Quality issues and proposals for improvements in the baseline adaption at geomagnetic observatories

Mandić, Igor

University of Zagreb

FACULTY OF SCIENCE

DEPARTMENT OF GEOPHYSICS

Igor Mandić

QUALITY ISSUES AND PROPOSALS FOR IMPROVEMENTS IN THE BASELINE ADAPTION AT GEOMAGNETIC OBSERVATORIES

DOCTORAL THESIS

Zagreb, 2017

University of Zagreb

FACULTY OF SCIENCE

DEPARTMENT OF GEOPHYSICS

Igor Mandić

QUALITY ISSUES AND PROPOSALS FOR IMPROVEMENTS IN THE BASELINE ADAPTION AT GEOMAGNETIC OBSERVATORIES

DOCTORAL THESIS

Supervisor:

Monika Korte, Ph.D.

Zagreb, 2017

Sveučilište u Zagrebu

Prirodoslovno-matematički fakultet

Geofizički odsjek

Igor Mandić

PROBLEMI KVALITETE I PRIJEDLOZI ZA POBOLJŠANJE PRILAGODBE BAZNIH LINIJA U GEOMAGNETSKIM OPSERVATORIJIMA

DOKTORSKI RAD

Mentor:

Dr.sc. Monika Korte

Zagreb, 2017.

Abstract

Data provided by geomagnetic observatories are fundamental in geomagnetic field studies and are widely used in other applications. Often they are combined with satellite and ground survey data. Unfortunately, the definitive observatory data are only available with a time lag ranging from several months up to more than a year. The main reason for this lag is the annual production of the final calibrated values, i.e. baselines that are used to correct preliminary data from continuously recording instruments at the observatory. To increase the prompt availability of calibrated observatory data, INTERMAGNET has recently started to distribute quasi-definitive data. These data are calibrated with temporary baselines and reported much faster than annual definitive data. In this thesis it is shown that the preparation of definitive geomagnetic data, i.e. definitive calibration values, is possible within a calendar year for most observatories of the INTERMAGNET type. An original method for prompt and automatic estimation of temporary quasi-definitive baselines is presented. Results of this baseline calculation obtained in a mostly automatic manner and comparisons with the baselines reported on INTERMAGNET DVDs for the 2009-2011 period are presented. The high quality of definitive and quasi-definitive baselines obtained by the new method indicate its suitability for data processing for nearly fully automatic observatories when automated absolute instruments will be deployed at remote sites. However, the automatic instruments show a larger scatter and an automated processing protocol should be robust to outliers. Data from Lonjsko Polje observatory are used to simulate datasets from an automated absolute instrument producing 24 observations per day. Results of these tests also confirmed robustness and reliability of the proposed method.

Key words: Geomagnetic observations, definitive data, quasi-definitive data, baseline fitting, data processing.

Sažetak

Podaci geomagnetskih opservatorija čine temelj u izučavanju geomagnetskog polja, nalaze široku primjenu u drugim geofizičkim disciplinama te se koriste za ostale primijenjene svrhe. Često se koriste zajedno sa satelitskim podacima i podacima terenskih izmjera. Nažalost, definitivni podaci geomagnetskih opservatorija su dostupni sa zakašnjenjem u periodu od nekoliko mjeseci, pa čak i više od godinu dana. Glavni razlog tog kašnjenja jest godišnja produkcija konačnih (definitivnih) kalibracijskih vrijednosti, tj. baznih linija koje se koriste za korekciju preliminarnih podataka s instrumenata koji kontinuirano mjere u geomagnetskim opservatorijima. U svrhu poboljšanja dostupnosti kalibriranih magnetskih podataka, u novije vrijeme INTERMAGNET je počeo publicirati kvazi-definitivne podatke. Ovi podaci su kalibrirani s privremenim baznim linijama te se izdaju puno brže nego godišnji definitivni podaci. U ovoj disertaciji je prikazano da je priprema definitivnih geomagnetskih podataka, tj. definitivnih kalibracijskih vrijednosti moguća unutar godine dana za većinu opservatorija mreže INTERMAGNET. Predložena metoda je također pogodna za promptnu i automatsku procjenu privremenih, kvazi-definitivnih baznih linija. Rezultati kalkulacije baznih linija predloženom metodom, dobivenih skoro u potpunosti automatskim putem, uspoređeni su s baznim linijama publiciranim na INTERMAGNET-ovim DVD-ima za period 2009-2011. Visoka kvaliteta definitivnih i kvazi-definitivnih baznih linija dobivenih novom metodom ukazuje da je predložena metoda prikladna za automatsku obradu podataka kada u potpuno automatiziranim opservatorijima (na udaljenim lokacijama) budu instalirani automatski apsolutni instrumenti. S druge strane, automatski instrumenti pokazuju veća raspršenja i pogreške u mjerenjima te bi iz tog razloga protokol za automatsku obradu podataka trebao biti robustan. Podaci iz opservatorija Lojsko polje korišteni su kako bi se simulirali podatkovni setovi automatskog apsolutnog instrumenta koji vrši 24 opažanja na dan. Rezultati ovih testova su također potvrdili robusnost i pouzdanost predložene metode.

Ključne riječi: geomagnetski opservatorij, apsolutna mjerenja, variometri, prilagodba baznih linija

Table of Contents

1. Introduction

1.1. The Earth's magnetic field and ground magnetic observatories

Around the Earth there is a natural shield, the so-called *geomagnetic* field that protects us from the solar wind and ensures sustainable environmental conditions. It deflects charged cosmic particles that would otherwise blow away our atmosphere and life on Earth would not be possible. Near its surface, Earth's magnetic field can be approximated (up to 90%) by the field of a magnetic dipole positioned at the centre of the Earth and whose axis is tilted about 11° with respect to the Earth's rotational axis. Earth's magnetic field observed all over the globe is a vector field (**F**) and three components are needed to describe the field. In the Cartesian coordinate system we describe it with X (North component), Y (East component) and Z (Vertical component, positive downwards). The elements describing the direction of the field are declination (D) and inclination (I). Aside from the rectangular system, the field can be represented in the cylindrical system *HDZ*, where H is the horizontal component in the direction of the magnetic meridian. Alternatively, we can also use two angular elements and the total intensity (F) to describe the field, i.e. the spherical *DIF* system.

Unlike the field of a bar magnet, the Earth's magnetic field is a very complex system that varies on a range of scales, in both the space and time domains. Variability of the Earth's field is the result of various processes, ranging from those in the Earth's deep interior, its crust, ionosphere, magnetosphere, all the way to the Sun. The geomagnetic field measured at the Earth's surface is a superposition of several contributions. More than 95% of the measured field originates from the electrically conductive fluid motions in the Earth's core (the main field). The lesser part is produced by the induced and remanent magnetization in the Earth's crust and upper mantle (the lithospheric field), and by time-varying current systems in the ionosphere and magnetosphere (the external field).

At Earth's surface, the main field has maximum intensity around 60 000 nT near the magnetic poles and minimum intensity about 30 000 nT at the magnetic equator. The spatial irregularities from the simple dipole model are caused mainly by instabilities of the electric currents in the Earth's core. Therefore, the field observed at the Earth's surface shows large regional anomalies with dimensions of thousands of kilometres. The non-uniform distribution of magnetic rocks in the Earth's crust and

accompanying induced effects in the upper mantle are seen as small-scale anomalies in the otherwise rather smooth field. The magnitudes of these local anomalies vary from several to hundreds of nT, but in some areas they reach a few thousand nT.

The temporal changes of the field occur on a time scale ranging from a fraction of a second (i.e. pulsations) to millions of years (i.e. pole reversals). The long-term variations of the main field, known as secular variation (SV), originate from physical processes in the Earth's core. These secular changes are noticeable on the annual timescales or longer. Short-term transient variations, from seconds to several days, arise mostly from the external field and associated induction effects.
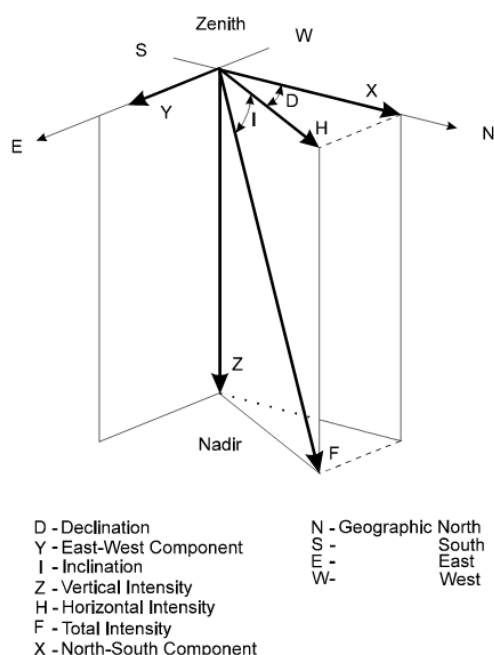
Figure 1.1 Geomagnetic elements (taken from St-Louis, 2012).

At any moment, the magnetic variations of extra-terrestrial origin are superimposed on the above described internal field (main field + lithospheric field). Except phenomena related with long-term solar activity (22 years solar magnetic reversal cycle and 11 year solar sunspot cycle), most contributors from the external field manifest themselves as short-term variations (from seconds up to time periods of a month). These short-term variations are mainly caused by: (1) thermal tidal forces in the atmosphere caused by solar heating, (2) interaction of the Earth's gaseous and plasma environment with charged particles and wave radiation intermittently emitted by the Sun, and (3) gravitational tidal pulls exerted on the Earth's gaseous environment, predominantly by Moon or to a lesser extent by the Sun. Some of well-known variations are: (1) 27-day variation connected with solar active regions rotating with the Sun's period of rotation, (2) 24-hour variation and its sub-harmonics connected with Sunrise and Sunset (referred to as S_q variation, Fig. 1.2), (3) variations of lunar origin with period 50.5-min longer than the S_q, (4) 2 to 4-day variation associated with the main phase and decay of

geomagnetic storms (Fig. 1.2), (5) 1 to 3-hour variation connected with the growth and decay of sub-storms, (6) periodicities of a few minutes to an hour which are set due to (i) X-rays from solar flares, (ii) decreased currents in the ionosphere caused by rapid recombination of ionization during a solar eclipse, and finally (7) pulsations with periods ranging from 0.3 seconds to 30 minutes, which originate in the distant magnetosphere (Fig. 1.3). Atmospheric lightning also leaves an oscillatory signature with periods of < 0.1 seconds. Amplitudes of the external variations vary between a fraction of nT (pulsations), through 10-100 nT (diurnal S_q variation) up to thousand nT in cases of geomagnetic storms. All these external contributions, of both regular and irregular kind, together with the internal field constitute the observed Earth's magnetic field.

In this short introduction on the geomagnetic field phenomena, many details have been omitted and I refer readers interested in more details to the textbook by Matsushita and Campbell 1967.
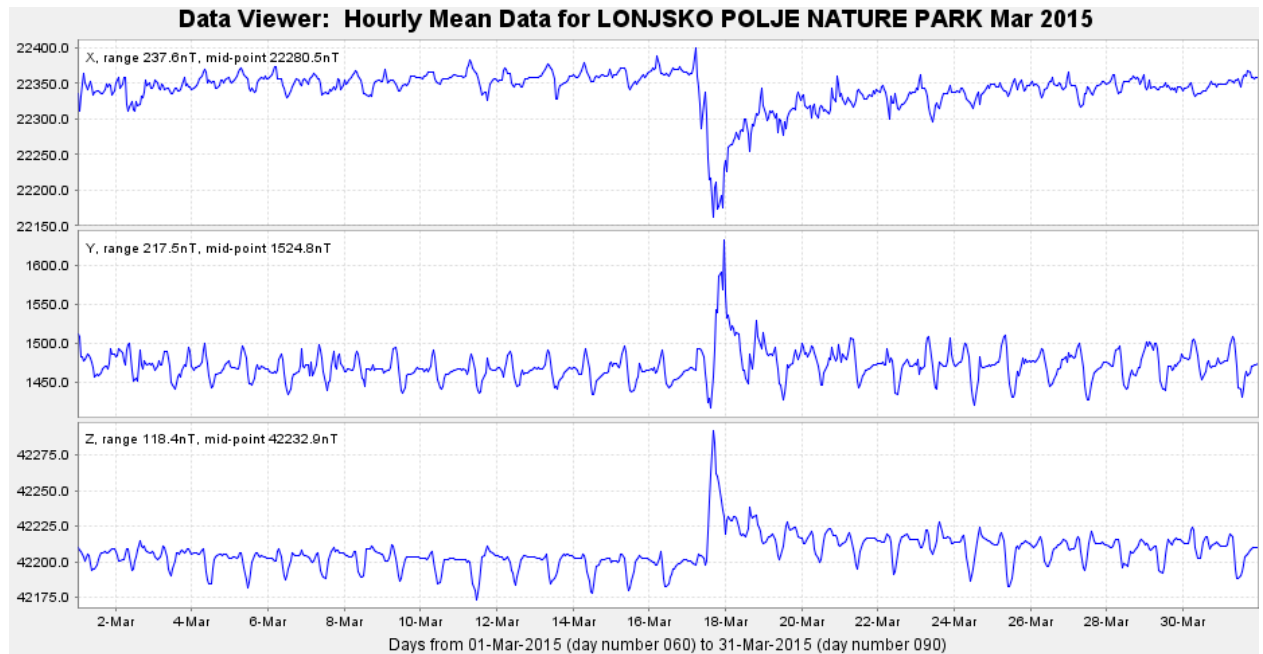
Figure 1.2 *X, Y* and *Z* components of the Earth's magnetic field recorded at LON during March 2015. Magnetograms show the diurnal S_q variation through the month. Except the regular S_q variation a sudden decay in *X*, i.e. increase in *Y* and *Z* components of the field is clearly noticeable on 17 and 18 March. This phenomenon is known as geomagnetic storm. The plot is created using IMCDVIEW software (www.intermagnet.org).

As stated previously, the geomagnetic field is a result of many geophysical processes inside and outside the Earth. In order to gain insight into the physics of these processes, we have to measure it, and develop models that reasonably fit the measured data. Like in many geophysical disciplines, the modeling is based on *inverse* techniques, i.e. the measured data are used for calculation of model parameters. Geomagnetic models (e.g. IGRF, Thébault et al. 2015) obtained in this way are used for scientific studies, the renewal of magnetic maps and various applied purposes like geology, mining, oil and gas exploration, archeology etc. Furthermore, these models are used for forecasting over a few

years to provide declination predictions for navigation purposes. Therefore, the high quality geomagnetic data are essential in scientific and other applications. These data are provided by geomagnetic observatories, extensive surveys made on land, at sea, and from aircrafts and satellites. Of all these, only the geomagnetic observatories can ensure continuous, high quality, long-term measurements (> 10yrs) of the geomagnetic field and its variations.
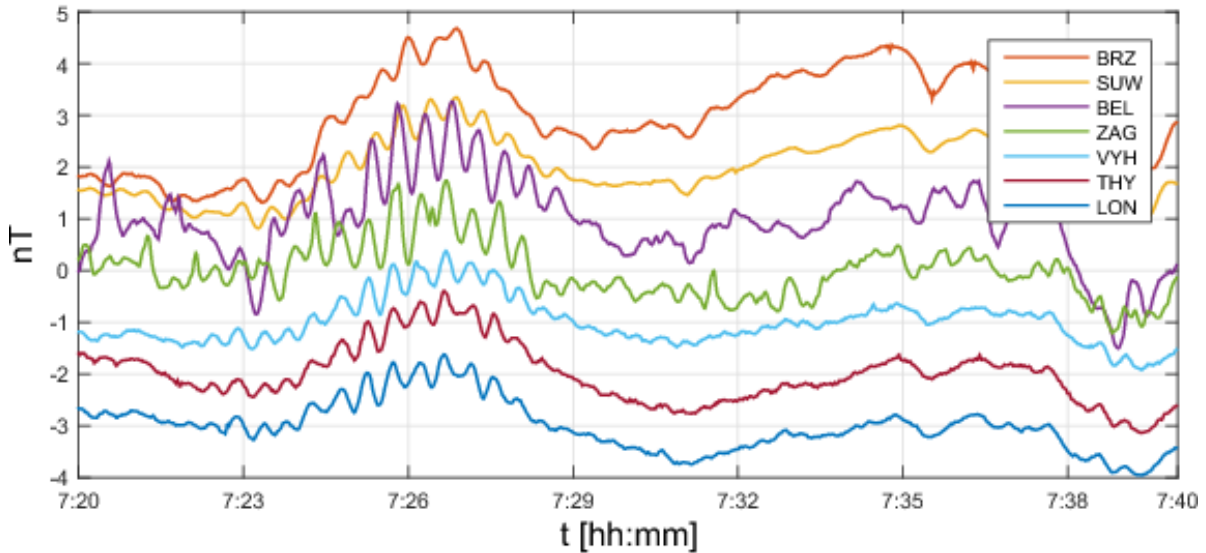
Figure 1.3 Stack plot of pulsation recordings along EMMA (European quasi-Meridional Magnetometer Array) on 15 July 2015 between 07:20-07:40 UT. Besides LON the recordings at THY (Tihany, Hungary),VHY (Vyhne, Slovakia), ZAG (Zagorzyce, Poland), BEL (Belsk, Poland), SUW (Suwalki, Poland) and BRZ (Birzai, Lithuania) are shown.

Magnetic observatories are designed to perform continuous and accurate measurements of the strength and direction of Earth's magnetic field over many years, or even centuries. The observatory locality must not be affected by artificial magnetic fields that could contaminate records. Ideally, the location should be free of crustal anomalies and have no lateral changes in electric conductivity in its vicinity (Wienert 1970, Jankowski and Sucksdorff 1996). Nowadays, the time resolution of the observatory measurements is one minute or less over a long period of time. These long-term data provided by global observatory network are mandatory for studies of the Earth's core dynamics, geomagnetic jerks and for investigating the relationship between the long-term solar and geomagnetic activity. A sufficiently dense global observatory network is essential in monitoring magnetic storms and other magnetic variations because these phenomena affect large areas of the Earth and have different effects in different areas. Ground observatories serve as base stations and are an important complement for various types of geomagnetic surveys (e.g. Newitt et al. 1996, Mandea and Korte 2011). They provide data from a different observation altitude and pure time series in contrast to the data obtained for example from the repeat station, airborne and marine surveys or satellite missions, containing both temporal and spatial variations. The main purpose of a survey is to find the spatial variations of the field (e.g. Brkić et al. 2013, Vujić et al. 2011). The temporal variation of the field during duration of a

4

survey distorts the actual picture of the spatial variation of geomagnetic elements over surveyed area. The observatory data are used to correct survey data for the temporal variations of the field in order to obtain a clear picture of the spatial variations. Usually the final product of a survey is magnetic chart (i.e. model) which is later updated at regular intervals with the help of the secular variation recorded at observatories, thus making a new detailed magnetic survey unnecessary. In many cases this means large savings of funds. Based on previous satellite missions (CHAMP, Ørsted, SAC-C) several studies have demonstrated (Lesur et al. 2006, Macmillan and Olsen 2013, Olsen et al. 2006) the importance of absolute observatory data for the ongoing *Swarm* mission, a constellation of three satellites (Friss-Christensen et al. 2006). The data from the *Swarm* satellites enable separation of the internal and external sources better than ever before. Processing, selection and validation of satellite data is usually based on data from ground observatories and their products, like geomagnetic activity indices. Absolute hourly mean values from observatories worldwide also play an important role in hour-by-hour spherical harmonic analysis used for deriving sophisticated magnetospheric models. Therefore, observatory data help to better constrain survey data and fill the gap between present and future satellite missions. Information from these different platforms offers the opportunity to exploit the geomagnetic field fully. From a local point of view, a magnetic observatory monitors the local magnetic variations, the knowledge of which is needed, for example in connection with observed power failures or difficulties in telecommunications. An observatory provides facilities for calibration of magnetic instruments. Very often the observatory is the only place to obtain information on local geomagnetic declination and its change. Local recording of magnetic variations is often needed by prospecting companies for the reduction of their data.

1.2. Motivation and outline

The objective of this thesis is to investigate the possibilities in producing the definitive geomagnetic observatory data in a more continuous manner without affecting the quality of the final definitive data. Until recently, magnetic observatories have been distributing two types of data: preliminary, available less than 72 hours in the case of INTERMAGNET observatories, and definitive baseline-corrected data, produced only once a year. The need for baseline-corrected observatory data released on a shorter time scale emerged within the community of global modelling. Based on the work of Peltier and Chulliat (2010) and Clarke et al. (2013) INTERMAGNET has defined a standard for a new data type called "quasi-definitive". As the name implies, these data should be close to the expected definitive vales, but delivered more rapidly than observatory annual definitive data. The purpose of quasi-definitive data is to fill the gap between preliminary and definitive data. These data are useful for a number of scientific activities, particularly in providing "ground truth" data for the satellite's

magnetometers. Today quasi-definitive data are used for many months or more than a year before they are replaced with definitive data. In this thesis, it will be shown that the preparation of definitive geomagnetic data, i.e. definitive calibration values is possible within a calendar year for most observatories of the INTERMAGNET type, and that the gap between preliminary and definitive data can be shorten significantly. Also, I will present an original method for prompt and automatic estimation of temporary quasi-definitive baselines. The results of this baseline calculation obtained in a mostly automatic manner and comparisons with the baselines reported on INTERMAGNET DVDs for the 2009-2011 period will be presented. The high quality of definitive and quasi-definitive baselines obtained by the new method indicate its suitability for data processing for nearly fully automatic observatories when automated absolute instruments will be deployed at remote sites.

In the first part of this thesis instrumentation and data processing techniques at geomagnetic observatories are presented. Problems in observatory practice and the state-of-the-art of preparing the observatory data are introduced and discussed through Chapter 2. In Chapter 3, a new scheme for the baseline adaption, based on smoothing spline modelling within windows is proposed. On several chosen examples, the advantages over classical methods are demonstrated. The data used for the analysis and verification of the proposed method are presented in Chapter 4. In Chapter 5, special attention is paid to demonstrating the robustness of the method and its applicability in automated processing. The last chapter, Chapter 6, summarizes the work and proposes some interesting concluding remarks.

2. Measurements in geomagnetic observatories

2.1. Instruments and basic principles of observatory operation – Example of Lonjsko Polje observatory

Nowadays in modern magnetic observatories the measurements of the Earth's magnetic field are performed with two types of instruments. These are absolute instruments and variometers. Magnetic variometers are magnetometers, which continuously measure and record three components of the magnetic field variations. Figure 2.1 shows the most commonly used variometers at modern magnetic observatories are three-component fluxgate magnetometers, or alternatively, variometers based on a scalar magnetometer (Jankowski and Sucksdorff 1996, Matzka et al. 2010, Mandea and Korte 2011). The data are samples of the magnitude of the field components variations. The primary samples are usually taken many times per second. Applying digital filtering techniques, one-minute or more frequent values are produced and stored. The samples represent only the varying part of the field, having a range within $\pm$ 5000 nT. To obtain the final value of the component a base value has to be added to the recorded value. The base values are determined by taking absolute measurements. Separate absolute instruments are used to determine absolute values of the field components. Today, the most popular combination for absolute measurements is a scalar magnetometer for measuring the total field intensity (F) and a fluxgate theodolite for measuring declination (D) and inclination (I), known as DI-flux (Lauridsen 1985, Kerridge 1988). Scalar magnetometers, like proton precession magnetometers, Overhauser magnetometers and optically pumped magnetometers are push-button devices, usually robust and waterproof with capabilities to continuously measure F with high-resolution and precision (Packard and Varian 1954, Alexandrov and Bonch-Bruevich, 1992, Gilles et al. 2001, Rasson 2007). In observatory practice, the set of three components provided by variometers is often complemented with a scalar F as an additional, absolute verification. The DI-flux magnetometers are based on a single-axis fluxgate sensor mounted on the telescope of a non-magnetic theodolite and the associated electronic unit (Fig. 2.2). Measurements with the DI-flux magnetometer are performed manually, usually once a week. In conjunction with F from scalar magnetometer we

obtain a complete set of absolute values of the field that is used to calibrate variometer recordings. Despite the vast progress in observatory instrumentation over the last two decades, it is still state-of-the-art to calibrate variation measurements with sporadic absolute instruments to obtain a high-resolution record of the field in terms of absolute values.

Figure 2.1 *Left*: Variometer based on a scalar magnetometer; a suspended dIdD magnetometer (manufacturer: GEM Systems, Canada), the main variometer at LON. *Top-right*: LEMI-035, three-component fluxgate magnetometer, the supplement variometer at LON (manufacturer: Lviv Centre of Institute for Space Research). *Bottom-right*: FGE, a very popular type of the suspended three-component fluxgate magnetometer (manufacturer: Danish Meteorological Institute, DMI). This type of instrument is used in many observatories wordwide.

The first observatories established in the 19th century performed only frequent absolute observations. The goal was to obtain daily and annual values. At that time, observing the geomagnetic field was quite laborious work due to long-lasting and complicated observational methodology. Also very well trained and skilful observers were needed for this job. With the development of the first analogue variometers, the principle of observatory measurements has remained the same until today. The use of continuously recording variometers had significantly decreased the number of absolute observations, but still the human intervention in observatory operation was substantial. For example, every day, the observatory staff needed to change photographic paper where magnetic variations had been recorded,

scale the abscissa and ordinate axes on raw magnetograms, estimate hourly means and write them down in tabular form, estimate geomagnetic indices by hand scaling, as well as perform occasional absolute observations in order to calibrate variation values. Thus, the traditional observatories, established many decades ago required a high quality infrastructure not only to provide accommodation and offices for the staff, but also to host traditional instruments. These instruments, generally large in size, were very sensitive to environmental changes and they required constant maintenance and care by the observatory staff.

Figure 2.2 Absolute instruments operating at LON. *Left*: DI-flux magnetometer (manufacturer: MinGeo, Hungary). It is based on a Zeiss 010A nonmagnetic theodolite and equipped with a DI fluxgate magnetometer (Model G, manufacturer: DMI). *Right*: Overhauser proton precession GSM-19F magnetometer (manufacturer: GEM Systems, Canada).

In the last few decades, with the development of digital instruments and progress in computer sciences and technology, geomagnetic instruments and acquisition systems have become more robust, compact, less power consuming and smaller in size. Nevertheless, variometers and absolute instruments cannot be placed on the same pillar. A relatively large separation is desirable (>10 m) in order to avoid mutual interference. In a geomagnetic observatory, at least two pillars are needed. One for the variometer, which has to be kept permanently in a stable environment, and one for the DI-flux, which has to be accessible to the observer and stabile for the duration of an individual absolute measurement. The scalar magnetometer can be put on an improvised pillar/placing since scalar sensors are not sensitive to moderate tilting and rotations. These pillars are usually in separate buildings/huts. Consequently, today a standard observatory for basic operation comprises a few simple nonmagnetic huts that host magnetometers, uninterrupted power supply, and systems for data acquisition and transmission. Many observatories are unmanned, and the staff visits the observatory only for occasional maintenance and for purposes of absolute measurements.
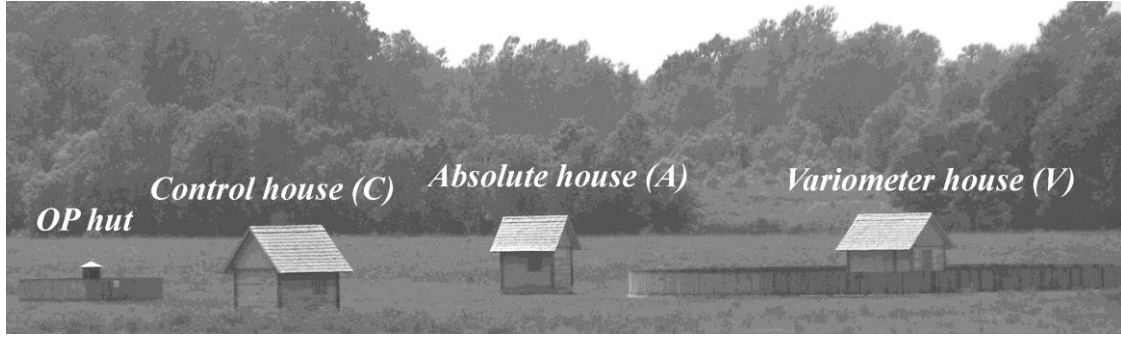
Figure 2.3 Four structures of the LON observatory: OP (Overhauser Proton) hut, control house (C), absolute house (A), and variometer house (V).

The recently established Croatian observatory in Lonjsko Polje (LON) is a typical unmanned observatory (e.g. Korte et al. 2009, Mandić et al. 2016). Many examples and some of the results in this thesis will be demonstrated on the LON data. Thus, for the sake of completeness, a detailed description of the observatory is given.

LON is comprised of several huts (Fig. 2.3) built from non-magnetic materials, mostly oak, and using styrofoam for insulation to allay temperature effects. The huts' foundations and inner pillars are constructed from white cement. The power supply of the observatory comes from solar cells mounted on the roof of the control house (C). House C is the only structure allowed to have a relatively small amount of magnetic materials due to the 90 m distance from the huts that host the magnetometer electronics and their sensors. The observatory operates several instruments, two scalar "Overhauser proton precession" magnetometers GSM-19 (manufacturer: GEM Systems, Canada) for measurement of the total intensity (F), with 0.2 nT absolute accuracy and 0.01 nT resolution. For measurements of the absolute values of declination (D) and inclination (I), we use a Declination-Inclination magnetometer, i.e. DI-flux magnetometer (manufacturer: MinGeo, Hungary). It is based on a Zeiss 010A geodetic theodolite with 1 second arc resolution converted into non-magnetic, and equipped with a DI fluxgate magnetometer Model G, with 0.1 nT resolution (manufacturer: Danish Meteorological Institute). The relative changes in inclination (dI) and declination (dD) are measured with a suspended dIdD magnetometer (manufacturer: GEM Systems, Canada). Beside variation recordings, the dIdD simultaneously provides total field recordings as well (Alldredge 1960, Hegymegi et al. 2004). Manufacturer specifications of this magnetometer are: dI and dD uncertainty is ≤ 1 arcsec and ≤ 4 arcsec rms, respectively, temperature drift is < 0.1 nT/°C and the long-term drift is < 2 nT/year. Furthermore, the observatory also hosts a Ukrainian three-axial fluxgate magnetometer LEMI-035 (manufacturer: Lviv Centre of Institute for Space Research). It is low-noise (< 10 pT at 1 Hz) with 1 pT resolution and temperature drift < 0.5 nT/°C, installed in the framework of the EU FP7 PLASMON Project (Heilig *et al.* 2013) in cooperation with the Tihany Observatory (MFGI – Geological and Geophysical Institute of Hungary).

The dIdD instrument records continuously in the variometer house (V), the GSM-19 is placed in the OP (Overhauser Proton) hut (Fig. 2.3), while absolute DI-flux observations are carried out with the DI-flux magnetometer on the absolute pillar standing inside the absolute house (A). A second scalar magnetometer is used for measurements of total field values on pillar A (except during periods when the DI-flux observations are performed). This pillar is the location where all observatory measurements are reduced to. Its WGS-84 coordinates are 45° 24' 29'' N, 16° 39' 33'' E, and altitude is 95 m above sea level. To achieve better temperature stability, the dIdD sensor is enclosed in a wooden box padded with 0.3 m-thick styrofoam panels. Currently, there is no active temperature control (cooling/heating) in house V, but comparison between temperature recordings inside (temperatures of dIdD electronic and sensor) and outside house V indicate that the diurnal temperature changes inside house V are significantly lower (around 80 %). Daily temperature variation around the sensor is kept within several degrees, with average amplitude 1.2 ± 0.7° C, and 2.6 ± 1.4° C for electronic. Since dIdD is based on a scalar magnetometer insensitive to temperature variation, most of the drift originates from the thermo-mechanical deformation of the spherical coil system around the sensor. According to technical specifications and temperature around the sensor, we assume there is no significant (< 0.5 nT) temperature drift superimposed to daily magnetic data. The LEMI sensor is buried 1 m under the ground, and its electronics unit and the data acquisition unit (DAQ) developed at MFGI (Merényi et al. 2013) are mounted in a shelter on the fence that surrounds house V. During the installation of the LEMI, we made sure that its sensor was far enough from the dIdD, which produces strong deflection fields during operation and could cause interference. Average daily temperature changes for the LEMI sensor and electronics are 0.07 ± 0.04° C and 6.8 ± 5.6° C, respectively. Unfortunately, due to the lack of suitable infrastructure, we could not provide a temperature-stable environment for the LEMI electronics, but luckily for the purposes of geomagnetic pulsation studies, temperature stability is a less important factor (Heilig et al. 2013). Both variometer systems are also subdued to long-term annual temperature changes around 20° C, and these drifts are eliminated by a standard procedure – baseline calibration (Jankowski and Sucksdorff 1996).

In house C is the main data acquisition system together with accompanying modules (GPS antenna, RS and A/D converters) for the collection and storage of data from the magnetometer systems in OP hut and house V. The main DAQ is basically the same as the LEMI's DAQ, only it has different operating settings. Through Internet communication provided by mobile Internet, all data are uploaded to the server of the Geophysical Institute in Zagreb every hour, while the LEMI data is also uploaded to the PLASMON server of the Tihany Observatory every 15 minutes. Both acquisition systems are connected via Ethernet to a third industrial PC, which serves as an in-situ server for storing the data, and which can be used for dIdD data logging in case of malfunction of the main DAQ. This PC has somewhat better performance than those used for primary data acquisition, thus enabling us remote access to LON through the Internet provided by a second modem. This allows us to check the dIdD

and LEMI systems remotely, and if necessary, modify the configuration settings, or reach data manually if there is a problem with the main Internet connection.
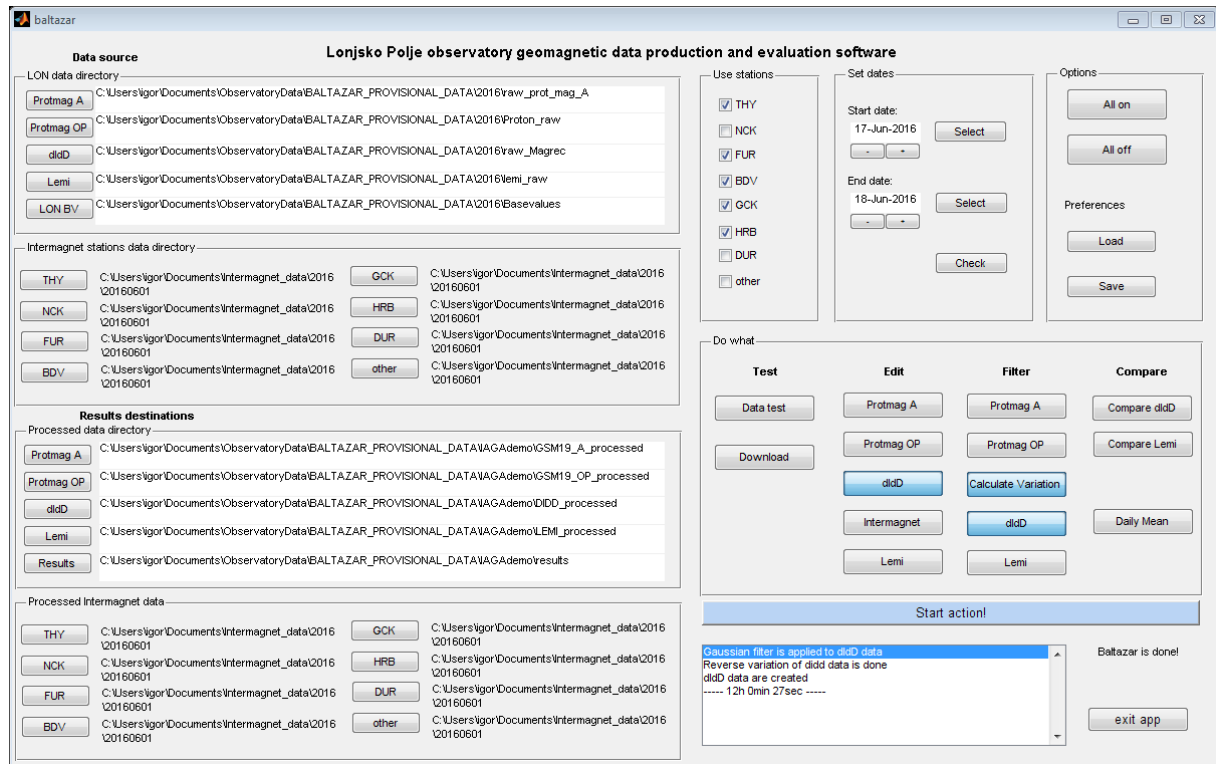
Figure 2.4 Main panel of "Lonjsko Polje data processing and evaluation software".

Except for the LEMI with 128 Hz data rate, all other recording systems are set to 5-second sampling. In the case of dIdD, this means that every 5 seconds, we have four biased total field readings and the unbiased ambient field reading, all required for deriving variation of inclination and declination (Schott and Leroy 2001, Hegymegi et al. 2004). The Gaussian low-pass filter is applied on the 5-second raw variation data and the total field recordings in order to obtain the standard INTERMAGNET (http://www.intermagnet.org/) minute means (St-Louis, 2012). Raw samples from the LEMI magnetometer are automatically filtered by two successive Gaussian digital filters embedded in the DAQ software. The first filter produces 16 Hz data, while the second produces 1 Hz data from which the standard minute means are obtained. After visual inspection of the GSM-19, dIdD and LEMI recordings together with simultaneous comparison with data from surrounding observatories (Fig. 2.14), artificial disturbances and spikes are identified and removed. Processing and cleaning of data is done using "Lonjsko Polje data processing and evaluation software" (Fig. 2.4). (This is non-commercial software created by the author of this thesis.) The final dIdD minute data are calibrated to the absolute level using adapted base values for declination and inclination, while total field is corrected for the *F* baseline which presents the offset between pillars A and V. All other components are then calculated from *D*, *I* and *F* values. In case the dIdD data are missing, they are complemented with baseline corrected LEMI data. Finally, the FMI algorithm (Menvielle et al. 1995)

is applied to produce local geomagnetic activity indices K with 350 nT as the lower $K = 9$ limit (Bartels *et al*. 1939).

The K index is a three-hour range index designed to measure the irregular deviations from the daily solar regular (S_R) variation of the geomagnetic field. Based on the difference between the highest and lowest deviation from S_R within a three-hourly interval, the K index is determined. The (dimensionless) logarithmic scale is used to obtain the index value (from 0 to 9) based on the amplitude of the disturbance in a three-hourly interval. In this way the deviations corresponding to the lower limit for $K = 9$ are 100 times larger than those corresponding to the upper limit for $K = 0$ and these limits give a reasonable frequency distribution for the nine values. However, due to statistical reasons it is also desirable to have indices on a linear scale. Therefore, along with calculation of K indices, a reconversion into equivalent linearly scaled ak index is done and a daily index, Ak, or equivalent daily amplitude, is determined as the average of eight ak values. The ak and Ak are expressed in units of nT. For more details on indices, see the textbook (Matsushita and Campbell 1967).

2.2. Absolute measurements and observatory baselines

Although INTERMAGNET does not forbid the use of other instruments, the DI-flux combined with a scalar magnetometer is the recommended pair of absolute instruments. The DI-flux features a fluxgate sensor mounted parallel onto the telescope of a non-magnetic theodolite. In practice, there will always be a misalignment which results in a collimation error. This, as well as most other errors, can be eliminated by proper observational procedure. There are two possible methods of observation: the null and residual method (e.g. Lauridsen 1985, Jankowski and Sucksdorff 1996, Worthington and Matzka 2017). Both methods require that the sensor be placed in four positions that cancel collimation and offset errors. The measurement procedure starts by placing the DI-flux on a pillar (or tripod). It is levelled with foot screws such that the theodolite's alidade rotates around a vertical axis, and its position has to be fixed during the measurement sequence. For convenient determination of geographic North with the DI-flux, a sighting mark is established with known azimuth in some 100 to 1000 m distance. The direction of the field vector is determined by measuring the horizontal and vertical angles, i.e. positions where the sensor is perpendicular to the horizontal component and the total field intensity. At these positions, the magnetometer shows zero output (or close to zero in the residual method), and it is important to note the precise time when zero reading is taken. From this, the declination and inclination are determined, as well as the fluxgate sensor offset and misalignment angles between the fluxgate sensor and the optical axis of the theodolite. The total intensity must be simultaneously recorded with a scalar magnetometer in order to obtain complete information about

absolute values of the field and to be able to compute base values for the vector magnetometer. A detailed procedure of absolute measurements and determination of base values is given in Appendix A.

Base values are found by comparing the results of absolute measurement to the variometer output (Appendix A). Figure 2.5 shows LON baselines for the year 2016. Each red point represents a base value determined from an absolute measurement, while the continuous lines represent the adapted baselines that were used to calculate definitive data. The measured and adapted baselines are an important indicator for the quality of observatory data. For example, continuously changing baselines suggest variometer drift, while steps in the baseline are often associated with certain events, like maintenance work or realignment of the variometer sensor.
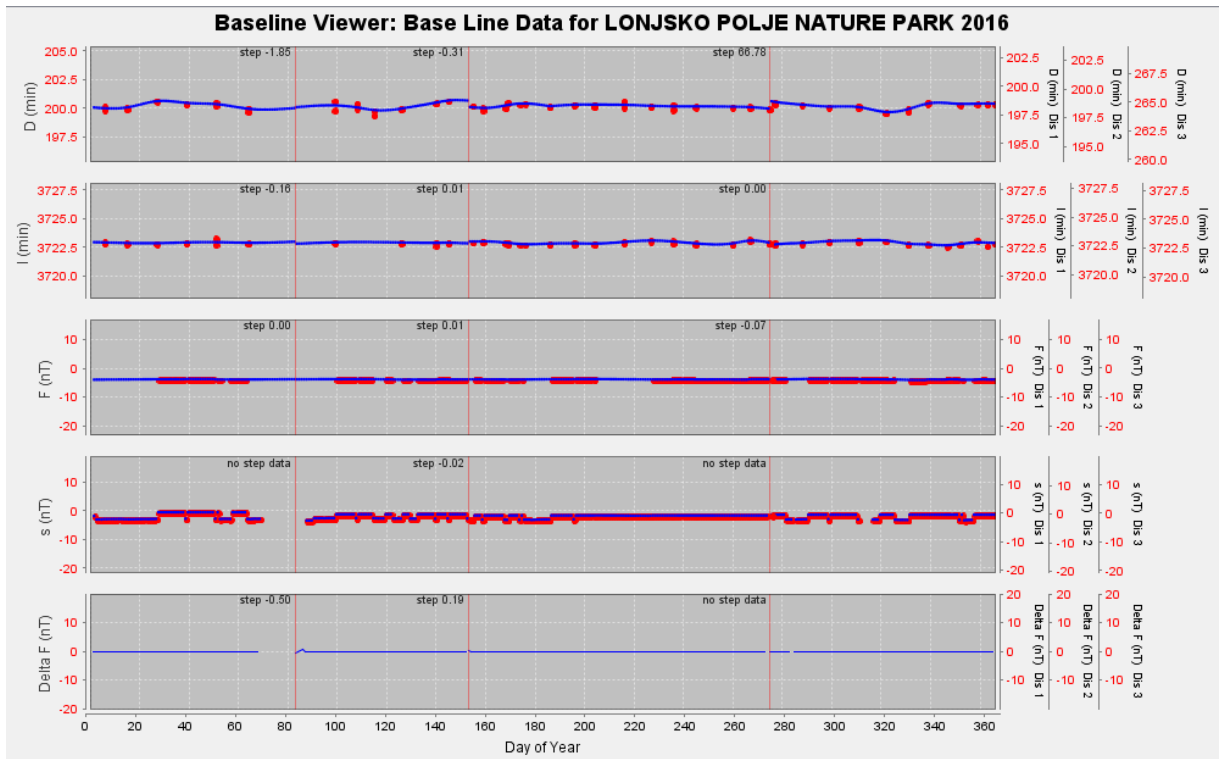
Figure 2.5 The dIdD baselines for the year 2016 at LON geomagnetic observatory. Observed baselines obtained from absolute measurements are presented by red dots. Continuous functions are fitted on the observed values to obtain adapted baselines (blue lines). The vertical red lines indicate the steps in the baseline. The baseline plot is created using IMCDVIEW software.

Baseline instabilities, so-called drifts, are mainly due to pillar tilts/rotation, temperature variations and the field gradients (Csontos et al. 2007, Chambodut et al. 2009, Iype et al. 2017). The drift of modern digital magnetometers is comparatively lower than those of classical age that were in use in the last two centuries. However, the drift of modern magnetometers is still large in comparison to the long-term week signals (secular variations, main field morphology, long-term external field variations, etc.). For studies in which absolute accuracy of the observatory data plays a crucial role, monitoring of

the baseline stability and baseline calibration is mandatory. Baselines are an important part of the metadata that geomagnetic observatories have to deliver to obtain definitive data accepted by INTERMAGNET (St-Louis, 2012).

2.2.1. Causes of baseline instabilities

Baseline instability is a variometer response to environmental instabilities in the vicinity of the variometer sensor and electronics. Thermal and mechanical stability (the sensor must not move) is of major concern for reliable variometer operation. In modern-day digital magnetometers, the temperature may affect the coil characteristic, temperature differences may cause strain on the mechanical system and also affect the electronic components. The problem of temperature can be circumvented by keeping both sensor and electronics in a thermostatically controlled, constant temperature environment. Tilting of the sensor is another problem that can seriously affect baseline stability. If the sensor is mounted on a pillar that moves for some reason; the freeze-thaw cycle, the wet-dry cycle, changes in temperature, then the orientation of the sensor assembly will change, and the sensor will no longer measure the three magnetic field components that they are supposed to measure. This is not a serious problem if the tilting progresses slowly and remains small. It is then manifested as a slow drift in one or more components, for which corrections can be applied by adding baseline values derived from absolute observations. One way to eliminate the problem of a small tilt is to place sensor assembly in a tilt-compensating suspension (Fig 2.1). Suspended sensors have solved the problem of drifting due to pillar tilts, but the drifting due to the rotation of the sensor caused by the twisting of the pillar still poses a problem. If tilting, twisting or thermo-mechanical effects progress rapidly, so that significant changes occur on a timescale shorter than the period between successive absolute observations, usually once a week, aliasing can occur. This means that it is impossible to obtain the true, properly baseline-corrected values of the magnetic field components on a minute-to-minute basis. In practice, even if almost ideal environmental conditions are ensured, we will still find some drifting due to aging of sensor windings and the electronic involved in magnetometers.

The variation in gradient field between the absolute pillar and variometer pillar also causes long-term drifts in baselines (Iype et al. 2017). While selecting a site for the establishment of an observatory, it is normal practice to choose a site with minimum magnetic gradients, preferably with less than 1 nT/m (e.g. Jankowski and Sucksdorff 1996, Verbanac and Vujić 2012, Mandić et al. 2016). However, in cases of many observatories this criterion could not be satisfied because of many constraints, and other factors and gradients at these observatories can be higher than the desirable limit. The gradients in the magnetic field between the pillars can be caused by many reasons, such as crustal field contributions, inhomogeneous electrical conductivity distribution in the ground from magnetized rocks and soil. This

means that the variation of *F* at the absolute and variometer pillar need not be the same. When we take the difference of these two, we expect to see an approximately constant offset, but we have examples from many observatories that this difference need not to be a constant. This can contribute to the gradient drift in the baseline.

Even if we manage to find ideal housing for the variometer and there are no instrumental or procedural errors from the variometer side, measurement errors in absolute observations will introduce errors in the baseline samples that may affect the quality of the final data.

2.2.2. Errors from absolute observations

The basic prerequisite for quality observatory data is the magnetic cleanness in the vicinity of the DI-fluxgate sensor, i.e. the geomagnetic theodolite must be completely free from ferromagnetic elements, and slightly magnetic materials have to be far from the sensor. In particular, the place for absolute measurements should be free of horizontal and vertical gradients (< 1 nT/m). The measurement of declination with the DI-flux requires referencing the observed value to a known azimuth. An error in the azimuth will result in a systematic error in declination. At a magnetic observatory, a professional surveyor should determine the azimuth of the reference mark to a very high degree of accuracy, so this should not be a source of error. A large temperature difference between the absolute building and the outside will cause an apparent erratic motion of the reference mark when viewed through an open window. Viewing through a glass window can lead to a systematic error due to the index of refraction of the glass. Natural magnetic perturbations are another potential source of error. In theory the null and residual method should be immune to the effects of disturbances because individual readings are corrected with synchronized recordings of the variometer. In practice, the ability to set the instrument in null position and to read the display with a timing error less than 1 s depends on the skill of the observer and the frequency content of the magnetic field variations. Therefore, performing observations during disturbed periods should be avoided. However, at high latitudes this is almost impossible and one should take several observation sets during one measurement session in order to improve the accuracy of the base values. Improper levelling of the theodolite will lead to errors in declination. This is another error that is completely preventable if a theodolite with a gravity-oriented vertical scale is used. Even if the base of the theodolite is slightly off-level (by less than 4 arc minutes), the vertical scale will indicate the true angle of the telescope relative to the horizontal. The telescope can then be placed in the horizontal by setting the vertical circle to exactly 90° or 270° before each reading (see Appendix A). If a theodolite without this feature is used, this source of error becomes much more important. Figure 2.6 shows empirical results of improper levelling, obtained from test measurements that I have are performed at Niemegk observatory (Germany) during my

research stay in the period between May and June 2014. The top subplots in Fig 2.6 demonstrate how errors in declination strongly depend on a small offset of the theodolite telescope relative to the horizontal. These errors can also be detected as errors in the electronic offset (S_{0D}) obtained from the declination observation. However, relatively high errors in D practically do not affect the quality of the I measurement. The positioning of the theodolite in the magnetic meridian is not very critical. Aligning the telescope within 5' of the true magnetic meridian is good enough. For values of inclination typical for mid latitudes 55° to 70°, failure to set the telescope within 5' will lead to errors of a few arc seconds or $\leq$ 1 nT. The theodolite parameters δ, ε, and S_0 (see Appendix) should be constant or slowly vary over time. A sudden change in these parameters without a known reason (for example adjusting the sensor axis or the electronic offset) is an indicator that there is some procedural error in observations. Deviation of δ_D, ε_D, S_{0D} or ε_I, S_{0I} from expected values indicates that there is an error in the D or I reading, respectively, or in the complete set.
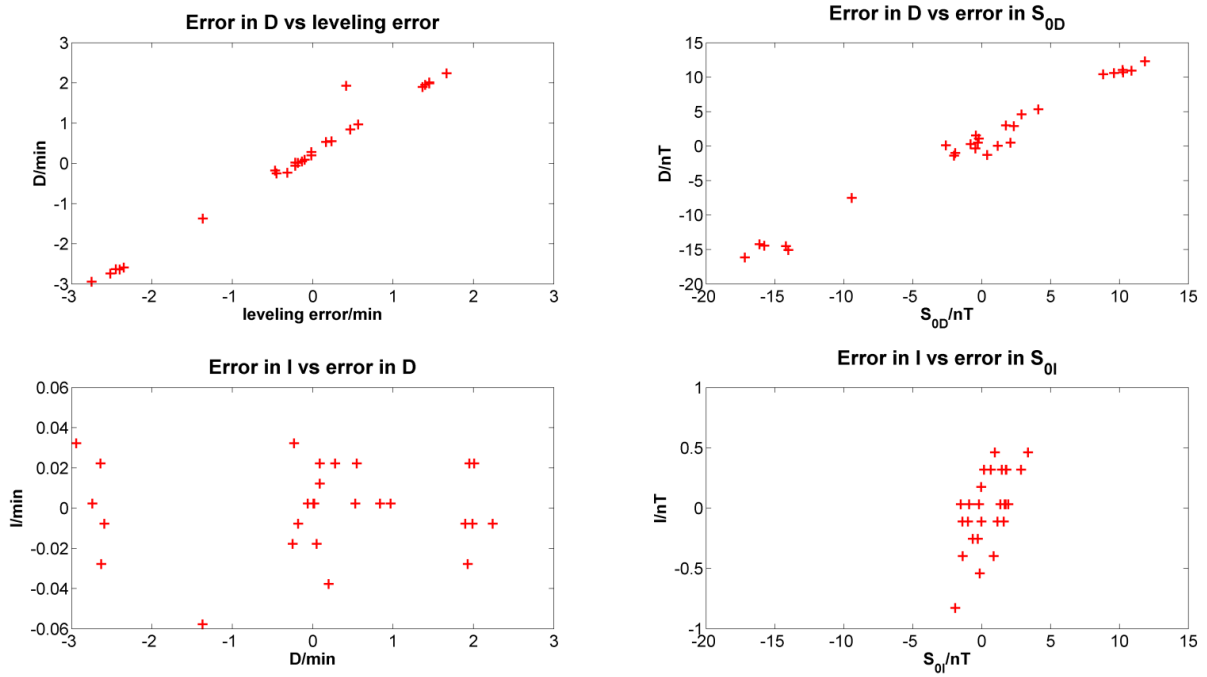
Figure 2.6 Results of test measurements performed at Niemegk observatory during May and June 2014. *Top-left*: Errors in D caused by improper levelling. *Top-right*: Errors in S_{0D} parameter are also linked with levelling errors. *Bottom-left*: Errors in I versus errors in D, i.e. error in setting the telescope in the magnetic meridian. *Bottom-right*: Errors in I versus errors in S_{0I} parameter. Note that D and I (arc minutes) on the left subplots are expressed in equivalent units in nT on the right subplots.

2.3. Baseline quality checks and preparation of the final data

The quality of observatory definitive data depends significantly on the suitable combination of manual

absolute measurements and variometer data used for calibration to obtain the absolute values of the geomagnetic field. The quality of a variometer can be evaluated by means of its base line plot for all its recorded components. Figure 2.7a (three top subplots) shows the base line plot of LEMI-035, the supplement variometer at LON. The vertical scale of 20 nT is often used by observatories because it is adequate for most baselines. However, due to increased variability of the LEMI-035 baselines, the vertical scale of 40 nT is used. The base line plot includes two types of information: the baseline variation and the uncertainty of the absolute measurements. By comparison of the baseline plots of the LEMI and dIdD magnetometer (Fig. 2.5 has the same ordinate scaling as Fig 2.7a), we immediately see the much better baseline stability of the dIdD magnetometer. The amplitude of LEMI baselines raise the question if absolute observations performed approximately every 10 days are frequent enough to avoid aliasing (Section 2.2.1).
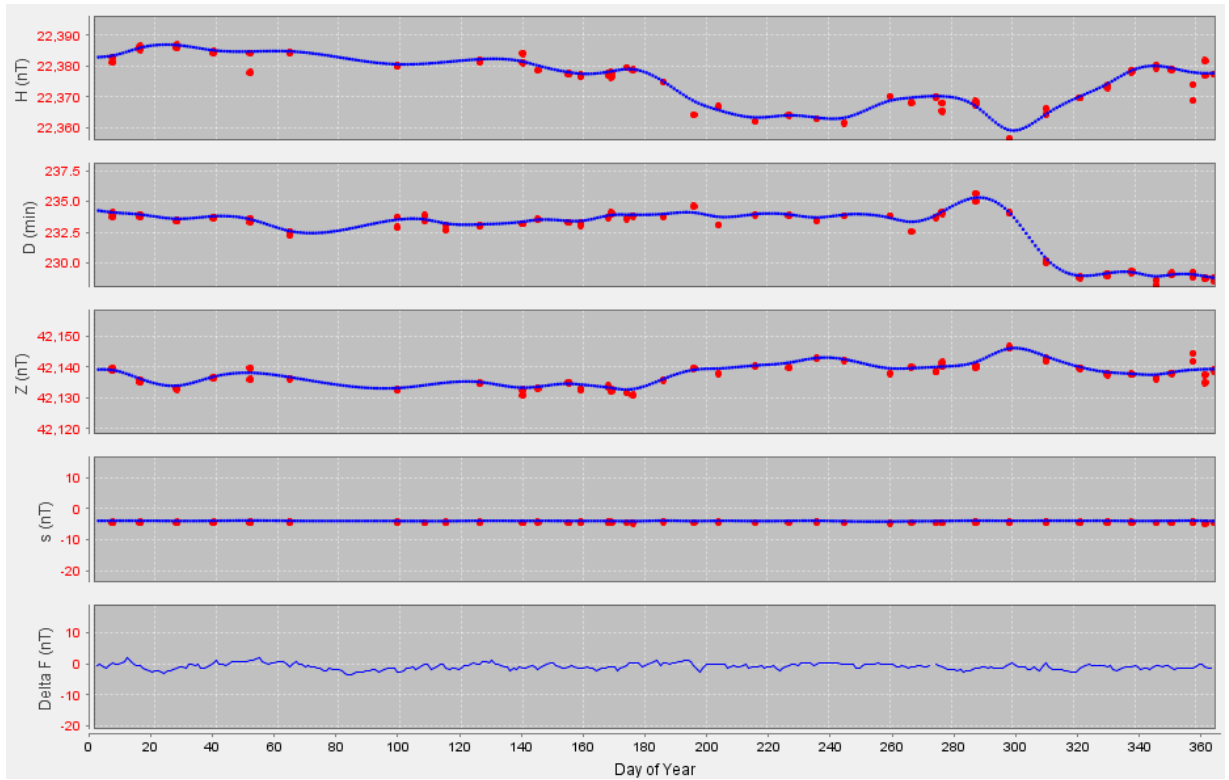
Figure 2.7a The LEMI baselines for the year 2016 at LON geomagnetic observatory. Observed baselines obtained from absolute measurements are presented by red dots. Continuous functions are fitted on the observed values to obtain adapted baselines (blue lines). The baseline plot is created using IMCDVIEW software.
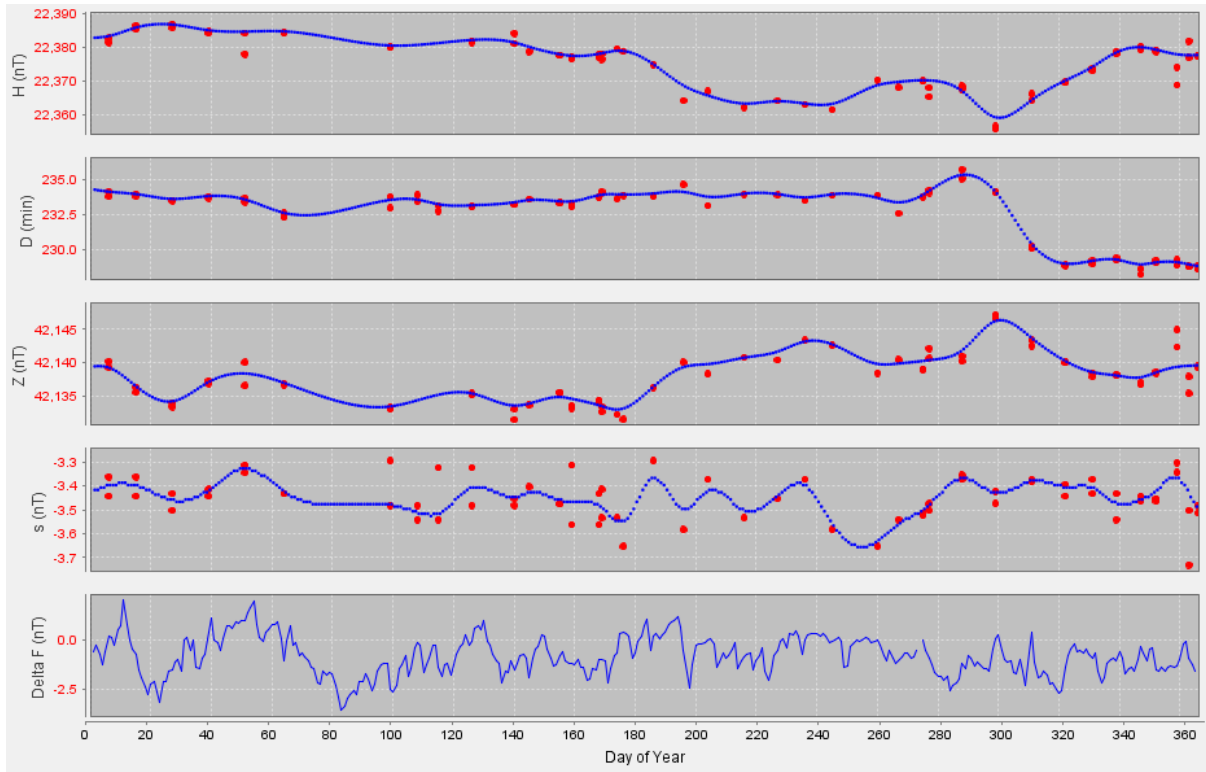
Figure 2.7b Same as Fig 2.7a, only the scaling on ordinates is automatic. The baseline plot is created using IMCDVIEW software.
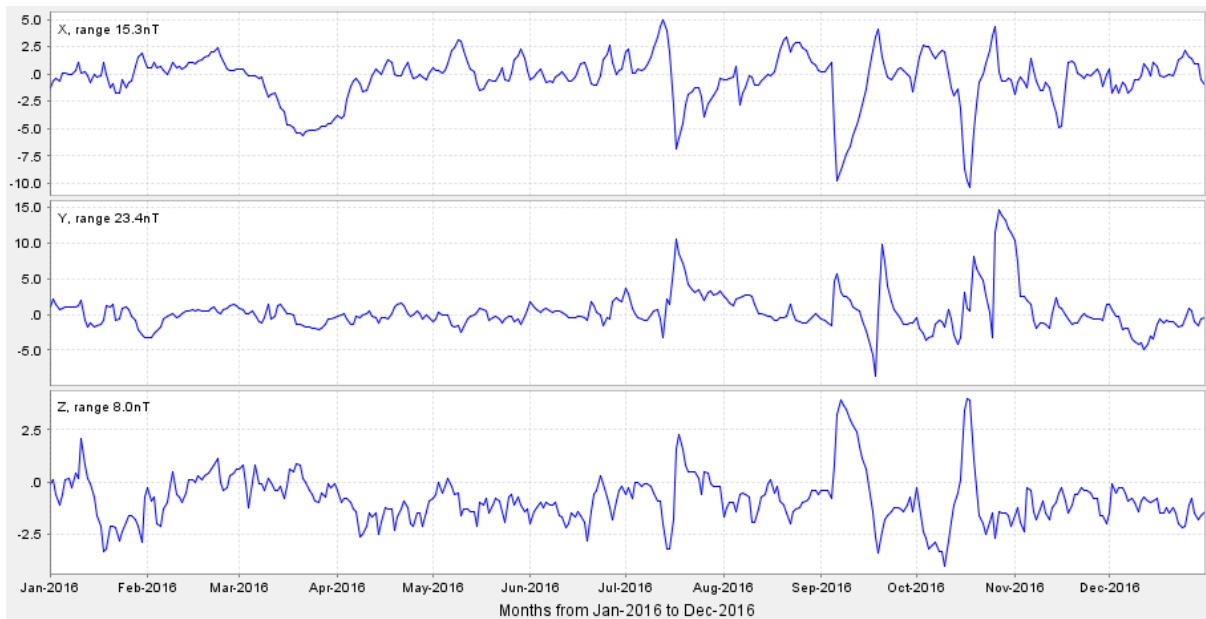
Figure 2.8 Difference between LEMI and dIdD daily mean values in 2016. The difference plot is created using IMCDVIEW software.

If we plot the difference between LEMI and dIdD data on the daily and hourly timescales, we can see obvious problems with the short- and long-term stability in LEMI data that could not be corrected by the standard calibration procedure. In 2016, sudden movements of the LEMI sensor occurred on

several occasions (Fig. 2.8 and Fig. 2.9). Since the (waterproof) sensor is installed at the bottom of the "waterproof-cylindrical-tube" and buried 1 m in the soil, the most probable reason of these movements are changes in the percentage of moisture in different layers of the soil. For example during the summer season, due to increased heating and lack of precipitation, the top layers of the soil cracks and may cause sudden movement of the tube/sensor. Beside these sudden and seasonal, i.e. gradual movements of the sensor, we can also see short-term diurnal drifts (Fig. 2.9) related to the temperature changes around LEMI electronics (Section 2.1). This type of drift can also be related to erroneous scale values. In the case of erroneous scale values, the difference plot should coincide with the diurnal variation of the magnetic field. Figure 2.10 shows the difference plot and changes in the field components on 21 June 2016. The temperature changes around LEMI sensor were practically constant (< 0.06 °C) and are not displayed on Fig. 2.10. From this figure, we may conclude that the drift in LEMI data originates from temperature changes in the surroundings of LEMI electronic unit.
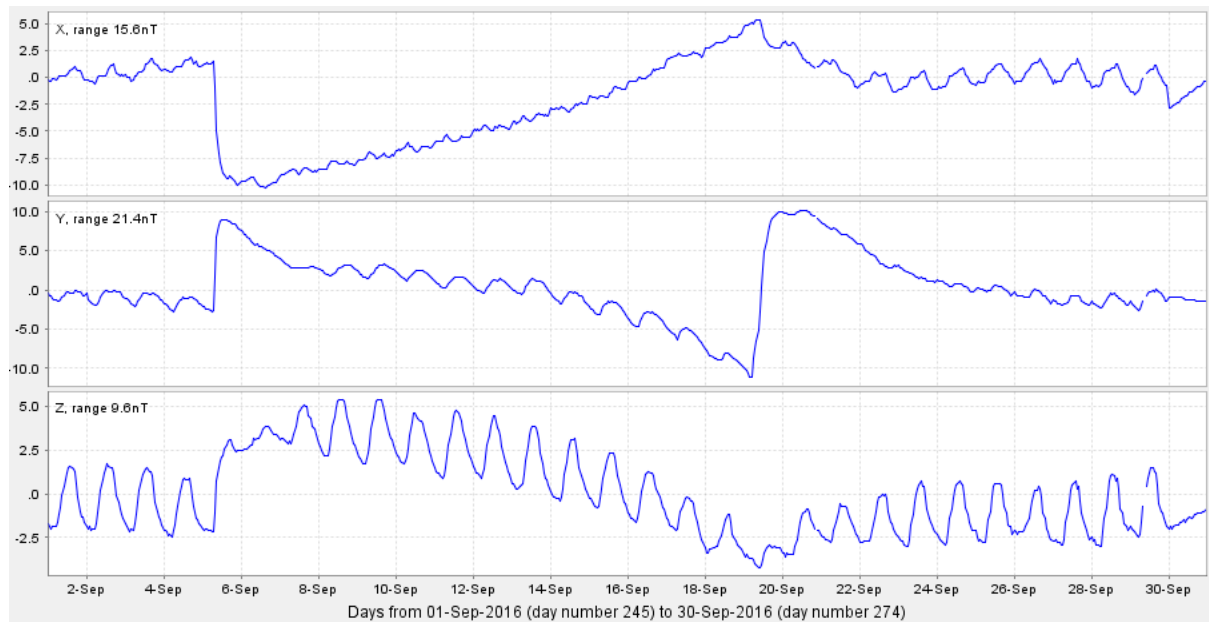
Figure 2.9 Difference between LEMI and dIdD hourly mean values in September 2016. The difference plot is created using IMCDVIEW software.

Further quality control is possible on the basis of certain special conditions existing at an observatory. If the observatory operates a scalar magnetometer independently, then the scalar baseline (*S*) and Delta *F* (Δ*F*) can be displayed as well. Δ*F* is the difference between the total field, calculated from the vector recordings and the total intensity recorded with the scalar magnetometer. The approximately constant diagram (Fig. 2.7a) or adapted blue dots around -3.4 nT (Fig. 2.7b) represents the offset between the *F* level at the position of the scalar magnetometer sensor and the position where the absolute measurements are carried out (absolute measurement pillar is the place to which all the observatory data refer). The equation for computing Δ*F* for a variometer orientated to measure components in *XYZ* is:

$$\Delta F = \left[(X_0 + \text{Var}_X)^2 + (Y_0 + \text{Var}_Y)^2 + (X_0 + \text{Var}_Z)^2\right]^{\frac{1}{2}} - (F_S + S), \qquad (2.1)$$

and for *HDZ* orientation:

$$\Delta F = \left[(H_0 + \text{Var}_H)^2 + (Z_0 + \text{Var}_Z)^2\right]^{\frac{1}{2}} - (F_S + S). \qquad (2.2)$$

Where:

H_0, X_0, Y_0, Z_0 – are baseline values for components *H*, *X*, *Y* and *Z*, respectively.

Var_H, Var_X, Var_Y, Var_Z – is the vector field component of the horizontal, north, east or vertical intensity recorded by the *H*, *X*, *Y* or *Z* sensor.

F_S – is the total field value recorded using a scalar magnetometer.

S – is the difference between the field value at the scalar sensor location and the field value at the absolute pillar.
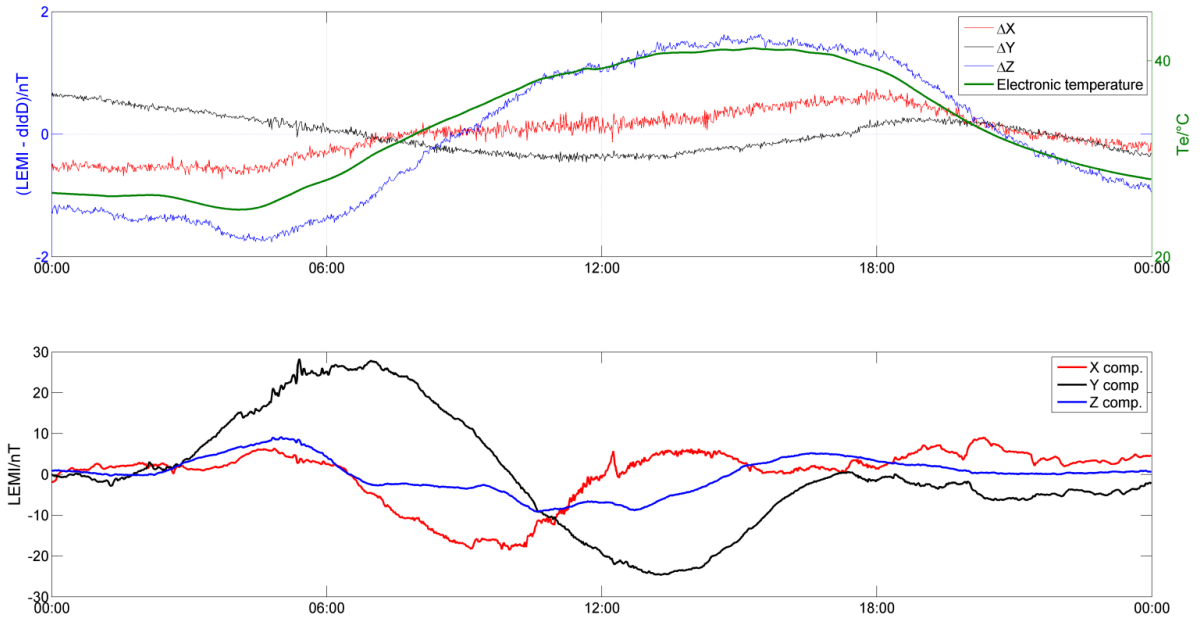
Figure 2.10 *Top*: Difference between LEMI and dIdD minute means on 21 June 2016. *Bottom*: Variations of the field components recorded by LEMI on 21 June 2016.

If there are problems in recordings at an observatory, the ΔF plot from minute, hourly and daily values is much more sensitive and can reveal problems not seen in individual data (minor magnetic contaminations are usually masked by natural geomagnetic variations). Jumps, spikes or drifts indicate problems of the baseline values, scale values, and internal or external magnetic perturbations. Spikes are caused mostly by external or internal perturbations. The length of the spike corresponds to

the time interval when any ferromagnetic material, for example, a vehicle, was placed too close to the variometer or when DC current has caused interference on the instrument.
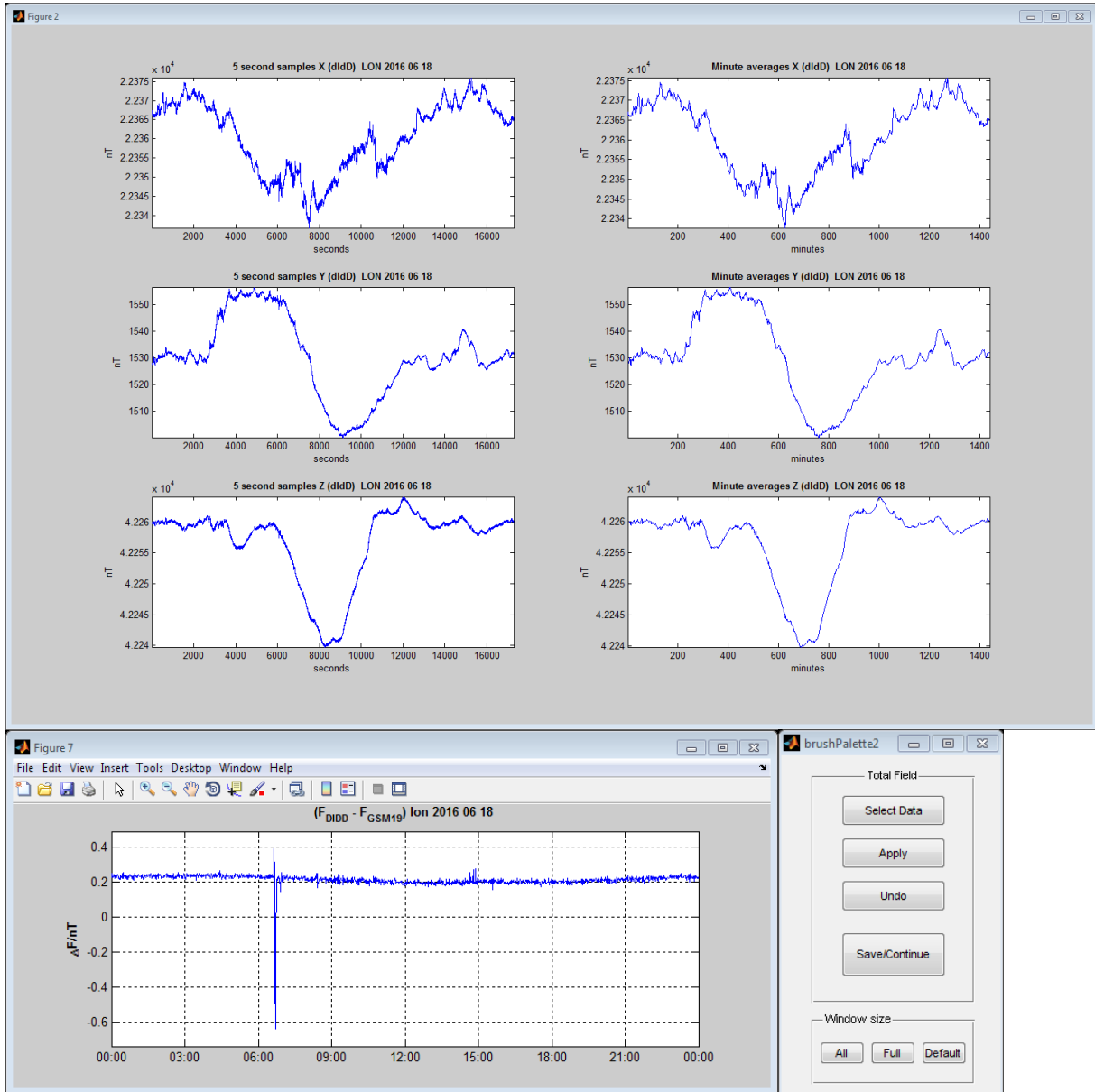
Figure 2.11 *Top*: Display of individual dIdD components on the day 18 June 2016 at LON. *Bottom*: ΔF plot, i.e. the total field difference between the vector dIdD and the scalar GSM-19 magnetometer. Diagrams are created in "Lonjsko Polje data processing and evaluation software."

Jumps or longer-term drifts in ΔF may indicate a baseline problem of the variometer. Figure 2.11 demonstrates how plots of individual components cannot reveal problems in observatory data. Degradations in magnetic recordings of a few nT or less will be masked by the natural magnetic short-term variations. However, the ΔF plot (Fig. 2.11) clearly reveals problems in LON data around 7 am. Although ΔF is a good indicator of problems in observatory data, with the single ΔF plot, we cannot detect which magnetometer has recorded the spike. Another scalar or vector magnetometer is required

to detect the instrument causing the problem. Instead of a third instrument, the data from neighbouring observatories can be used. Figure 2.12 shows additional ΔF plot (LEMI – GSM-19) obtained using LON supplement variometer. Apart from the diurnal variation, there are no spikes in the graph, and the spike (Fig. 2.11) may be uniquely ascribed to the dIdD recordings. One should note that in the dIdD case, ΔF cannot be used for detecting problems caused by longer-term drifts, because it is the vector magnetometer based on the scalar magnetometer. In general, for 3-component magnetometers, ΔF is calculated as the square-root of the sum of squares of the components. The sensitivity of the ΔF plot is dependent on the magnitude of the components aligned with the variometer sensor. For the *HDZ* orientated variometer errors on the *D* sensor are undetectable. If the variometer is orientated geographically (*XYZ*), the East component sensor (*Y*), due to its small value in comparison to both other components, contributes very little to ΔF at most locations of geomagnetic observatories. Further, note that ΔF cannot be used to detect drifts caused by purely mechanical movement of the sensor. This is demonstrated on Fig. 2.8, where yearly difference plot (LEMI-dIdD) reveals a quite share of uncorrected mechanical drift in individual components, which cannot be identified through the ΔF plot in Figs. 2.7a and 2.7b.
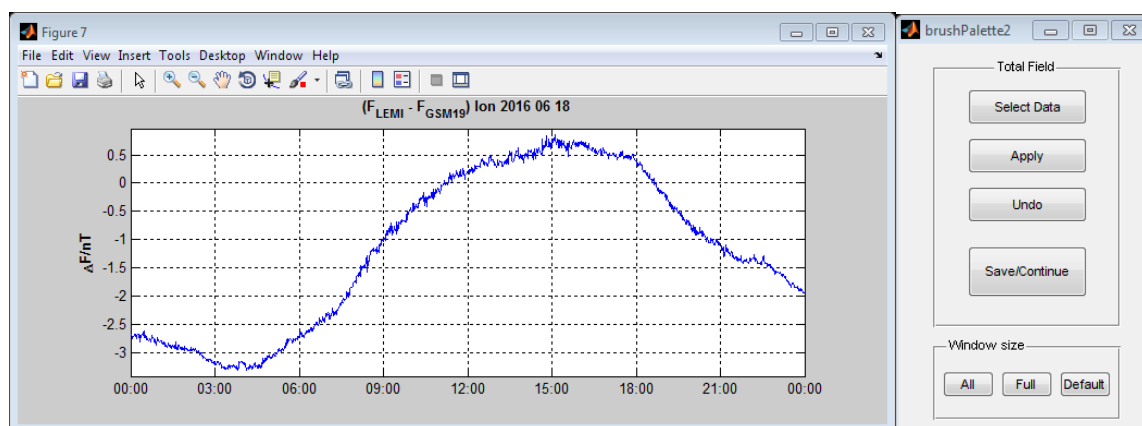
Figure 2.12 ΔF plot, i.e. the total field difference between the vector LEMI and the scalar GSM-19 magnetometer. Diagram is created in "Lonjsko Polje data processing and evaluation software."

If an observatory operates more than one variometer, an inter-comparison can be carried out to detect problems in single components. In Fig. 2.13, we may observe that the horizontal components are mostly affected by magnetic perturbation. Again, we see the sinusoidal drift caused by the temperature variation of LEMI electronic unit. A further example of the use of variometer inter-comparison is improving the baseline stability of LEMI recordings. Since the dIdD drift is slower and linear than the drift of LEMI, the baseline-corrected dIdD values can be used to compute baselines for LEMI magnetometer on a minute-by-minute basis.
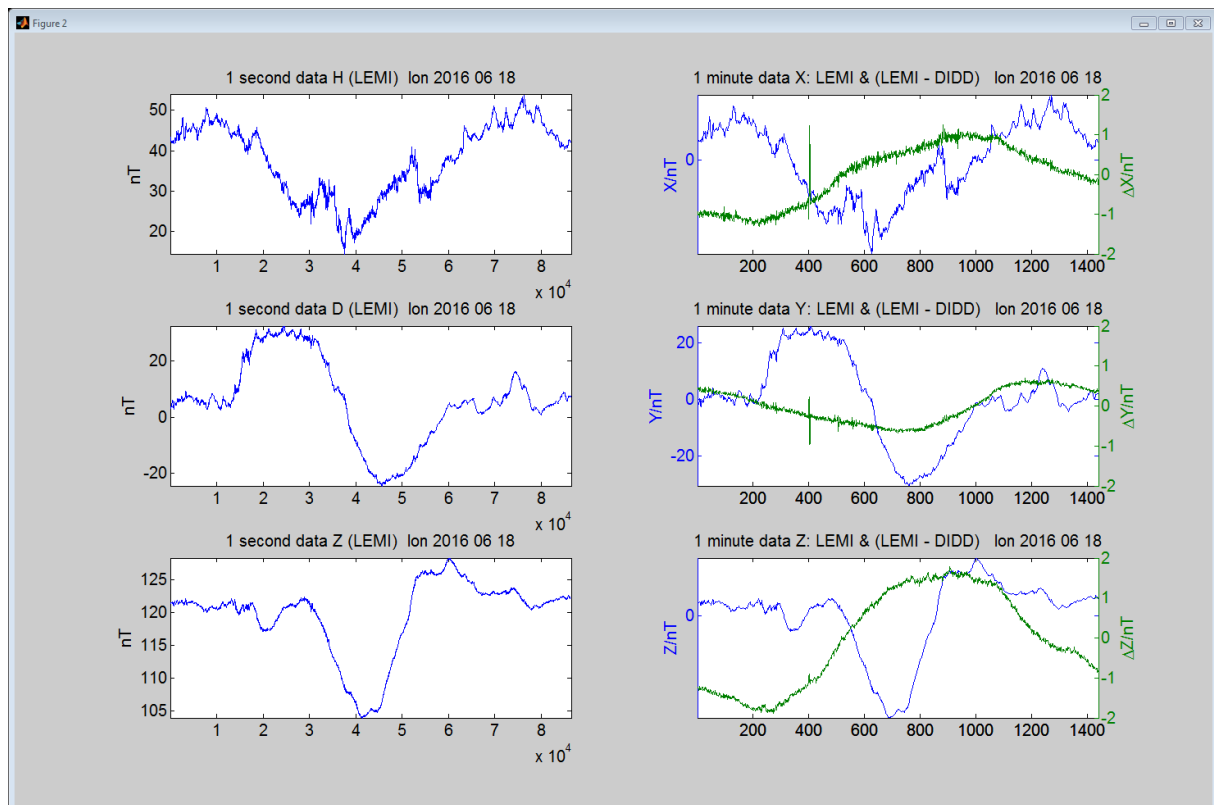
Figure 2.13 Display of individual LEMI components on the day 18 June 2016 at LON. Green lines on the graphs to the right show the difference between LEMI and dIdD recordings. Diagrams are created in "Lonjsko Polje data processing and evaluation software".
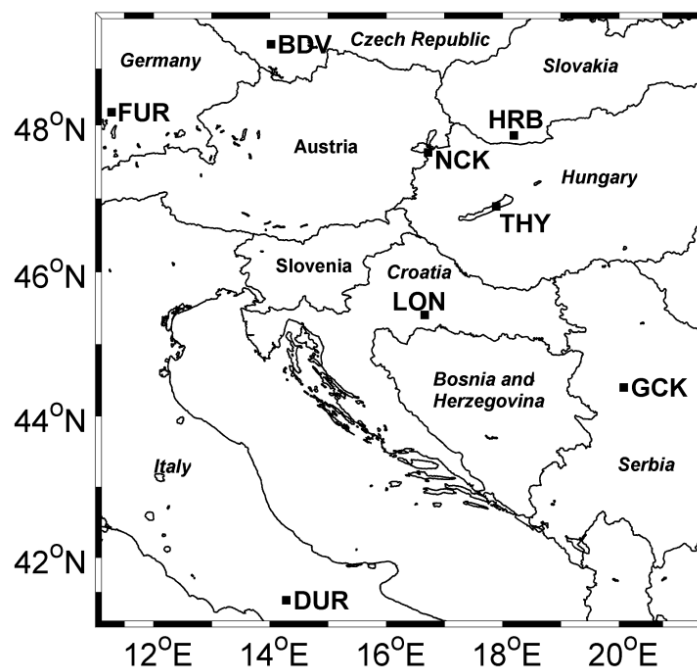
Figure 2.14 Positions of LON observatory and surrounding INTERMAGNET observatories Budkov (BDV), Fürstenfeldbruck (FUR), Grocka (GCK), Hurbanovo (HRB), Nagycenk (NCK), Tihany (THY) and Duronia (DUR).

A very fortunate situation exists if the observatory operates three variometers continuously. In that case, the instrument which causes the problem can be identified easily and uniquely. A further possibility of variometer inter-comparison is the check of data from one observatory by means of the data from neighbouring observatories. At LON, the final comparison (Fig. 2.15) of dIdD and LEMI data also includes data from three neighbouring observatories, as shown in Fig 2.14. Availability and quality of the data determines which observatories will be used. This way it is possible to uniquely detect problems in LON data even if one variometer system was out of operation. Due to differences in the diurnal variation of the magnetic field between different observatory locations, this type of plot cannot be used for checking the short-term stability of variometers, only jumps and spikes are detectible. Except the difference plot the rate of change *dB/dt* (Worthington et al. 2009) for LON and nearby observatories is also calculated and displayed.

After detecting problems in the data, by same or similar techniques that are described above, degradations should be corrected or removed. The presence of artificial disturbances and spikes is strictly forbidden and they have to be removed from the final data. In the case of larger data gaps, the time series from the main variometer should be complemented with the data from the backup variometer, if possible. All mentioned procedures should be done before publishing of the final definitive data.
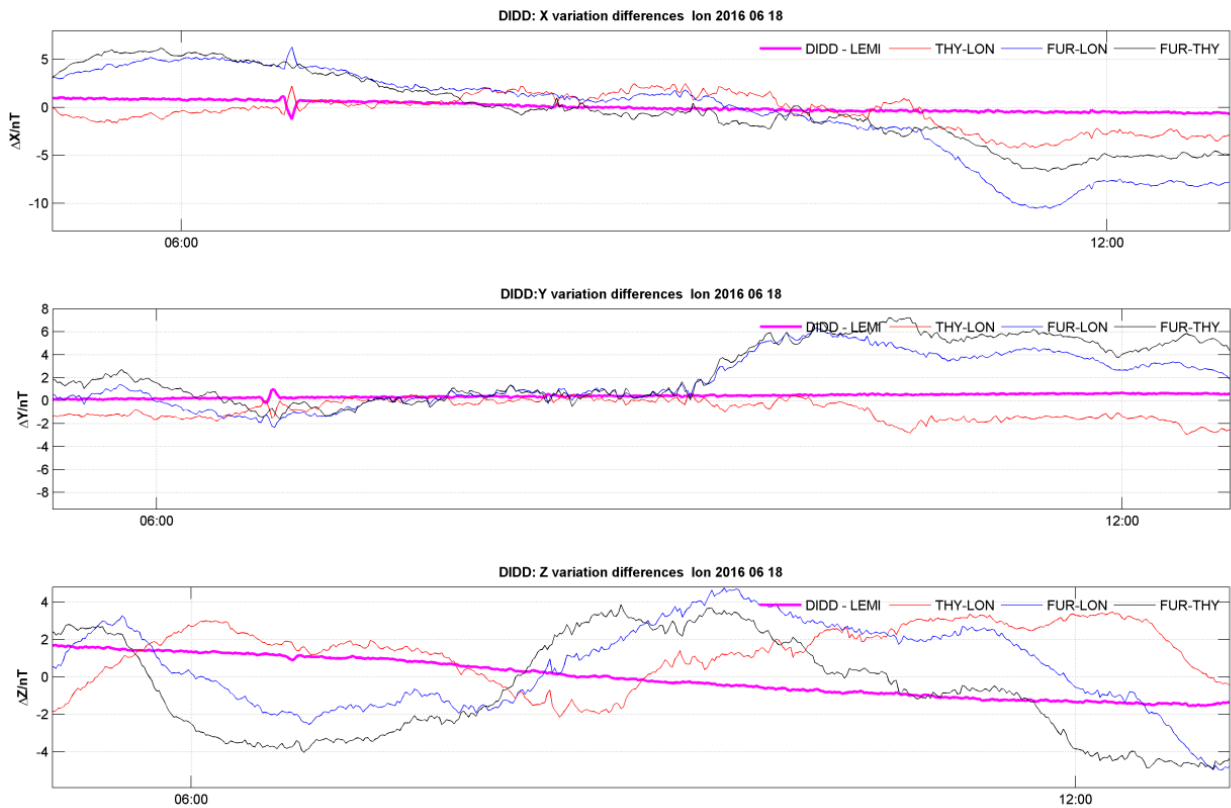
Figure 2.15 The difference plot between LON and nearby observatories on the day 18 June 2016. Figure is created in "Lonjsko Polje data processing and evaluation software."

2.4. The global observatory network and data types

Geomagnetic observatories have been the backbone of ground geomagnetic measurements for almost 200 years. As to be expected, the network has considerable gaps, the largest being on the southern hemisphere and in oceanic regions. The network is presented in Fig 2.16, with a distinction made for observatories which have attained certification from "International Real-time Magnetic Observatory Network" (INTERMAGNET, more details at www.intermagnet.org). INTERMAGNET is an international, voluntary organisation promoting high-quality standards for magnetic observatories and facilitating data distribution. Today, the INTERMAGNET consortium encompasses 63 institutes from 43 countries supporting 133 observatories. Several procedures help ensuring the highest quality for data produced by INTERMAGNET magnetic observatories (IMOs). Prior to its acceptance in the network, an observatory has to demonstrate compliance of its data with the standards set by INTERMAGNET. Once in the network, its definitive data are carefully reviewed by a committee of experts before publishing on a DVD and the organization's website. Also, the overall performance of each IMO is reviewed on a continuous basis. Another service provided by INTERMAGNET is distribution of preliminary data in near-real time on a single website. Data from each IMO are first transmitted to a Geomagnetic Information Node (GIN), either via the Internet or via satellites, then to the central website. There are currently six such nodes, two in Europe (Edinburgh and Paris), two in North America (Golden and Ottawa) and two in Japan (Hiraiso and Kyoto).

Since the establishment of INTERMAGNET in the late 1980s, IMOs have been reporting three types of magnetic data until recently: definitive and preliminary data. Definitive data are produced through processing, combining variometer data with auxiliary measurements of the absolute field direction and intensity to correct for variometer orientation and baseline drift (Section 2.2 and 2.3). Preliminary data comprise two types of data products: reported and adjusted data. Reported data are raw data of the geomagnetic field variation measured with the variometer and should be available within 3 days from acquisition. These data are only suitable for studies of the rapid field variations (and may contain spikes, gaps and discontinuities). Within 7 days from transmission, observatories are allowed to modify reported data to produce adjusted data by removing the spikes, filling the gaps or to modify baselines. However, adjusted data do not have sufficient absolute accuracy and are not free from drift. On the other hand definitive data required in particular for studies of secular variation and the geodynamo process in the Earth's core are reported only after the end of a calendar year with a time lag from several months up to more than a year. Unlike observatory data, fully calibrated data from satellites are available within a few days from acquisition.

To increase the usefulness of observatory data and fulfil the needs of the community for global modelling and other user groups, INTERMAGNET has defined the new type of "quasi-definitive" data (e.g. Clarke et al. 2013, Peltier and Chulliat 2010, Matzka 2013). Quasi-definitive data are

corrected with temporary baselines, should be close to expected definitive values and are delivered much sooner (1-3 months) than the final definitive data. The variation part of quasi-definitive data should have the same (or similar) quality as definitive data, i.e. without spikes or noise. Quasi-definitive data bridge the gap between preliminary and definitive data, and pave the way to a more efficient combination of ground observatory data and satellite, marine and airborne survey data.
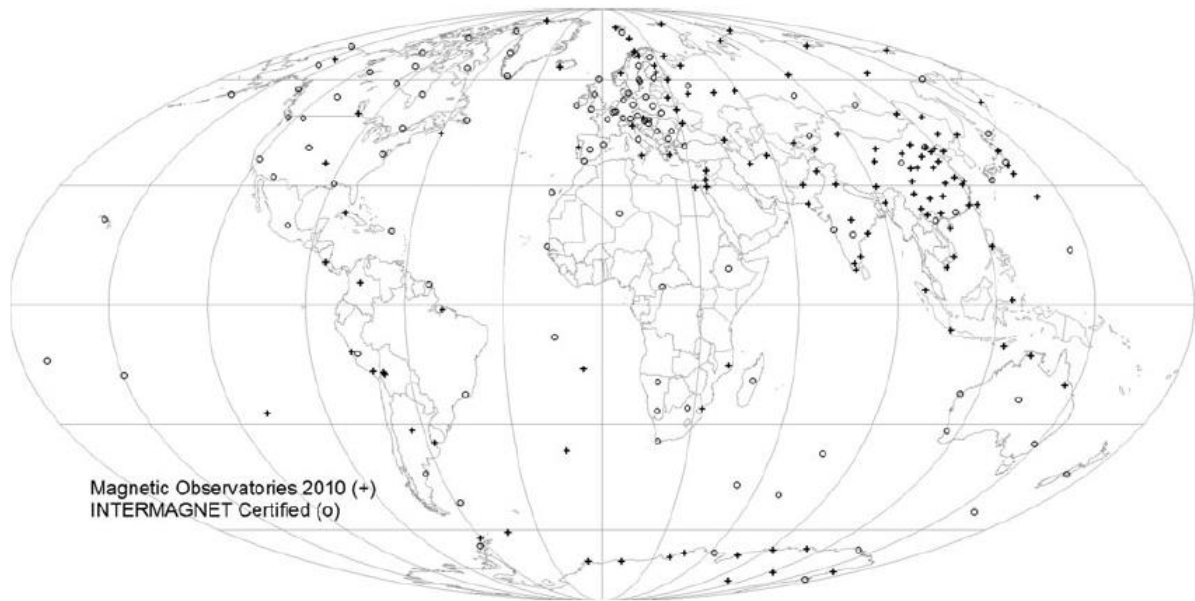
Figure 2.16 Global network of geomagnetic observatories in 2010 (taken from Rasson et al. 2011).

3. Proposed method for the baseline adaption

As already discussed in detail in Chapter 2, continuously recording vector magnetometers do not provide absolute field component values, but might be influenced by temperature variations, instable pillars or instrumental drifts. Although there have been several attempts to automate absolute observations (see Chapter 5), manual absolute observations are still mandatory at modern magnetic observatories to calibrate the continuous recordings and are usually done once a week. These observations are used in conjunction with the data from the variometer and an independent scalar magnetometer to derive observed base values. These values later serve for calculation, i.e. adapting of definitive baselines (DBLs) which are used to obtain absolute variometer data free from drift or environmental variations. Adapted values are derived by fitting, interpolation or hand scaling from the observed base values. Today, final baseline fitting is performed on an annual basis and data calibrated with these final baselines are labelled as definitive (D) data. The final D data should also be free from spikes, jumps and other degradations in continuous recordings. For details of preparation of the final observatory data see also Section 2.3 or Jankowski and Sucksdorff (1996).

Temporary quasi-definitive baselines (QDBLs) required for producing quasi-definitive (QD) data are estimated from all absolute measurement results available in the current year. Peltier and Chulliat (2010) proposed a method where QDBLs are calculated every month, shortly after the end of month M of year Y (noted M/Y hereafter). Calculation of temporary baseline is done using observations from 1st December of year Y-1 to the last day of M/Y. They use cubic smoothing splines with a constant smoothing parameter to obtain adapted baseline. Using this method, twelve quasi-definitive datasets are successively produced during year Y; each dataset replacing the previous one. The processing is very similar to that for producing definitive data, except that time interval for the baseline calculation is shorter. In a similar way in the BGS (British Geological Survey) method (Clarke et al. 2013) the continuous baselines are adapted using a series of piecewise polynomial fits, which are subjectively chosen. The BGS observatories also report their QD data in near-real time using baselines obtained by extrapolation. A projection into the future is based on the baselines on the day of computation. The extrapolation is usually constant (order 0), although account can be taken of any current increasing or

decreasing linear trends (order 1). In these cases, the annual baseline amplitude should not exceed 5 nT, and this also requires prompt processing of the variation data by observatory staff. Nowadays, despiked and magnetically clean variation data and other observatory products, like geomagnetic activity indices can be obtained relatively promptly, within several days from recording. Of course, this depends on the available observatory staff, amount and complexity of the encountered problems in the data, and efficiency of processing protocols. The same is true for the absolute control of data, only on longer time scales. Human intervention is essential for the absolute control of observatory data. This includes manual absolute observations, retyping and processing of the observational results, quality checks and validation of results, decisions during baseline calculation etc., both for temporary QDBLs and for DBLs. Nowadays, the timescales for production of QD and D data correspond to 1-3 months and more than a year, respectively.

Today, most observatories use parametric (e.g. polynomial) or semi-parametric (e.g. smoothing splines) fits in the global domain, i.e. on an annual basis to derive DBLs. Similarly stands also for QDBLs, except that the time interval is shorter and it is constantly increasing throughout a year. Obtaining baselines (QDBL and DBL) in such manner has some disadvantages: 1) A full year of observed values has to be collected before calculating DBLs; 2) In the case of parametric fits, the convergence of temporary QDBLs toward the DBL is slow, i.e. the overlap between cumulative QDBLs and the DBL might not be good. The same is true for semi-parametric fits in the case when the distribution of observed values is non-uniform or the smoothing parameter of the spline functions is changed as the observational dataset is updated. This means that we need to have good baseline stability (i.e. high quality observatory infrastructure) in order to produce high quality QD data. In general, global fits are good for estimating general trends in the observational dataset. On the other hand, if we have rapid trending of samples during a short period of time (for example, due to temporary problems with the mechanical stability of the variometer sensor), global fits may not be the appropriate tool to fit these short-term variations without affecting the baseline quality in other parts of the domain. Increasing the polynomial degree or flexibility of smoothing splines, to track samples when the baseline varies more rapidly, can cause "overfitting" or artificial variations in other parts of the domain, particularly in parts where observations are sparse (an example is given in Section 2.2).

In the next section of this thesis, a new method for the baseline modelling is proposed. The proposed method uses the advantage of a modelling within fixed time frames. This enables production of the final D data within the timespan less than a year and many of abovementioned problems that can occur with fits on an annual basis can be avoided. The method is based on assumption that it is enough to collect a reasonable number of observed values during some period that enable us to do an accurate local fit and determine DBL for that period. With absolute sampling performed (usually) once per week, we can collect enough samples within a few months to calculate one piece of DBL within a year. By constructing piecewise continuous fits, with smooth transitions on the edges of these pieces

(windows), we are effectively constructing DBL by pieces. The advantage of the piecewise fitting is that observations in the future will not affect the shape of a baseline in the past, which is clearly justified from a physical point of view. Observed base values reflect the instrument response in the current environmental conditions, and they are in fact independent from those in the future. We only need a reasonable number of good quality observations for some period of time to obtain a correct estimation of the baseline trend for days without observations. Correct approximation of samples in the periods when the baseline varies more rapidly, and avoiding overfitting when we have good baseline stability are further advantages of the piecewise fitting.

The developed routine can determine the "best fit" as candidate for QDBL and DBL without human intervention, although it is emphasized that QDBL or DBL should always be reviewed by experienced observatory staff. In the next chapters it will be shown that the proposed method gives high quality results in nearly automatic manner. Thus, it can find its applicability in continuous baseline fitting when automated absolute instruments (Gonsette et al. 2013, Korte et al. 2013, Poncelet et. al. 2017) become supplemental or standard observatory equipment. The increase in the number of automatically collected observations (let say every 30 min, Gonsette *et al.* 2013), will require a routine robust to outliers because the automatic instruments show a larger scatter than the standard DI-flux measurements.

3.1. Method

Motivated by the work of Peltier and Chulliat (2010) and their results it was decided to design a routine based on cubic smoothing splines (De Boor 1978). The aforementioned authors tested their method for producing QDBLs on nine IPGP (Institut de Physique du Globe de Paris) observatories (AAE, BOX, CLF, KOU, LZH, MBO, PHU, PPT, TAM) for the year 2008, and showed that the production of accurate QD data is possible even in cases where baselines vary more rapidly throughout a year. The differences between definitive and temporary baselines, calculated after the end of each month, were within a fraction of nT. However, the obtained results might be too promising and unrealistic. The authors determined an optimal smoothing parameter for the dataset on an annual basis. They then simulated the production of QDBLs in retroactive manner with *a priori* known optimal smoothing parameter (see Peltier and Chulliat 2010, for details). In reality, in most cases, the optimal smoothing parameter cannot be known in advance and in many cases simple smoothing splines will not give satisfactory results. This will be demonstrated in the next subsection.

To obtain high quality baselines in an automatic manner, cubic smoothing splines are used in conjunction with additional constraints. Firstly, a baseline pieces (inside windows) were calculated. It

was empirically determined that a length of eight observational days ($L = 8$) to be a good choice in most cases (one observational day can have several observation sets). Depending on the observation frequency the time span of a window may vary from a week up to several months depending on the observatory. Additionally, samples from two ($d = 2$) observation days before and after the window are used for calculation of a baseline within the window. This alleviates edge effects between neighbouring baseline segments. The baseline within a window is a cubic smoothing spline function $f(t)$ that minimizes the expression

$$p\sum_{i=1}^{n} w_i (y_i - f_i)^2 \quad + \quad (1-p)\int_a^b \{f''(t)\}^2 \, dt, \tag{3.1}$$

where $f_i = f(t_i)$ are values of the baseline $f(t)$ at the observation times t_i, $f''(t)$ stands for the second derivative. In the integral expression, a and b are the limits of the extended window containing $L + 2d$ observations. Observations are denoted with y_i and w_i are corresponding weights. The smoothing parameter $p \in [0,1]$ controls the smoothness of $f(t)$. For higher values of p the baseline will be closer to the observations. In the case $p = 0$, the baseline will be a straight line and for $p = 1$, the interpolating baseline will pass exactly through the data points. To obtain weights, estimation of a preliminary baseline $\tilde{f}(t)$ is performed with assumption that all observations have weights equal to 1. Then, using the residuals $y_i - \tilde{f}_i$, the weights are estimated according to the most frequent value (Steiner 1988). This way, relatively flexible baseline segments (high values of p) are robust to bigger outliers or low-quality observations. Determination of the optimal smoothing parameter is performed automatically according to relation (De Boor 2003)

$$p = 1/(1 + h^3 / c), \tag{3.2}$$

where h is the average sampling, i.e. average period between observation days. The current version of the program assumes the same coefficient c for three vector components, while the scalar c may be the same or different. Coefficient c is varied in the range from 10^{-3} up to 10^2, and for each c (vector and scalar) baselines are calculated.

In order to determine the suitable value for c and check the quality of the determined baselines, the so-called Delta F (ΔF) values are calculated. ΔF represents the difference between the total field intensity obtained from vector and independent scalar magnetometers (Section 2.1). Here, the scalar total field is corrected for the field difference between the sensor site and the absolute pier (for details see Section 2.3). The best c corresponds to the minimum value of ΔF. For this purpose the routine requires the variometer and scalar recordings in addition to the observations themselves. In case no scalar magnetometer data are available, it is not possible to perform the ΔF check and the default value of c

= 0.5 is used.

In some cases of IMOs, the annual long-term baseline drift is comparable or order of magnitude larger than random fluctuations of samples. On the other hand, some observatories have very frequent absolute observations (several sets, almost every day) in some time intervals. In this case, observations can show random fluctuations, which are not expected in the nature of the underlying baseline. Note also that p increases with the decrease of h (frequent observations). According to eq. (3.1), this means the baseline will attempt to follow the same random fluctuations by remaining close to the observations. Thus, in general, "smoothness" over "staying close to the data" is preferred. By choosing the default $c < 1$, the spline function is restrained to be smooth enough to capture the trend and not to follow random scattering or erroneous observations.

Once when piecewise baselines according to equation (3.1) are obtained, with several constraints as described above, the resulting baseline pieces will have similar (but not equal) values on the edges toward neighbouring windows. Thus, a final smoothing by a spline function with the default $c = 0.005$ for vector, and $c = 0.0005$ for scalar, is applied to piecewise baselines in order to obtain smooth transition on the edges of the windows for which the baselines are calculated. In this way, smooth, continuous baselines over the whole domain are obtained. Optionally, the final vector and scalar c can be set manually by the user. Except in the last window, the shape of a baseline obtained in this manner will not be affected as we add new observations.

Realignment or relocation of a magnetometer sensor (or some other reason) may result in discontinuities, i.e. jumps in the variometer or scalar baseline. Generally, the number of discontinuities may be different for the vector and scalar instrument. These discontinuities are usually known at the observatories and are marked with "d" in the INTERMAGNET baseline files. The marker "d" and originally reported baseline values are used to identify jumps and their magnitudes. The routine requires a reference list with times and values of discontinuities. For test purposes in this study, the list is created from the information provided in the INTERMAGNET baseline files. Observations are then corrected to a single reference level to obtain accurate estimations of the new adopted values. In the figures in supplemental materials (see sub-Appendix B1), discontinuities are denoted with green and magenta vertical lines for vector and scalar components, respectively.

3.2. Special cases: data gaps and disagreeing intensity in scalar baselines

The BOX example from Peltier and Chulliat (2010) was chosen to demonstrate how non-uniformity of sampling and assumption of an *a priori* "known" smoothing parameter could introduce artificial baseline variation that is not supported by samples. In Fig. 3.1, only the horizontal (*H*) and vertical (*Z*)

baseline components are displayed, together with ΔF. Original baselines and ΔF (reported on the INTERMAGNET DVD) are obtained taking into account all observations. Now, let us imagine that the observations were not possible during spring due to some operational problems (e.g. the observatory location was unreachable for some reason or problems occurred with the DI-flux magnetometer). The results obtained under the assumption that some observations in spring are missing with the IPGP and the newly proposed method are presented by blue and black lines, respectively. Vertical grey lines designate the automatically defined windows in the proposed method (Section 3.1). The IPGP and original baselines overlap perfectly everywhere except in the third window. Clearly we can see that the IPGP method gives a more erroneous estimation of the baseline than the new method, if observations in spring are omitted. The initially chosen smoothing parameter in the IPGP method will no longer be a good choice since the smoothing splines in the BOX case are quite flexible and we have no samples in spring to restrain the spline wiggling. The new baselines give more reasonable values due to several constraints that are described in Section 3.1. On the other hand, Fig. 3.1 shows somewhat smoother baselines obtained with the new method during November and December. Too smooth values of the new baselines are caused by the missing information about the total field difference between the scalar sensor and absolute (i.e. reference) site. Prior to 2009, observatories did not report this information about scalar baselines. In addition, there is no information about ΔF in December, i.e. data from the scalar magnetometer are missing. Thus, the proposed baselines in the last two windows were obtained without any information about the scalar baseline and ΔF in December.
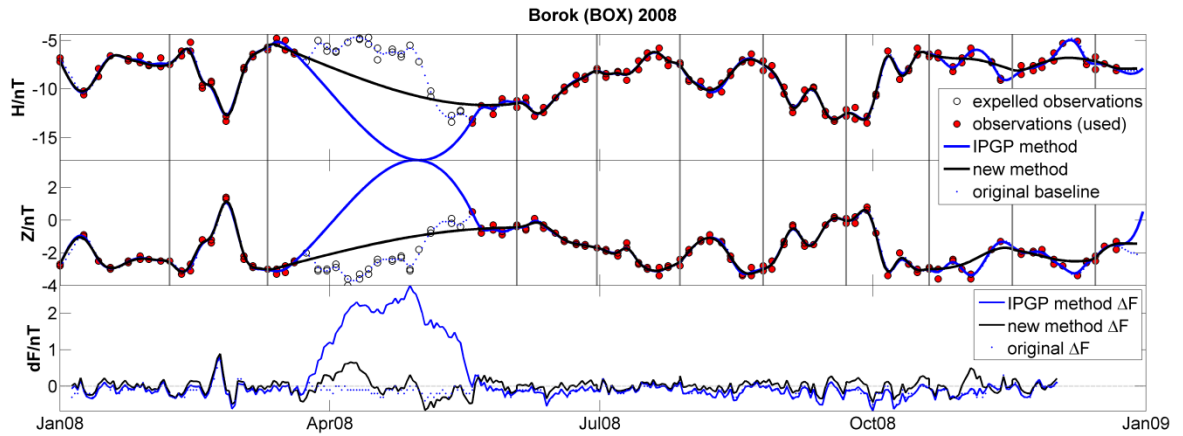
Figure 3.1 Baselines calculated with the IPGP and new method (default settings) under the assumption that observations from spring (white circles) are missing. Original baselines and ΔF (blue dotted line) were obtained by taking all observations (red and white circles).

In many cases, the scalar baseline has the greatest impact on the ΔF residual, and sometimes the baseline obtained from scalar samples cannot properly reduce the total field recordings from scalar magnetometer to the reference site. Although scalar magnetometers in general are absolute

instruments, a potentially time-varying baseline results come from the fact that vector, scalar and absolute observations are carried out at different sites. All measurements in the end are referred to the same reference site. The difference between values at the site of the scalar instrument and the reference site determines the scalar baseline. As demonstrated in Fig. 3.2 ("*S*" diagram) in the case of the reported data we have an obvious degradation in ΔF in this example. (IMOs in Figs 3.2. to 3.4b and also in Appendix B are left as anonymous.) The main reason is the presence of a constant offset (approximately -0.5 nT) in the reported scalar baseline. For additional examples of disagreeing intensities in scalar baselines, see supplemental figures (sub-Appendix B2). I presume the presence of the offset in scalar samples in Fig. 3.2 is a consequence of erroneous or outdated information about the field difference between the scalar and reference site in the protocol for processing absolute observations. Generally speaking, the representativeness (offset, variability and scattering) of the scalar samples also depends on the magnetic homogeneity of the observatory site. We need to keep in mind that recordings and observations in the observatory are performed at three different sites. The gradiometer difference and its variation over a certain time, between the reference and scalar site should be as small as possible. The same is true for the difference between the variometer and scalar site. Also, scalar and vector recordings during absolute observations must be free from spikes and the differences between natural short-term variations at all observatory sites should be negligible. These are basic prerequisites for obtaining quality base values and a proper reduction of the variometer and scalar data to the reference site.
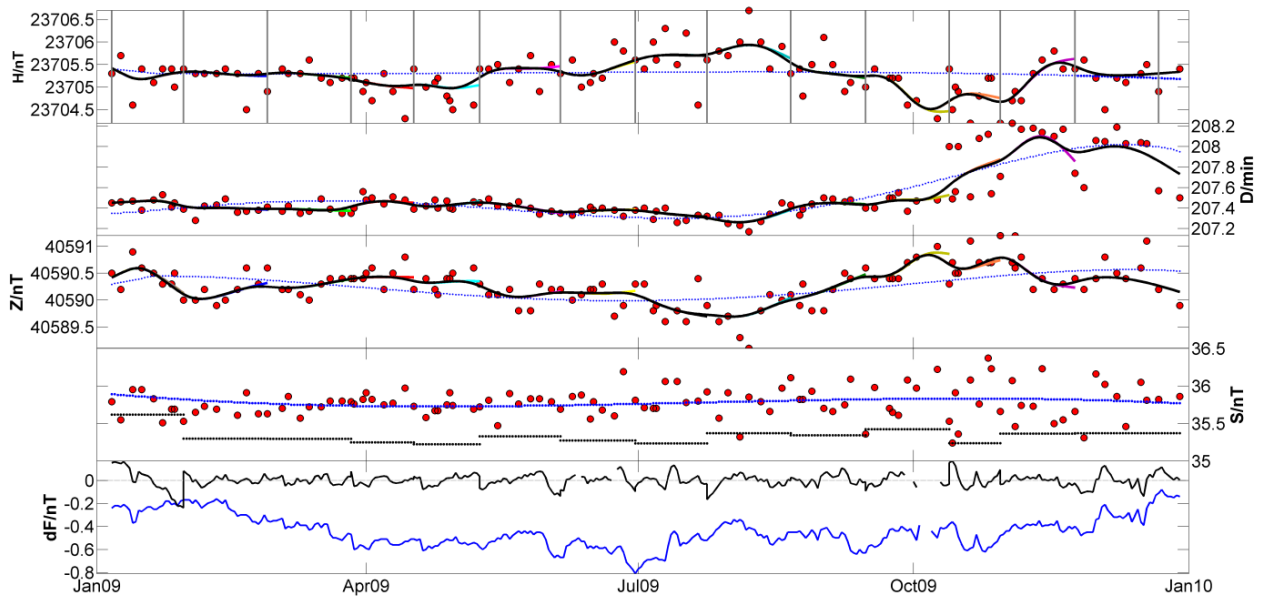
Figure 3.2 Vector baselines obtained with the new method (black line) and original baselines (blue dotted line). Scalar baseline obtained with the new method is displayed by black dotted lines and original by blue dotted line. Observations are denoted with red circles. Original ΔF (blue line) corresponds to original baselines (blue dotted lines).

In situations when we have disagreeing intensity in the scalar baseline (i.e. offset in ΔF) or increased scattering of S samples, the new method estimates the S baseline as a de-trended value of ΔF obtained in the iterative manner described in Section 3.1 under the initial assumption that S baseline is zero. The baseline obtained in this way is shown by black dotted lines in Fig. 3.2 ("S" diagram). Each piecewise constant segment of the annual baseline is estimated for each of the windows shown in the "H" diagram (Fig. 3.2, grey vertical lines). At many observatories, the number of scalar samples is significantly smaller than the number of vector samples, in some periods or during a whole year. In case there is no information on the scalar baseline or there are less than 3 samples necessary for spline calculation within the window, the routine assumes that the scalar baseline is a constant. This assumption is also valid if ΔF, calculated using the spline scalar baseline, obtained from scattered S samples, is larger than ΔF obtained with a constant scalar baseline. Furthermore, if we obtain discontinuities larger than 0.5 nT between piecewise constant scalar baselines, then these constant baselines are smoothed by a final spline with default $c = 0.0005$ (see Section 2.1) to avoid sudden jumps in F from the independent scalar instrument. An example of a small jump (< 0.5 nT) can be seen in Fig. 3.2 in ΔF and S (on the edge of the first and second window). In Fig. 3.3 ("S" diagram), we can see preliminary piecewise constant baselines (coloured dotted lines). The final adopted baseline obtained by smoothing the constant baseline segments is represented by a black dotted line.
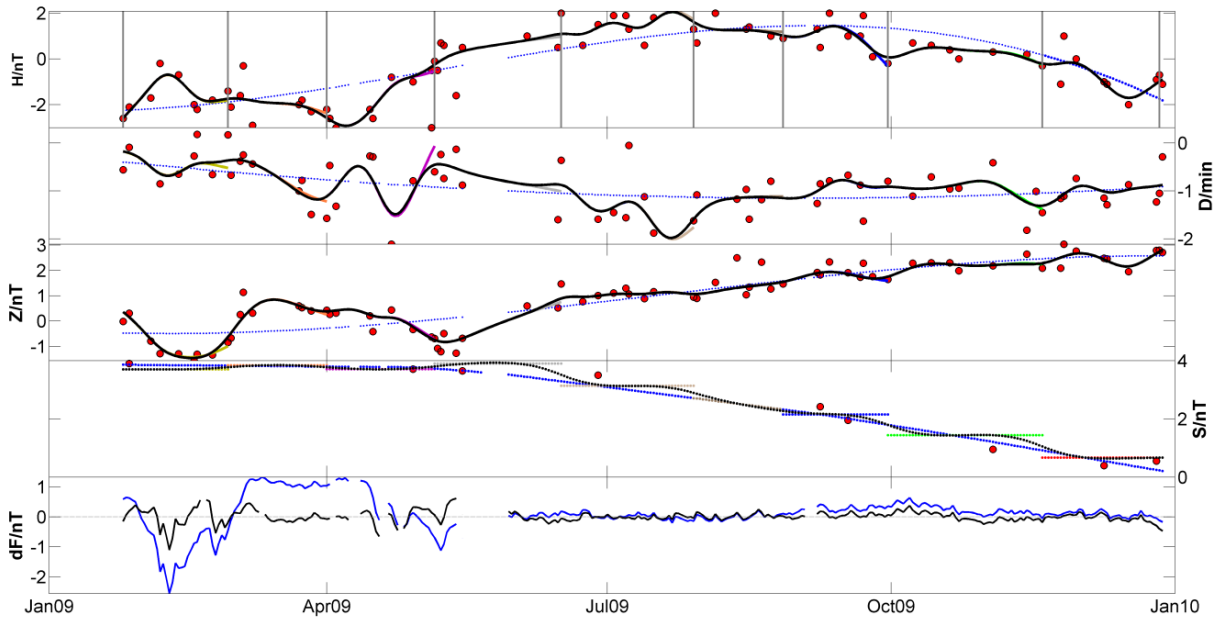
Figure 3.3 Vector baselines obtained with the new method (black line) and original baselines (blue dotted line). Scalar baseline obtained with the new method (black dotted line) and original baseline (blue dotted line). The new temporary scalar baselines (within windows) are displayed by coloured constant lines. Observations are denoted with red dots. Original Delta F (blue line) corresponds to original baselines.

Looking at the fit of the vector baselines in Figs 3.2 and 3.3, we see that new baselines capture the trend of the samples much better than the original baselines. This is especially pronounced in the Z

component in Fig. 3.3. In the first half of the year, the originally adopted values could not completely compensate a drift in the Z component. Consequently, the ΔF residuals are increased in this period. Note that, in this period, the original and new values of the scalar baseline are practically identical. In Fig. 3.2, we see a long-term drift throughout the whole year in addition to a constant offset in the original ΔF. The reported baselines in this case also underestimate the baseline trends indicated by samples in H and Z.

3.3. Manual adjustment and quasi-definitive baselines

A single computational method may not be appropriate to handle all different dataset types and in some cases might not give satisfactory results. This could occur especially in cases where we have a relatively small number or different numbers of samples in each component, non-uniform sampling, sudden discontinuities and when every dataset has its own characteristics (like trends, amplitudes and sampling quality). All these are potential features of observational datasets obtained from standard absolute measurements in geomagnetic observatories. Testing the new routine for all IMOs showed that, in some cases, improved results were obtained with manual adjustments of the automated procedure following visual inspection of the data and calculated baselines. This is done by manual adjustment of L and d parameters (see Section 3.1), or by adjustment of the smoothing parameter of the final spline which is used to join sub-splines within windows. This procedure is demonstrated in Figs 3.4a and 3.4b. Results obtained with default settings are presented in Fig. 3.4a. In this case the new baselines are not flexible enough to fit rapid baseline variability at the start of the year. This clearly leads to degradation in ΔF.

By manual increase of coefficient c in relation (3.2) of the final spline that smooths the baselines within individual windows, a more flexible baseline will be obtained. This is illustrated in Fig. 3.4b. With this minor intervention (L and d were not changed), significantly better results were obtained.

In Figs. 3.2, 3.3, 3.4a and 3.4b, the new temporary QDBLs (coloured lines) are simultaneously plotted under DBL. However, due to practically perfect overlapping between cumulative QDBLs and the final baseline, only small segments of QDBLs are visible in Figs. 3.2 and 3.3. A fraction of QDBLs, barely noticeable, can be seen on the right edges of some windows. For example, in Fig. 3.2 near the edge of the eleventh window, part of the vector QDBLs (orange line) are noticeable, which are slightly different from final DBLs calculated from all observations in the year. Similarly, in Fig. 3.3 this can be seen in declination (D) near the edge of the third window. The residuals between QDBL and DBL (QD_{RSD}) are plotted separately in Figs. 3.4a and 3.4b for better visibility. Here we see that small differences between QDBL and DBL exist only near the right edge of a window. If we denote the

number of windows with *N*, then we have perfect overlapping QDBLs with DBL within all windows from *1* to *N-1*, i.e. QD_{RSD} are exactly zero. This means that DBLs are calculated within all windows, from first up to *N-1*. Only near the right edge of the *N-th* window, small differences exist and until we define the *N+1*, window the baseline is labelled as QD. Generally, for all observatories used in this study, these small differences are within fractions of a nT.
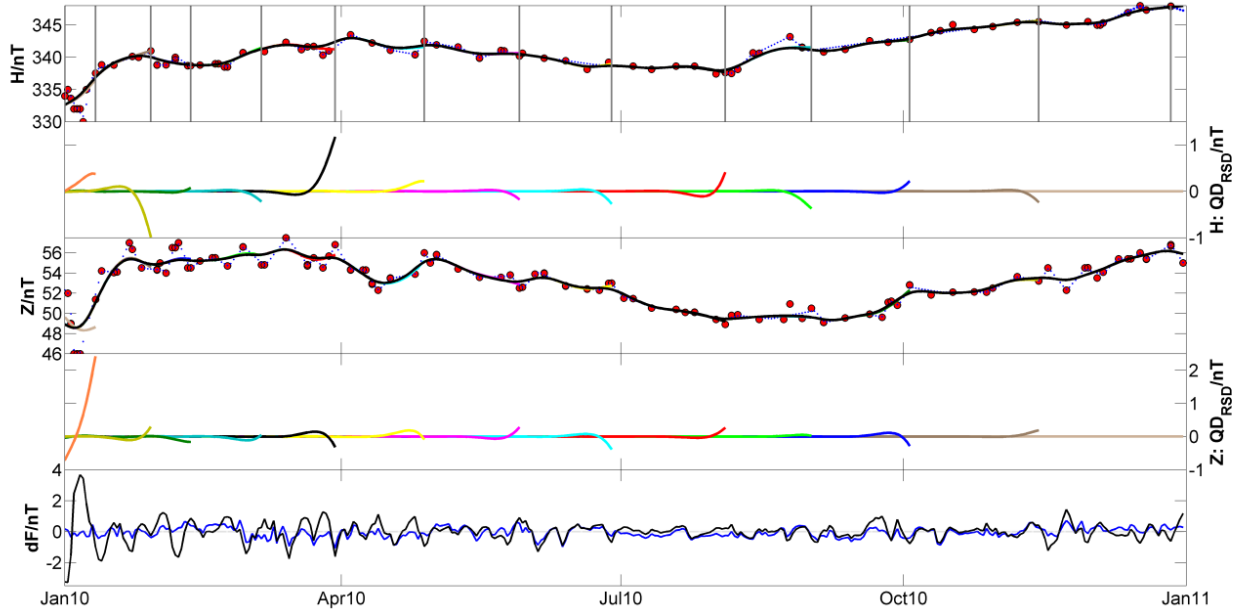
Figure 3.4a *H* and *Z* baselines obtained with the new method (black lines) and original baselines (blue dotted lines). Residuals between QDBLs and DBLs are shown with coloured lines. Observations are denoted with red dots. Original Δ*F* (blue line) corresponds to original baselines.
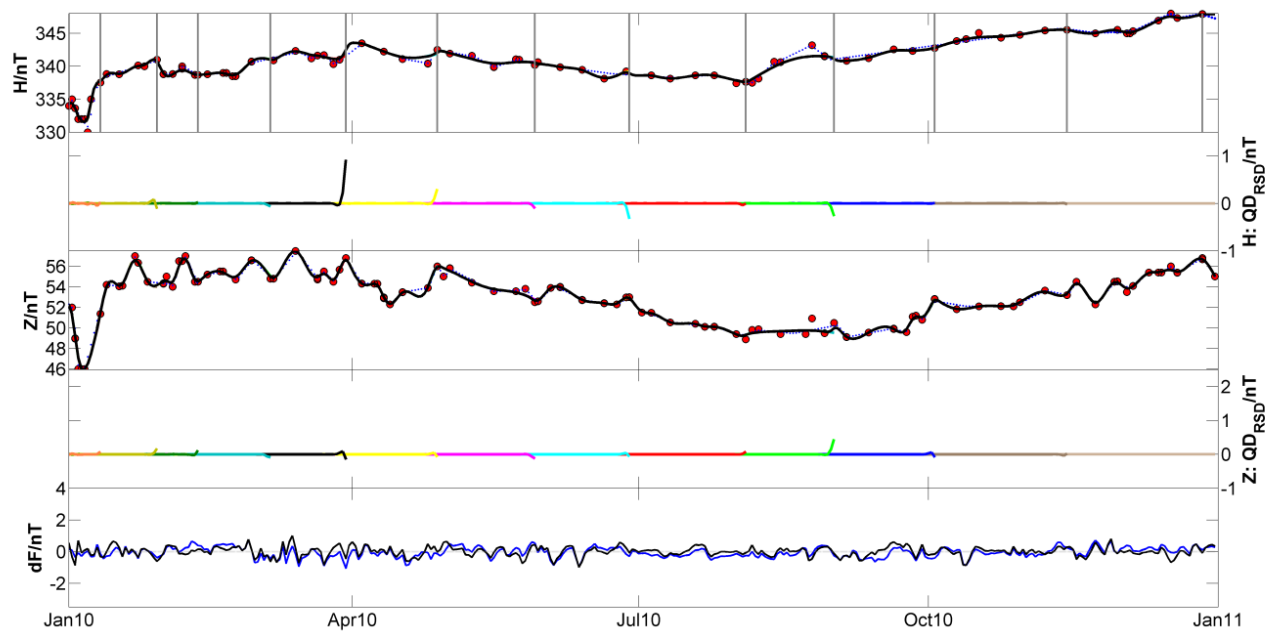
Figure 3.4b Same as Fig. 3.4a only the new *H* and *Z* baselines are obtained with manual adjustment. Results are presented with the same ordinate scaling as used in Fig. 3.4a.

4. Verification of the proposed method

4.1. Data selection and statistical analysis of results

To compare the obtained baseline calibration results with those reported by IMOs, the data in the period 2009-2011 were used. This period was chosen because calibration data from the independent scalar magnetometer were not available before 2009. Also during the preparation of this thesis the last available INTERMAGNET DVD was published for 2011. In this period, only data from observatories that report ΔF results have been used. This way, it is possible to estimate the adoption quality according to the ΔF check. The overall number of observatories that reported ΔF in this three-year period is 255.

In Chapter 3 only a few examples of the 255 analysed cases have been presented. To show all results in summarized form, some statistics are presented further herein.

To obtain an idea about the goodness of fit with the new and reported DBLs, squared correlation coefficients (R^2) between observed and adopted values have been calculated and used for this purpose. Table 4.1 shows results of examples presented in Figs 3.2, 3.3, 3.4a and 3.4b. From the numerical values in Table 4.1 and from the plotted results, we can see that R^2s are quite good indicators of the goodness of fit. Also, the maximal absolute residuals ($max|RSD|$) and the average absolute residuals ($avg|RSD|$) between the new and reported baselines were then determined on a yearly basis. This was done for each of the 255 cases, for vector and scalar baselines and ΔF residuals. We have rejected 5 cases, where $max|RSD|$ and $avg|RSD|$ were outside two standard deviations from the average results. In all rejected cases, the new baselines gave better results in ΔF and according squared correlation coefficients between observed and adopted values as a measure of the fit. The remaining residuals are sorted into 0.5 nT bins and presented in the form of histograms.

A similar analysis was done for the new, cumulative temporary baselines (i.e. QDBLs) within a year. Here, the residuals (QD_{RSD}) were determined only with respect to the new DBL. In the QD case, only the maximal absolute residuals within windows are determined ($max|RSD_{QD}^i|$), where $i = 1, \ldots, N$ and

N is the number of windows. The maximal ($max(max|RSD_{QD}^i|)$) and average ($avg(max|RSD_{QD}^i|)$)

values from all windows within a year were then determined. By considering only $max|RSD_{QD}^i|$,

periods of perfect overlapping among the new QDBL and DBL (Figs 3.4a and b, residual diagrams)
have been excluded. Otherwise, we would obtain unreasonably small residuals (less than 0.01 nT), i.e.
much smaller than the achievable absolute accuracy of the baseline calibration procedure. Residuals
between the new QDBLs and reported DBLs were not calculated separately. These residuals
correspond approximately to residuals between the new DBLs and reported DBLs. In other words,
$avg|RSD_{QD}^i|$ are much smaller than $max|RSD|$ and $avg|RSD|$.

Table 4.1

Squared correlation coefficients (R^2) between observed and adopted values presented in Figs. 3.2, 3.3, 3.4a and
3.4b. Four coefficients ($R_1^2,... R_4^2$) correspond to three vector and one scalar component. R_2^2 and R_4^2 are not
given for Figs. 3.4a and 3.4b because examples of these plots are not shown there.

case/comp.	DBL type	R_1^2	R_2^2	R_3^2	R_4^2
Fig. 3.2	reported DBL	0.036	0.643	0.261	0.001
	new DBL	0.450	0.724	0.653	0.003
Fig. 3.3	reported DBL	0.674	0.198	0.787	0.978
	new DBL	0.869	0.526	0.943	0.972
Figs 3.4a and 3.4b	reported DBL	0,990	-	0.990	-
	new DBL	0.949	-	0.899	-
	new manual DBL	0.986	-	0.990	-

4.2. Results and discussion

In Fig. 4.1, (upper panels) the maximum and average absolute ΔF values are presented. New
baselines, automatically calculated, with default settings are displayed with black histograms. Results
of originally reported ΔF are presented with white histograms. We clearly see that new baselines in
general give slightly better results according to the ΔF check. However, it should be emphasized that,

in some individual cases, human intervention is crucial for improving the baseline fit. Minor manual adjustments were done in 46 cases (i.e. 18 %) for this purpose, based on visual inspection. After re-calculation of baselines, small improvements can be seen in ΔF (Fig. 4.1, grey histograms). More significant improvements in trends of the new baselines obtained by manual adjustment are noticeable in the supplemental figures (sub-Appendix B3).
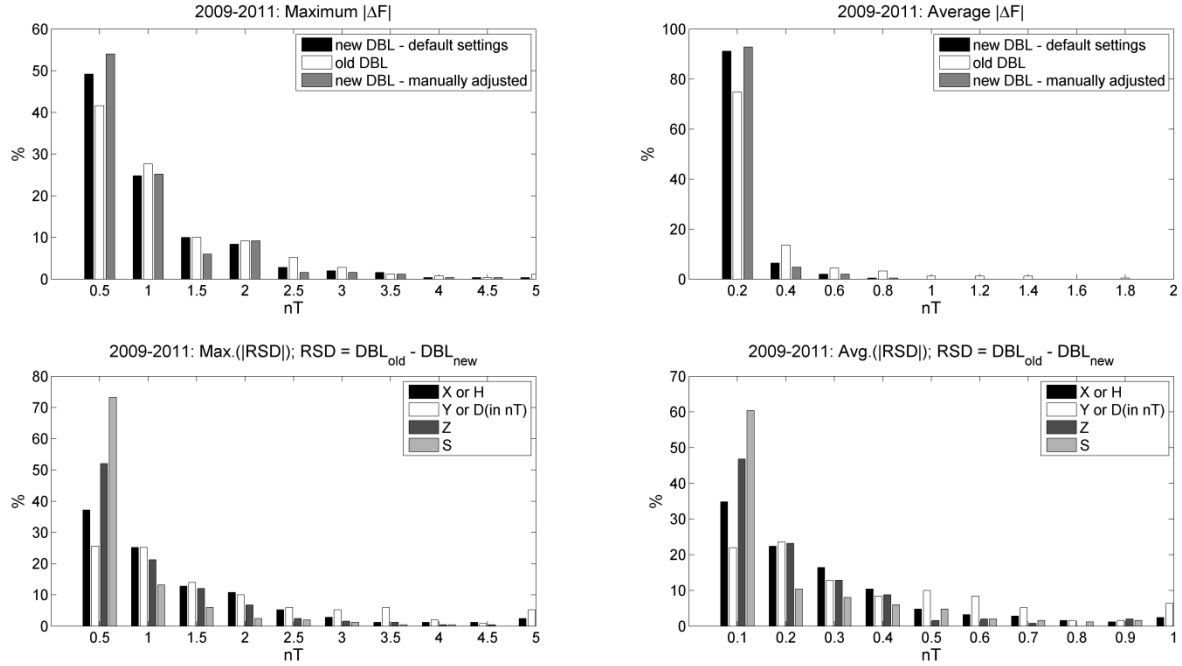
Figure 4.1 Upper panels: Histograms of the absolute maximum and average absolute ΔF. Lower panels: Residuals between the new DBL (without manual adjustment) and reported DBL for three vector and the scalar component.

Histograms of differences between the new DBLs obtained in automatic manner, and reported DBLs show that $max|RSD|$ are within 1 nT and $avg|RSD|$ are within 0.2 nT in approximately 80 % of the cases. The largest residuals are obtained in the Y (or D) component and the smallest are in the S component. These results are expected, because usually the baseline variability is largest in Y (or D), while the S baseline is the most stable. Stability of the S baseline is also evident from Fig. 4.2, where around 30 % of S baselines are approximated by constant or piecewise constant fits, i.e. R^2s are ≤ 0.1. For the vector components, we clearly find a higher number of cases with R^2 between 0.5 and 0.9 obtained with the new baselines than with the originally reported baselines.

A somewhat higher number of observatories with R^2 around 1 in the case of originally reported baselines is mostly due to observatories that determine their DBLs by linear interpolation or piecewise linear fits (see sub-Appendix B4). In this case, human intervention is essential. Here all outliers and low-quality observations are excluded from the observational datasets. Also, during piecewise fitting, the data processor makes decisions, for example, which observations should be used to calculate one

piece of a baseline, where to join the baseline pieces, which may be defined differently for different components, etc. These cases also show that, in order to obtain high quality data, in some cases, the intervention of a skilful and experienced data processor is essential.
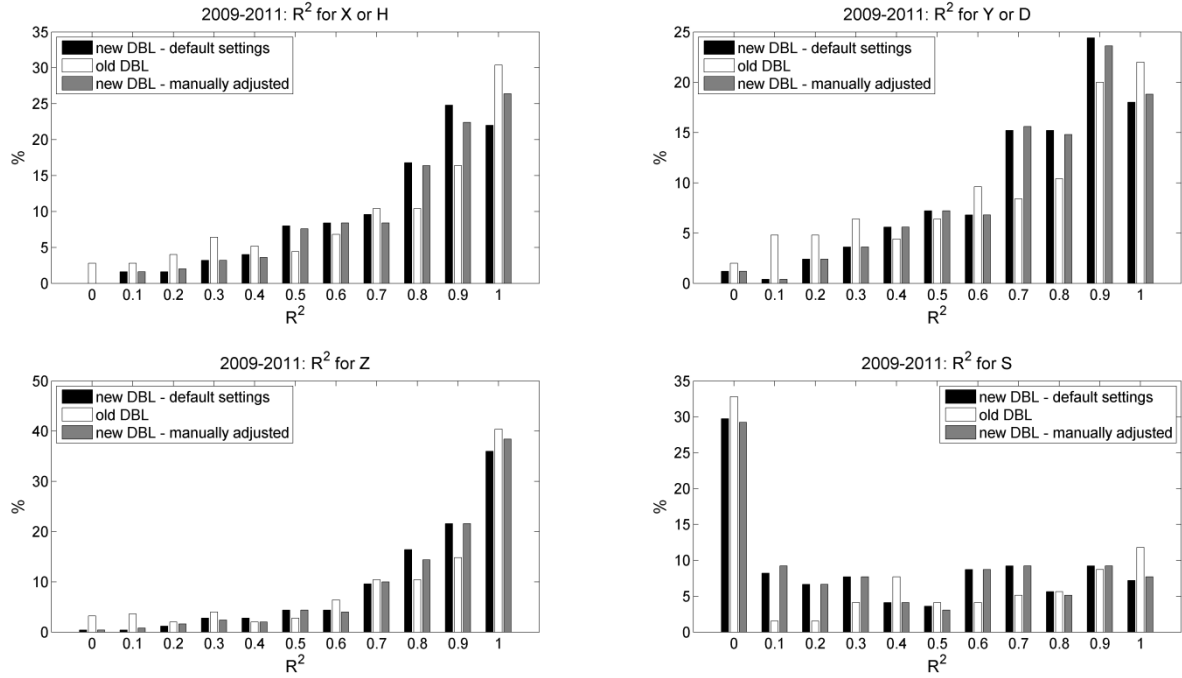
Figure 4.2 Squared correlation coefficients (R^2) between adopted and observed values for three vector and the scalar component. Three cases are presented. R^2 obtained for newly automatically calculated baselines (black), reported baselines (white) and newly calculated after manual adjustment for some observatories (grey).
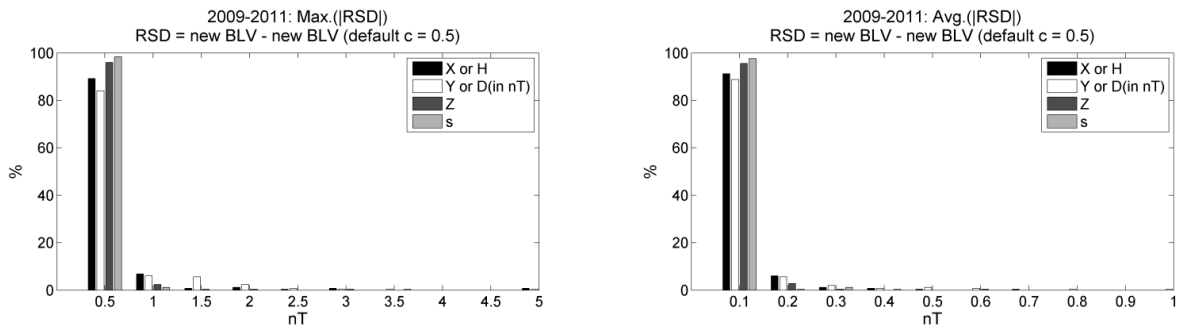
Figure 4.3 Histograms of the maximal and average (absolute) residuals between the new DBL (without manual adjustment) and the new DBL with default parameter $c = 0.5$, for three vector and the scalar component.

The same test was performed with the new baselines that are calculated using the default c parameter for the splines within windows. This means that fitting was not performed iteratively in order to minimize ΔF, i.e. to find an optimal c. The overall average differences between baselines with default c and automatically determined c are quite small. For all components, more than 90 % of average/maximal residuals are < 0.1 nT / 1 nT, while 0.3 nT / 1 nT are rarely excited. Detailed distribution of these residuals is shown in Fig 4.3. However, in some cases, by visual inspection,

significant improvements can be seen in the fit quality for baselines that are determined by minimization of ΔF.

Thus the new method has several advantages compared to traditional methods. Firstly, the new baselines are indeed more accurate, since in most cases they track the observations better than the original baselines and consequently give a smaller ΔF (e.g. Figs. 3.2 and 3.3). Secondly, residuals between the new DBL and QDBLs are practically negligible (Fig. 4.4). Small differences exist only near the right edge of the last window for which baseline is calculated. On average, more than 90 % of these residuals are < 0.3 nT (Fig. 4.4 right), while yearly maximum residuals in all 250 cases rarely exceed 1 nT (Fig. 4.4 left). Note that this discrepancy occurs only for a small time period, as demonstrated in Figs. 3.4a and 3.4b. Immediately after calculation of a new baseline using samples from the consecutive window (i.e. baseline update), this discrepancy is corrected. Last, but most important, the new DBLs are determined within a year. The time delay of DBL production may vary from several weeks up to several months, and depends only on the frequency of absolute observations.
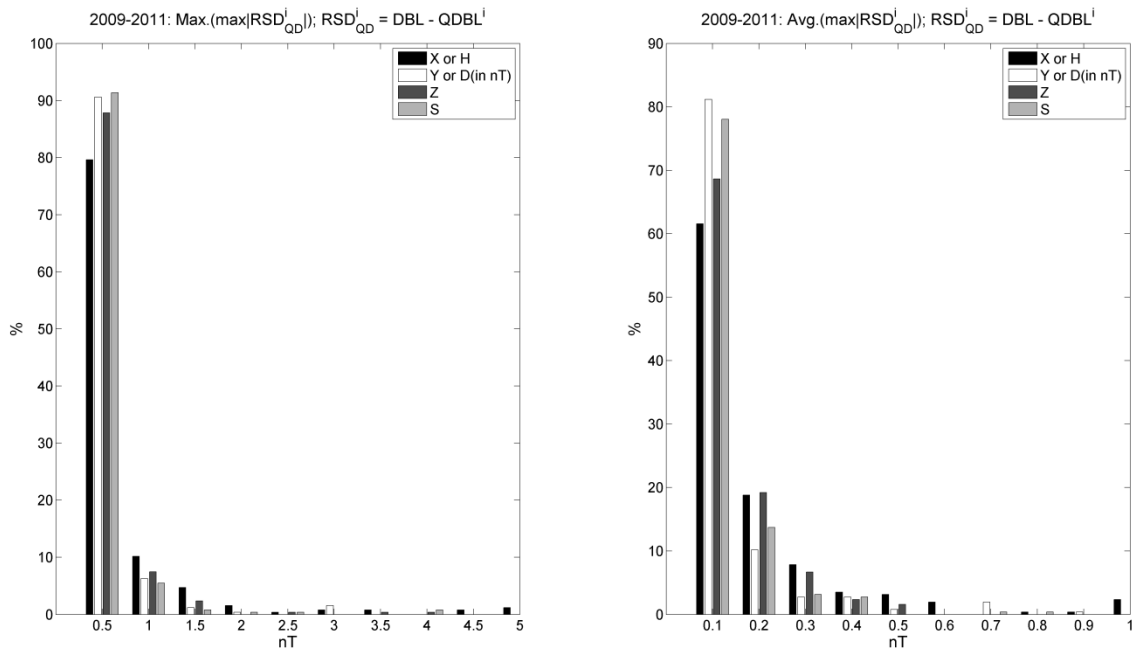
Figure 4.4 *Left*: Annual maxima of the maximal residuals between the new DBL and its temporary baseline segments (QDBL), i.e. each maximal residual correspond to one baseline window. *Right*: Annual averages of the same residuals presented in the left subplot.

New temporary baselines also clearly fulfil the requirements to define them as QDBLs with respect to the reported DBLs. According to INTERMAGNET standards, the (average) differences between QDBLs and DBLs should be less than 5 nT, and for many observatories these differences are within 1 nT. From Fig. 4.1, we can see that average $avg|RSD|$ are within 1 nT in all components and that about 80% are within 0.2 nT. Here, the assumption have been made that the new temporary baselines

have perfect overlapping with the new DBLs. This assumption is valid, because the differences between the new DBLs and their temporary segments are much smaller than the differences between the new and original DBLs. Note that Fig. 4.1 shows maximum and average residuals, while Fig. 4.4 shows annual maxima and averages of the maximal residual within all windows.

5. Applicability of the method in near real-time processing

Automated observatories that reach INTERMAGNET standards would be a major breakthrough in geomagnetic measurements. True global coverage with an even distribution of geomagnetic observatories is only possible with automatic observatories. These observatories could be set up in areas lacking infrastructure, the ocean floor or uninhabited remote areas without the possibility of intervention from trained personnel. Newitt (2007) lists six elements of observatory operations that must be fully or partially automated before an observatory can truly be called automated: data collection, data telemetry, data processing, data dissemination, error detection and absolute observations. Nowadays, except absolute observations and preparation of the final definitive data, all elements in of observatory operations are fully or at least partly automated. Therefore, the automation of absolute observations is of particular importance, since it would remove the necessity of having a trained observer on site. At present, there have been several attempts to automate absolute observations. One of them is AUTODIF an automated DI-flux for making unattended measurements of declination and inclination (van Loo and Rasson 2006, Rasson et al. 2009, Gonsette et al. 2013). Another approach is based on developing a new generation of ultra-high-resolution optically pumped [4]He magnetometers (Gravarand et al. 2001) or on optically pumped tandem magnetometers (Pulz et al. 2009). Another one is GAUSS, the Geomagnetic AUtomatic SyStem based on the method of rotating a three-axis fluxgate magnetometer around a defined axis, in order to determine the field component along that axis (Auster et al. 2007a, 2007b, Korte et al. 2013).

Very different but promising concepts are currently explored by continuous development and improvement of prototypes towards reliable automatic absolute instruments. If these prototypes prove to be stable enough in the long-term testing at conventional observatories, in the near future some magnetic observatories could operate without the need of absolute measurements for extensive periods of time.

5.1. Calibration of the LEMI data

As already shown in Sections 2.2 and 2.3, due to the lack of suitable infrastructure for LEMI system, in 2016, drifting of the LEMI baselines has been occurring on various timescales. Sudden movements of the sensor occurred also. To obtain a clear picture of LEMI baseline behaviour, the centred differences between dIdD definitive data and LEMI variations are shown in Fig 5.1. Together with the differences, the DI-flux observation results (also centred) are shown. One can conclude that, using the standard DI-flux observations, in conjunction with the standard baseline adaptation procedure, it is impossible to completely eliminate the drift from LEMI data. The attempt to correct LEMI data by means of the standard protocol is shown on Figs. 2.7a and 2.7b. Sudden drifts, within a day (like those in Fig. 2.9, on 5th and 19th September) and diurnal drifts will still be present in the data.
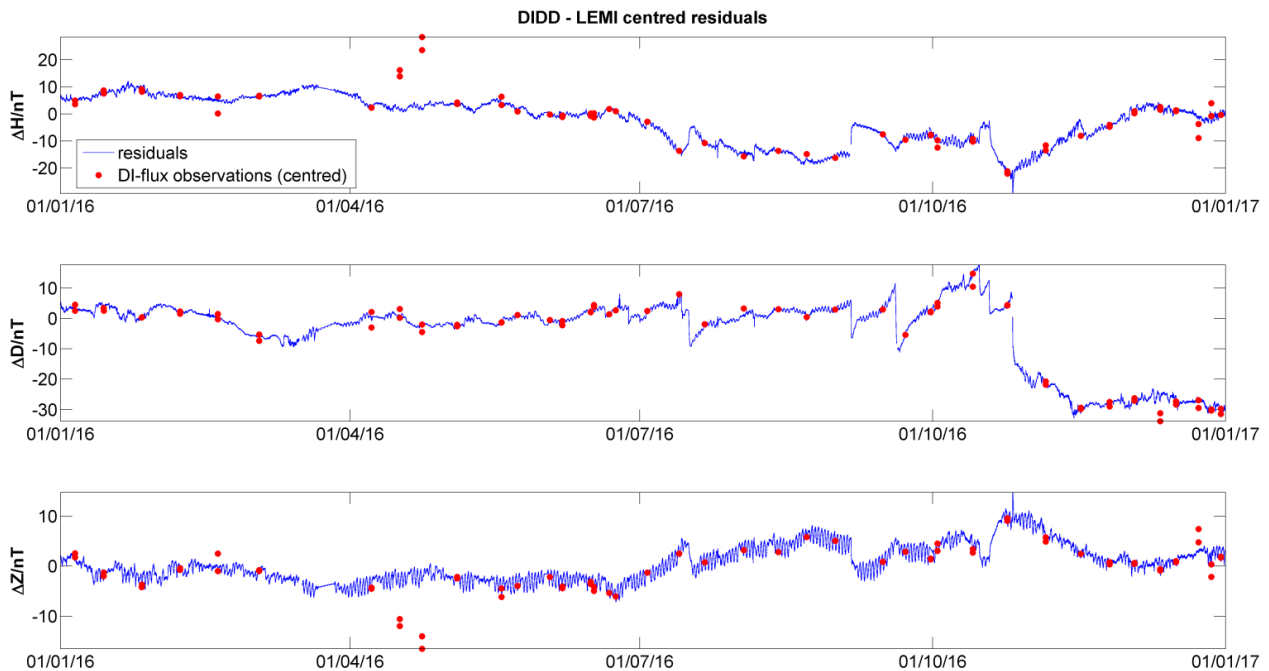
Figure 5.1 Centred differences between LON definitive data (dIdD) and LEMI variations in 2016. LEMI base values obtained from the DI-flux measurements are also displayed.

In this and similar cases, very frequent absolute observations are a basic prerequisite for quality correction of variometer data. In the near future, we can expect that development of automated absolute instruments will enable this requirement. Due to imperfection of instruments, with an increase in the number of measured absolute values (e.g. once per day, or per hour), the number of outliers and erroneous values will also increase. Therefore, it would be convenient to have a tool that is robust to outliers, for the near real-time calibration of variometer data without major revision of the input dataset. In this chapter, it will be demonstrated that the proposed technique may find its applicability in fully automated observatories operating automated absolute instruments that provide

many (digital) baseline samples in a day. Availability of frequent baseline samples in near real-time will also enable verification of calculated baselines with a delay of several days. This means that the final definitive data could be produced within several days from acquisition on a day-by-day basis.

5.2. Simulation of observations provided by an automatic absolute instrument

LON definitive data in 2016 are absolute values of the geomagnetic field vector. These data are referred to the main pillar and obtained from dIdD magnetometer in combination with sporadic absolute measurements. Therefore, LON definitive data can be used to obtain frequent base values for LEMI magnetometer. These base values will be used to calibrate LEMI data applying the proposed method.
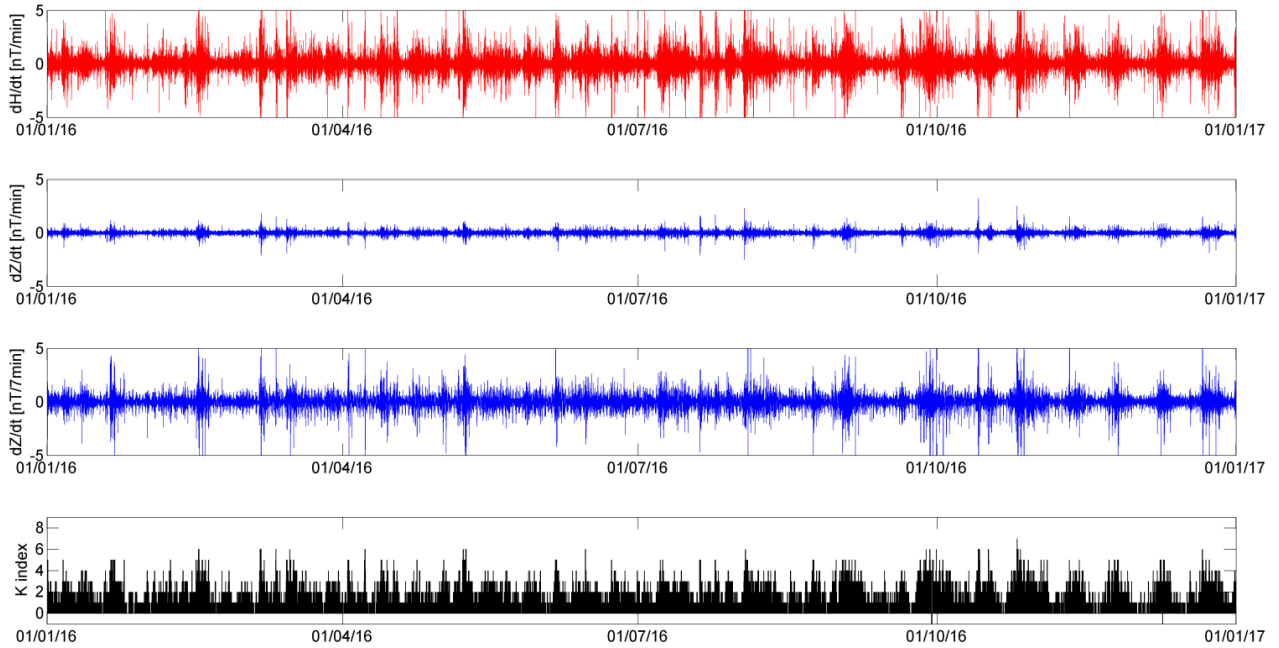
Figure 5.2 Rate of change *dB*/*dt* for *H* and *Z* components of LON time series during 2016 (see text for details). In the first and third subplots at some periods (enhanced geomagnetic activity), values exceed ±5 nT. The ordinate scaling of ±5 nT is used for better visibility. The bottom subplot displays local geomagnetic indices during 2016.

Periodical, definitive, momentary values are used to simulate samples from automated absolute instrument. For example, every 15th minute of each hour are used to obtain absolute samples that are used to find base values for LEMI magnetometer. This way, I have simulated observations, provided by automated absolute instrument, at every hour in the day. In reality, automatic instruments will have limited accuracy, and in some periods, measurements may be more erroneous. The lack of utopian laboratory conditions for instrument operation at remote sites could also affect operation of automated

47

absolute instruments. In order to make the situation more realistic, errors in observations are also introduced.

Instead of using some numerical algorithm for generating random errors (in otherwise perfect observations), natural magnetic perturbations are used for this purpose. To introduce a certain amount of error in the observation, instead of true value spotted in the 15th minute of each hour, the value preceding/following the 15th minute value by a few minutes before/after is taken. This "wrong" value with the time stamp hh:15 ± mm :00 contains a deviation from the true field. The magnitude of this deviation will depend on geomagnetic activity. During the higher geomagnetic activity, we will have larger errors, and smaller during the low geomagnetic activity. Therefore, periods of a few days during magnetic storms and sub-storms can be considered as periods when the automated absolute instrument had some (major) temporary problems with operation due to external or internal reasons. These kinds of problems are expected in observatory practice and they also occur with continuously recording variometers and scalar magnetometers.

Figure 5.2 shows dB/dt (Worthington et al. 2009) of LON time series for H and Z components together with geomagnetic activity indices. The rate of change dB/dt is calculated as simple forward differences of original time series; $dB/dt = B(i+1) - B(i)$ for $i = 1,\dots N$, where $N = 527040$ is the overall number of minutes from 1 January 2016 at 00:00 UT to 31 December 2016 at 23:59 UT. At LON the magnitude of dB/dt is approximately the same for horizontal components H and D (or X and Y), and Z component is about an order of magnitude smaller than horizontal components (Fig. 5.2, second subplot). Standard deviation of dH/dt is 0.5 nT for the whole year. This means if I use the H absolute value at hh:16:00 to derive the base value (H_0) at hh:15:00, H_0 will contain an error of a fraction of nT up to several nT (Fig. 5.2, first subplot) or 0.5 nT on average on the yearly basis. It is also reasonable to assume that the magnitude of this simulated error should be similar in the vertical component. From Fig 5.2 (second subplot), one can see that the rate of change dZ/dt is significantly smaller than dH/dt. But, if I calculate dZ/dt as $Z(i+7) - Z(i)$, the magnitude will be similar to dH/dt with standard deviation of 0.5 nT (Fig. 5.2, third subplot). Thus, the Z absolute value at hh:22:00 is used to derive the base value (Z_0) at hh:15:00. To introduce even greater errors around 1 nT on the yearly basis, the H absolute value at hh:17:00 and the Z absolute value at hh:29:00 are used to obtain H_0 and Z_0. Standard error of 1 nT correspond to rates of change $H(i+1) - H(i)$ and $Z(i+14) - Z(i)$. Expressions for rate of changes that are used to estimate errors in H and Z components can be rewritten in general form:

$$dH / dt = H(i+m) - H(i)$$
$$dZ / dt = Z(i+n) - Z(i)$$

(5.1)

Finally, a few datasets are created with different amounts of errors in data, i.e. for a few cases of m and n. Errors in D are simulated in the same manner as for H component. Cases and standard errors on the yearly basis are listed in Table 5.1.

Table 5.1

Annual standard errors of simulated absolute observations, i.e. base values for LEMI magnetometer (see text for details).

H m	*Z* n	std. error nT
1	7	0.5
2	14	1
3	21	1.3
4	28	1.6
5	35	2

Figure 5.3 displays simulated base values of LEMI magnetometer obtained by an imaginary absolute instrument. Red dots are true base values, while more scattered, red dots represent a more realistic situation, i.e. measurements with some uncertainty and errors. Periods with increased scattering correspond to higher geomagnetic activity and can be considered as periods when the performance of an imaginary absolute instrument was not so good.
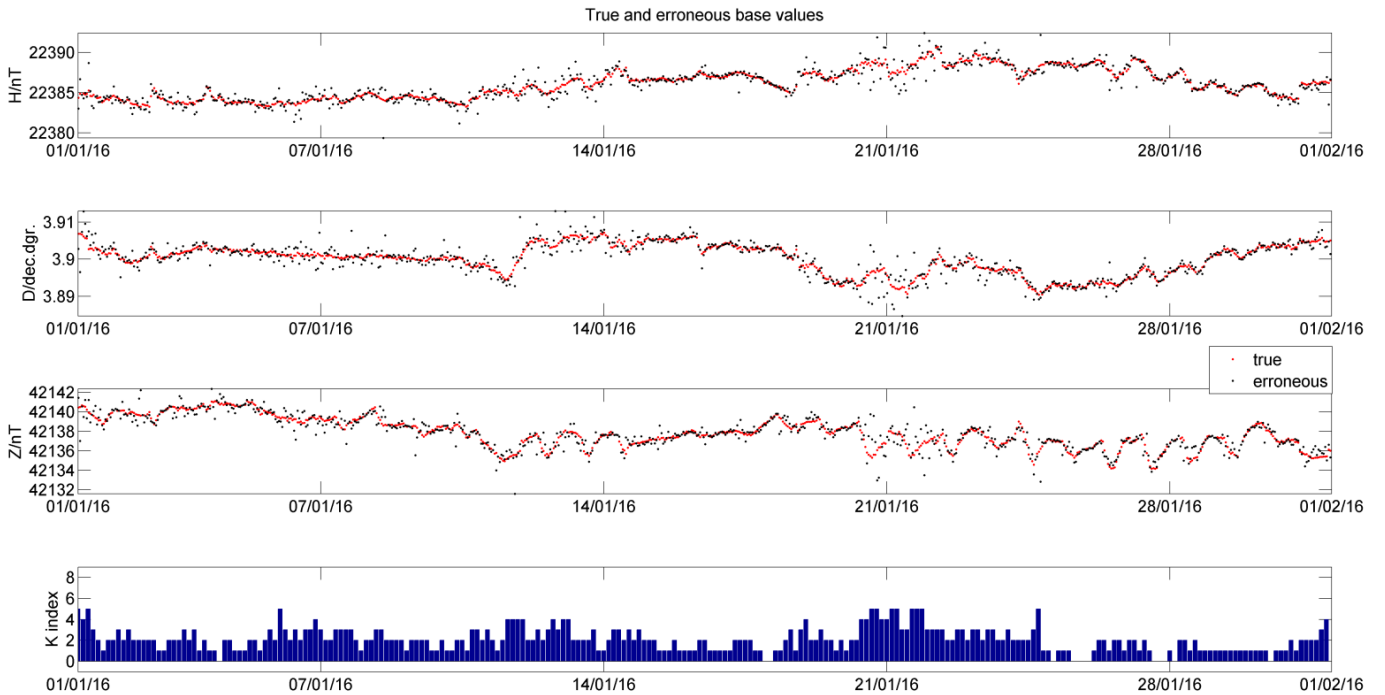

Figure 5.3 Simulated hourly base values for LEMI magnetometer in January 2016. Red dots represent true (i.e. perfect) observations, and black dots represent erroneous observations for the second case in Table 5.1. The bottom subplot displays local geomagnetic indices during January 2016.

5.3. Modification of the proposed method

Automated absolute instruments will provide many absolute samples per day in equidistant time intervals. In my particular case, observations are simulated once per hour, i.e. in a day there are 24 samples. For this purpose I decide to define windows with the predefined time span (is Section 3.1 the time span of a window was not fixed). Pieces of a baseline are calculated within a day, i.e. the span of a window is 24. Same as in Section 3.1, two samples from neighbouring windows are used to alleviate possible edge effects between neighbouring baseline segments. The smoothing coefficient c is varied in the range from 0.0725 up to 0.00725, and splines within windows are joined by the final smoothing spline with coefficient $c = 0.725$. One can notice that this varying range has the span of one order of magnitude in contrast to one in the Section 3.1 (five orders of magnitude). There are several reasons for this. Here, we have much more observational data and optimal c, i.e. p is determined by minimization of ΔF obtained from the minute data. By narrowing the varying range, the computational efficiency is increased. Secondly, in Section 3 the data from many observatories worldwide are used, and most of the datasets have non-uniform sampling with different sampling rate, i.e. interesting range of c for each observatory is different. Thirdly, the interesting range for the smoothing parameter p is extremely sensitive to the scaling of the spacing between data sites. In the LEMI case, with 24 samples per day ($h = 0.042$), the splines outside the varying range ($c = [0.0725, 0.00725]$, i.e. $p = [0.990, 0.999]$) converge very fast toward a last-squares straight line to the data on the one side, or toward a cubic spline interpolant on the other side.

In Fig. 5.4, the first three subplots show observations presented in Fig 5.3 and adapted baselines obtained with the modified proposed method. Erroneous observations (case 2, Table 5.1) are used to calculate adapted baselines. Generally, adapted baselines overlap good observations (red dots) quite well. As expected, in some parts the uncorrected drift is still present due to errors in observations (fourth and fifth subplots). On the other hand, we can see that the occasional a few nT outliers did not distort the baselines. Figure 5.5 demonstrate further the robustness of the method to outliers. In this figure, additional larger, monotonically increasing outliers are added to the horizontal and vertical component. Declination is free from larger outliers to demonstrate how the proposed method and simple smoothing splines have similar performance on the frequent data with moderate scattering. The fourth subplot is the same as in Fig 5.4, and residuals plotted in both figures are practically identical, i.e. the results of adaption with the proposed method are not affected by outliers. On the other hand, baselines obtained with cubic smoothing splines are strongly affected by outliers. (Median value of all smoothing parameters that are used to obtain 31 baseline pieces in January is used as the smoothing parameter throughout January in the case of adaption with simple smoothing splines.) Therefore, in the near real-time processing, automatic adaption with the smoothing spline can introduce significant degradation in the reported data.

In the case of variable baselines, an automated absolute instrument with quite large scattering can still provide valuable data that can be used to correct longer-term drifts within a month or year. In the LEMI case in January 2016, we can note that the long-term drift within the month is completely eliminated, i.e. differences in the fourth subplot, Fig. 5.4 are centred to zero. Figure 5.6 shows differences between dIdD and LEMI data after adaption using the standard DI-flux results (Fig. 2.7a), and after adaption (Fig. 5.4) using data provided by automatic absolute instrument.
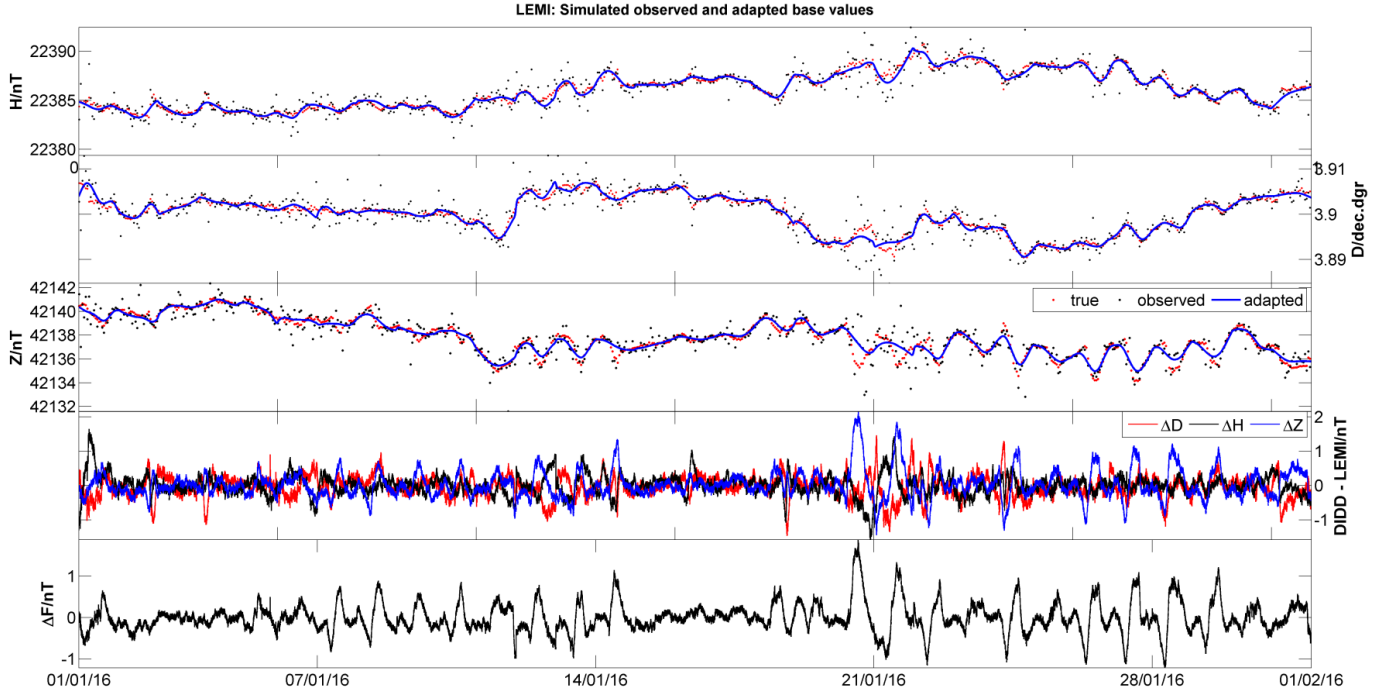
Figure 5.4 Adapted baselines with same observations as in Fig. 5.3 (first three subplots). Differences between dIdD (LON definitive data) and LEMI calibrated data (fourth subplot). The difference between LEMI vector *F* and scalar *F* (fifth subplot).
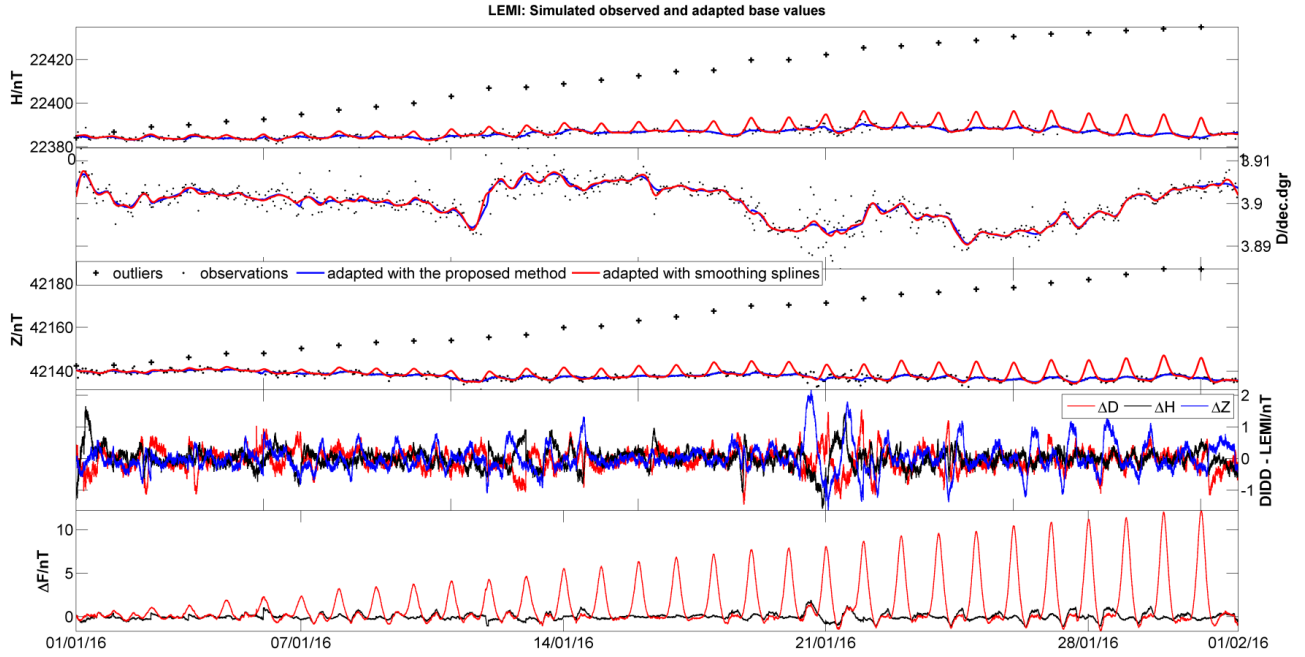
Figure 5.5 The first three subplots show adapted baselines with the proposed method (blue line) and with simple cubic smoothing splines (red line). Additional outliers (one per day) are added to *H* and *Z* component. Fourth subplot is the same as in Fig 5.4. Differences between dIdD and LEMI calibrated data (fourth subplot). The final subplot shows Δ*F* diagrams. Black corresponds to the adaption with the proposed method, and red to the adaption with simple smoothing splines.
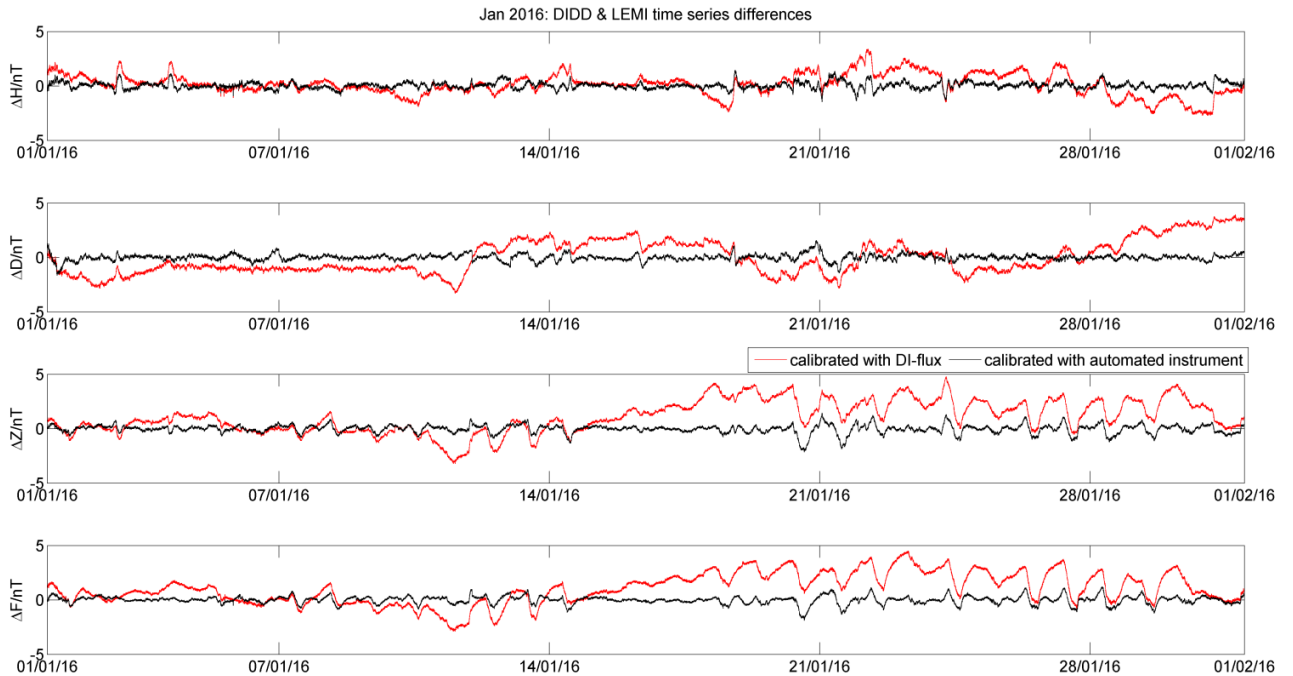
Figure 5.6 Comparison of differences between dIdD (LON definitive data) and LEMI calibrated data. Red line represents the difference after calibration of LEMI data by means of DI-flux measurement (Fig. 2.7a). Black line represents the difference after calibration of LEMI data with the proposed method and simulated data from automated absolute instrument.

52

5.4. Results and discussion

From Fig. 5.6, it is obvious that drifts within a month or longer will be corrected successfully due to a frequent sampling of the baseline changes. Here, we are interested in how successfully the proposed method corrects diurnal drifting for the several simulated cases in Table 5.1. Due to approximately sinusoidal shape of diurnal drift with magnitudes up to a few nT during most days, especially for H and D, the daily drift averages (or absolute averages) are small ($\leq$ nT) and are not suitable for analysis. Instead, amplitudes of the drift are compared with the observational errors. Firstly, for uncorrected LEMI variations for the whole 2016, the daily drift amplitudes are estimated. Then, after adaption with the proposed method (for cases in Table 5.1), amplitudes are estimated again. Finally, the time series of amplitudes are compared with simulated observational errors and initial daily amplitudes (of uncorrected LEMI series). Days when sudden movements of the sensor had occurred (Fig. 5.1) are not used in this analysis.

In the case with the "perfect" observations, the adaption gives almost perfectly calibrated LEMI data, up to the noise level (Fig. 5.7). Generally, this noise is a consequence of imperfections of recording systems, time stamp accuracy, local anthropogenic noise and two instruments at different sites do not record the identical magnetic field. At LON, this noise level is approximately ± 0.3 nT, i.e. 0.6 nT amplitude.
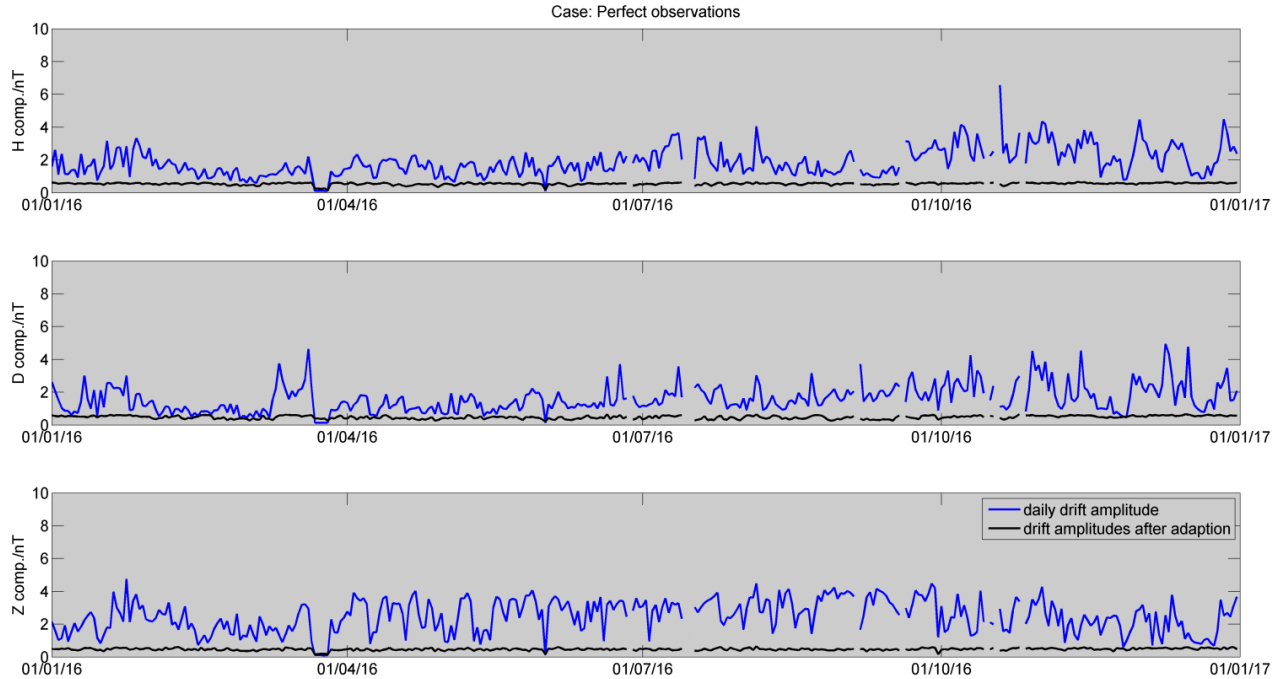
Figure 5.7 Daily drift amplitudes of uncorrected LEMI series (blue line). Drift amplitudes after calibration of LEMI series with "perfect" observations (black line).
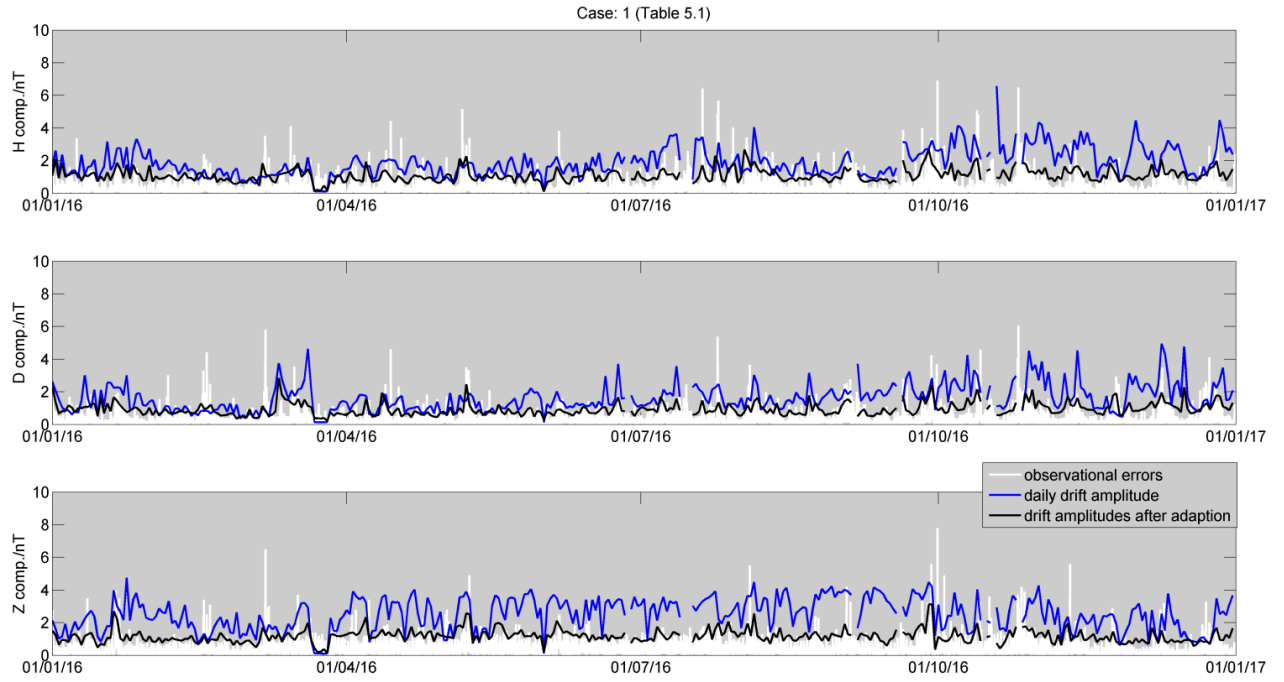
Figure 5.8 Daily drift amplitudes of uncorrected LEMI series (blue line). Drift amplitudes after calibration of LEMI series with erroneous observations (black line), case 1 in Table 5.1. Observational errors are presented with the white line.
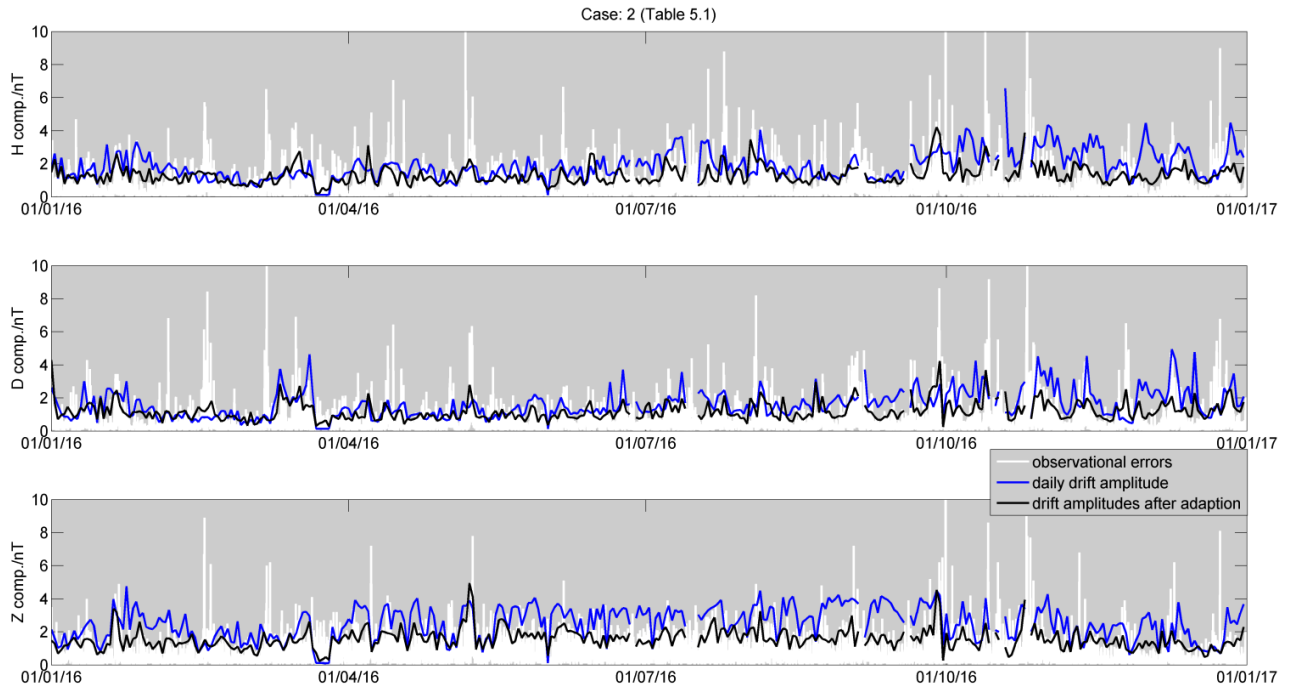
Figure 5.9 Same as Fig 5.8, only for case 2 in Table 5.1.
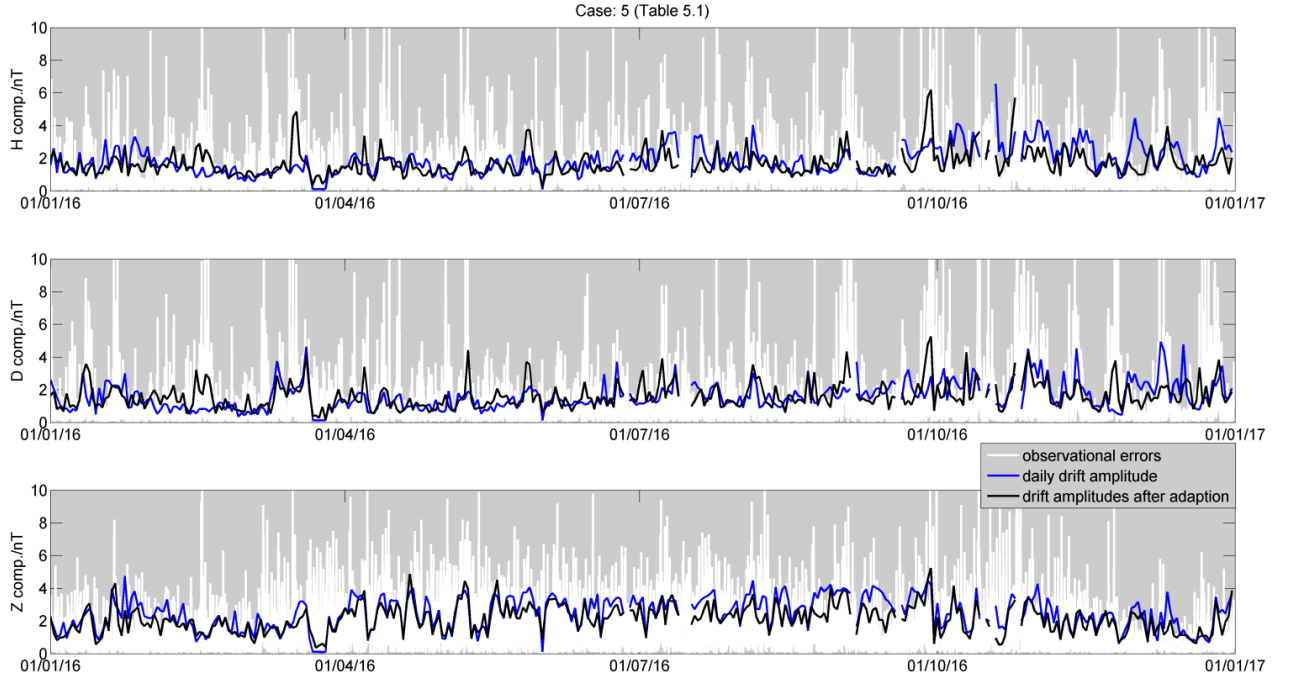
Figure 5.10 Same as Fig 5.8, only for case 5 in Table 5.1.

Figures 5.8 to 5.10 display the daily drift amplitudes of uncorrected LEMI series (blue line), simulated observational absolute errors (white line) and the drift amplitudes after calibration of LEMI series with erroneous observations (black line). Figures 5.8, 5.9 and 5.10 correspond to the first, second and fifth cases in Table 5.1. As expected, the quality of adaption depends on the quality of absolute observations. In Fig 5.8, improvements are clearly visible in all three components. In Fig 5.9, improvement is still clearly visible in the vertical component. This is because the vertical component has larger and more regular (sinusoidal) drifting than the other two horizontal components (Fig 5.1). In Fig. 5.10, many errors are larger than 10 nT, but for the purpose of better visibility, the ordinate span is set to 10 nT. Even if we have very large outliers and scattering of samples (Fig. 5.10), the performance of the proposed method is quite satisfactory, thus demonstrating the robustness of the method. General conclusion is that the adaption performed in fully automatic manner did not introduce additional degradations in data. Later, after detailed revision of the observational dataset, the data quality can be additionally improved.

6. Conclusions

Traditionally definitive geomagnetic observatory data are published annually with a delay ranging from several months up to more than a year. The reasons being that it may be difficult to produce high quality recordings (visually checked, de-spiked, corrected for jumps, etc.) soon after acquisition due to lack of observatory staff and processing protocols, or simply because the calculation of definitive baselines and calibration of recorded data on a yearly basis is currently standard procedure.

In this study, the possibility to produce definitive observatory data more continuously with smaller time lags was investigated. The new method for reliable baseline adoption in a nearly fully automatic manner is proposed. Definitive baselines can be estimated by pieces from a sufficient number of observations in a way that the future results will not affect the shape of baselines from the past. This way, it is also much easier to fit flexible baselines in case of rapid variation of the absolute observations within some period without overfitting surrounding observations that are stable. By re-processing the published baseline observations of the INTERMAGNET observatories from 2009 to 2011, it has been shown that definitive baselines calculated with the new method, in most cases, give the same or better results (as indicated by ΔF and R^2) than definitive baselines determined by experienced observatory staff. However, in some cases manual intervention is necessary to obtain good results with the new method. Furthermore, it is planned to develop a graphical user interface (GUI) that will allow others to use the method with options for manual intervention to improve results. For example, before fitting the user will be able to remove larger outliers, define knots (i.e. window edges) differently in each component and modify the automatically determined smoothing parameter within the window and for each component separately.

Most of the results in this study are obtained relying on the ΔF check. Continuous and accurate scalar observations are essential to obtain correct scalar F at the reference site in order to obtain reliable ΔF. Due to increased scattering or absolute inaccuracy in many cases the proposed method estimates scalar baselines as piecewise constant functions that do not fit observations. Examples similar to the one shown in Fig. 2 (results obtained with the proposed method), can also be found on INTERMAGNET DVDs 2009-2011. Thus the best observatory practice would be to set scalar baseline to zero, i.e. to perform continuous scalar measurement at the reference site (except during manual DI-flux observations). Alternatively, the gradiometer difference between the scalar and reference site, which is

required for processing of the DI-flux observations and obtaining accurate scalar observations, should be updated regularly after each absolute DI-flux observation.

It has been demonstrated that most INTERMAGNET observatories should be able to distribute definitive data relatively soon after acquiring recent absolute measurements. Availability of the best existing data, i.e. definitive data, within less than a year will be highly appreciated from the side of the observatory data users. With weekly absolute observations, most observatories should be able to produce their definitive data more continuously with a delay between two and three months. Increasing the number of observations, or shortening the window size, could significantly shorten this delay. In addition, with the proposed technique maximal discrepancies between definitive and quasi-definitive data (which can be available within a few days/weeks) rarely exceed 0.3 nT.

The fact that in many cases the new method gives good results without human intervention paves the way towards automating the whole data processing chain, and towards fully automated observatories when automated absolute instruments become supplemental equipment or the only absolute instrument at remote (unmanned) observatories (e.g. Korte et al. 2009, Mandić et al. 2016). These instruments will provide information about the absolute values of the field and variometer base values much more frequently than today. The increase in the number of automatically collected observations (e.g. every 30 min, Gonsette *et al*. 2013) will require a routine for baseline fitting and calibration of variometer data continuously in near real-time. However, the automatic instruments show a larger scatter and we have to expect increased number of outliers. Thus, an automated processing protocol should be robust to outliers.

In the last section, data from LON observatory are used to simulate datasets from an automated absolute instrument producing 24 observations per day. These observations are used for calibration of LON supplement variometer with variable baselines. Even if we have scattering comparable or larger than the drift amplitude, together with large outliers, the proposed method shows good performance. Results of these tests confirmed robustness and reliability of the proposed method, i.e. the quality of calibrated data will not be undermined by occasional outliers. To summarize: the quality of adaption (performed in fully automatic manner), i.e. accuracy of calibrated data will depend on the data quality provided by an automated absolute instrument. This means that the overall accuracy of absolute observations must be better than the amplitude of the drift, and sampling frequency should be higher than the highest frequency in the drift signal. When prototypes of automated absolute instruments prove sufficient long-term stability and accuracy, and fulfil requirements to become standard instrument in a magnetic observatory, this will bring the opportunity to produce definitive data within several days from acquisition on a day-by-day basis. In this scenario, the proposed method could find its use in automated calibration protocol, and in this way contribute to dissemination of preliminary data with the high absolute accuracy and near real-time availability.

7. References

Alexandarov, E.B. and Bonch-Bruevich, V.A. (1992), Optically pumped magnetometers after three decades, *Optical Engineering*, **31**, 4, 711-717, DOI: 10.1117/12.56132.

Alldredge, L.R. (1960), A proposed automatic standard magnetic observatory, *J. Geophys. Res*. **65**, 11, 3777-3786, DOI: 10.1029/JZ065i011p03777

Auster, H.U., Mandea, M., Hemshorn, A., Pulz, E., Korte, M. (2007a), Automation of absolute measurements of the geomagnetic field, *Earth planets Space*, **59**, 9, 2007-1014.

Auster, H.U., Mandea, M., Hemshorn, A., Korte, M., Pulz, E.(2007b), Gauss: a geomagnetic automated system, *Publ. Inst. Geophys. Res. Pol. Acad. Sci.* C **99**, 398, 49-59.

Brkić, M., Vujić E., Šugar D., Jungwirth E., Markovinović D., Rezo M., Pavasović M., Bjelotomić O., Šljivarić M., Varga M., Poslončec-Petrić V. (2013), Osnovna geomagnetska mreža Republike Hrvatske 2004 - 2012, s kartama geomagnetskog polja za epohu 2009.5 / ISBN: 978-953-293-521-9 / Brkić, Mario (ur.), Zagreb: Državna geodetska uprava, 2013.

Bartels, J., Heck, N.H. and Johnston, H.F. (1939), The three-hour range index measuring geomagnetic activity, *J. Geophy. Res*. **44**, 4, 411-454, DOI: 10.1029/TE044i004p00411.

Clarke, E., Baillie, O., Reay, S.J. and Turbitt, C.W. (2013), A method for the near real-time production of quasi-definitive magnetic observatory data, *Earth Planets Space*, **65**, 11, 1363-1374, DOI: 10.5047/eps.2013.10.001.

Chambodut, A., Di Mauro, D., Schott, J.J., Bordais, P., Agnoletto, L. and di Felice, P. (2009), Three years continuous record of the Earth's magnetic field at Concordia station (DomeC, Antartica), *Ann. Geophys.-Italy*, **52**, 1, 15-26.

Csontos, A., Hegymegi, L. and Heilig, B. (2007), Temperature tests on modern magnetometers, *Publs. Inst. Geophys. Pol. Acad. Sc*., C-99 (398), 171-177.

De Boor, C. (2003), *Spline Toolbox for Use with MATLAB*, The MathWorks, Inc.

De Boor, C. (1978), *A practical guide to splines*, Springer Verlag, New York.

Friis-Christensen, E., H. Lühr, and G. Hulot (2006), Swarm: A constellation to study the Earth's magnetic field, *Earth Planets Space*, **58**, 4, 351-358, DOI: 10.1186/BF03351933.

Gilles, H., Hamel, J. and Cheron, B. (2001), Laser pumped ^{4}He magnetometer, *Review of Scientific Instruments*, **72**, 2253-2260.

Gonsette, A., Rasson, J. and Marin, J.L. (2013), AUTODIF: Automatic absolute DI measurements, *Proc. 15th IAGA Workshop on Geomagnetic Observatory Instruments, Data Acquisition, and Processing*, Boletin ROA, No. 03/13, 16-19.

Gravarand, O., Khokhlov, A. Le Mouë, J.L., Leger, J.M. (2001), On the calibration of a vectorial ^{4}He pumped magnetometer. *Earth Planets Space*, **53**, 949-958.

Hegymegi L., B. Heilig, and A. Csontos (2004), New suspended dIdD magnetometer for observatory (and field?) use, *Proceedings of the XIth IAGA Workshop on Geomagnetic Observatory Instruments*, *Data Acquisition, and Processing*, Kakioka and Tsukuba, Japan, 28-33.

Heilig B., J. Lichtenberger, M. Vellante, J. Reda, T. Rita, P. Sutcliffe, M. Váczyová, D. Herak, M. Neska, L. Merényi, A. Csontos, P. Kovács, M. Srbecky, and I. Mandić (2013), EMMA for near real time Monitoring of the Plasmasphere, *Proceedings of the XVth IAGA Workshop on Geomagnetic Observatory Instruments, Data Acquisition, and Processing*, San Fernando, Spain, 127-130.

Iype, A., Deshmukh, A.T. and Veenadhari, B. (2017), Long term drifts in baselines of ground magnetic observatories, *Measurement*, **102**, 33-41.

Jankowski, J. and Sucksdorff, C. (1996), *Guide for Magnetic Measurements and Observatory Practice*, International association of Geomagnetism and Aeronomy, Boulder, USA.

Kerridge, D.J. (1988), Theory of the fluxgate-theodolite, Report WM/88/14, British Geological Survey.

Lauridsen, K.E. (1985), Experience with the DI-fluxgate magnetometer inclusive theory of the instrument and comparison with other methods, *Geophysical Papers R-71*, Danish Meteorological Institute, Copenhagen.

Lesur, V., S. Macmillan, and A.W.P. Thomson (2006), Deriving main field and secular variation models from synthetic Swarm satellite and Observatory data, *Earth Planets Space*, **58**, 4, 409-416, DOI: 10.1186/BF03351937.

Korte, M., Brunke, H.P., Bronkalla, O. and Pulz E. (2013), Status of the geomagnetic automated system GAUSS. In: *Proc. 15th IAGA Workshop on Geomagnetic Observatory Instruments, Data Acquisition, and Processing*, Boletin ROA, No. 03/13, 20-23.

Korte, M., Mandea, M., Linthe, H.J., Hemshorn, A., Kotze, P. and Ricaldi, E. (2009), New geomagnetic field observations in the South Atlantic Anomaly region, *Ann. Geophys.-Italy*, **52**, 1, 65-81.

Macmillan, S., and N. Olsen (2013), Observatory data and the Swarm mission, *Earth Planets Space*, **65**, 15, 1355-1362, DOI: 10.5047/eps.2013.07.011.

Mandea, M. and Korte, M. (Eds.) (2011), *Geomagnetic Observations and Models*, IAGA Special Sopron Book Series, Springer, Dordrecht Heidelberg London New York, DOI: 10.1007/978-90-481-9858-0.

Mandić, I., Vujić, E., Heilig, B., Pelajić, I. and Herak, D. (2016), Recent efforts toward the establishment of the Lonjsko Polje geomagnetic observatory, *Acta Geophys.* **64**, 5, 1311-1339, DOI: 10.1515/acgeo-2016-0051.

Matsushita, S. and Campbell, W.H. (1967), *Physics of Geomagnetic Phenomena*, Academic Press, New York and London, USA.

Matzka, J. (2013), Preparation of quasi definitive (QD) data for the observatories Narsarsuaq, Qeqertarsuaq and Tristan Da Cunha. In: *Proc. 15th IAGA Workshop on Geomagnetic Observatory Instruments, Data Acquisition, and Processing*, Boletin ROA, No. 03/13, 50-53.

Menvielle, M., Papitashvili, N., Häkkinen, L. and Sucksdorff, C. (1995), Computer production of K-indices: Review and comparison of methods. *Geophys. J. Int.* 123, 3, 866-886, DOI: 10.1111/j.1365-246X.1995.tb06895.x

Merényi L., B. Heilig B., and L. Szabados (2013), Geomagnetic Data Acquisition System developed for PLASMON project, *Proceedings of the XVth IAGA Workshop on Geomagnetic Observatory Instruments, Data Acquisition, and Processing*, San Fernando, Spain, 54-56.

Newitt, L.R. (2007), Observatory automation. In: Gubbins, D. and Jerrero-Bervera E. (Eds.), *Encyclopaedia of Geomagnetism and Paleomagnetism*, Springer, Dordrecht, Netherlands.

Newitt, L.R., Barton, C.E. and Bitterly, J. (1996), *Guide for magnetic repeat station surveys*, International Association of Geomagnetism and Aeronomy, Warszawa, Poland.

Olsen, N., R. Haagmans, T.J. Sabaka, A. Kuvshinov, S. Maus, M.E. Purucker, M. Rother, V. Lesur,

and M. Mandea (2006), The Swarm End-to-End mission simulator study: A demonstration of separating the various contributions to Earth's magnetic field using synthetic data, *Earth Planets Space*, **58**, 4, 359-370, DOI: 10.1186/BF03351934.

Packard, M. and Varian, R. (1954), Free nuclear induction in the Earth's magnetic field, *Phys. Rev.*, **93**, 941.

Peltier, A. and Chulliat A. (2010), On the feasibility of promptly producing quasi-definitive magnetic observatory data, *Earth Planets Space*, **62**, 2, e5-e8, DOI: 10.5047/eps.2010.02.002.

Poncelet, A. Gonsette, A. and Rasson, J. (2017), Several years of experience with automatic DI-flux: theory, validation and results, *Geosci. Instrum. Method. Data. Syst.*, **6**, 353-360, DOI: 10.5194/gi-6-353-2017.

Pulz, E., Jäckel, K.H., Bronkalla, O. (2009), A quasi absolute optically pumped magnetometer for the permanent recording of the Earth's magnetic field vector, *Proceedings of the XIIIth IAGA Workshop on Geomagnetic Observatory Instruments, Data Acquisition, and Processing*, U.S. Geological Survey Open-File Report, 216-219.

Rasson, J.L., Toh, H. and Yang, D (2011), The global geomagnetic observatory network, in *Geomagnetic Observations and Models*, Eds. Mandea, M. and Korte, M., pp. 1-25, IAGA Special Sopron Book Series, Springer, Dordrecht Heidelberg London New York, DOI: 10.1007/978-90-481-9858-0.

Rasson, J.L., van Loo, S.A. and Berrami, N. (2009), Automatic DIflux measurements with AUTODIF, in *Proceedings of the XIIIth IAGA Workshop on Geomagnetic Observatory Instruments, Data Acquisition and Processing*, Ed. Love, J.J., U.S. Geological Survey Open-File Report, pp. 220-224.

Rasson, J.L. (2007), Observatories, instrumentation, in *Encyclopaedia of Geomagnetism and Paleomagnetism*, Eds. Gubbins, D. and Herrero-Bervera, pp. 711-713, Springer, Heidelberg.

Schott, J.J. and Leroy, P. (2001), Magnetic components measured with the DIDD, *Contribution to Geophysics and Geodesy*, **31**, 1, 35-42.

Steiner, F. (1988), Most frequent value procedures, *Geophysical transactions*, **34**, 2-3, 139-260.

St-Louis, B. (2012), Intermagnet Technical Reference Manual (Version 4.6).

Thébault, E., Finlay, C. C., Beggan, C. D., Alken, P., Aubert, J., Barrois, O., Bertrand, F., Bondar, T., Boness, A., Brocco, L., Canet, E., Chambodut, A., Chulliat, A., Coïsson, P., Civet, F., Du, A.,

Fournier, A., Fratter, I., Gillet, N., Hamilton, B., Hamoudi, M., Hulot, G., Jager, T., Korte, M., Kuang, W., Lalanne, X., Langlai, B., Léger, J.M., Lesur, V., Lowes, F. J., Macmillan, S., Mandea, M., Manoj, C., Maus, S., Olsen, N., Petrov, V., Ridley, V., Rother, M., Sabaka, T. J., Saturnino, D., Schachtschneider, R., Sirol, O., Tangborn, A., Thomson, A., Tøffner-Clausen, L., Vigneron, P., Wardinski, I. and Zvereva, T. (2015), International Geomagnetic Reference Field – The Twelfth generation, *Earth Planets Space*, **67**, 79, 1-19, DOI: 10.1186/s40623-015-0228-9.

Van Loo, S.A. and Rasson, J.L. (2006), Development of an automatic declination-inclination magnetometer, in *Geomagnetics for Aeronautical Safety*, Eds. Rasson, J.L. and Delipetrov, T. NATO Science for Peace and Security Series C, Springer, Norwell, pp. 177-186.

Verbanac, G. and Vujić, E. (2012), Determination of the Croatian geomagnetic observatory location, *Acta Geophys.*, **60**, 2, 337-356, DOI:10.2478/s11600-012-0001-4.

Vujić, E., Brkić, M. and Radović, N. (2011), Analysis of Croatian geomagnetic repeat station surveys in 2004 and 2007, *Stud. Geophy. Geod.* **55**, 4, 737-753, DOI: 10.1007/s11200-010-9037-6.

Wienert, K.A. (1970), Notes on geomagnetic observatory and survey practice. UNESCO, Brussels.

Worthington, E.W., Sauter, E.A. and Love J.J. (2009), Analysis of USGS one-second data, *Proceedings of the XIIIth IAGA Workshop on Geomagnetic Observatory Instruments, Data Acquisition, and Processing*, U.S. Geological Survey Open-File Report, 262-266.

Worthington, E.W. and Matzka J. (2017), USGS Experience with the residual absolutes method, *Geosci. Instrum. Method. Data. Syst.*, DOI: 10.5194/gi-2017-24.

8. Prošireni sažetak

8.1. Uvod

Podaci geomagnetskih opservatorija čine temelj u izučavanju geomagnetskog polja, nalaze široku primjenu u drugim geofizičkim disciplinama te se koriste raznim primijenjenim svrhama. Često se koriste zajedno sa satelitskim podacima te podacima terenskih izmjera (npr. sekularna, marinska, aeromagnetska mjerenja, istraživanja ležišta ugljikovodika itd.) čija je osnovna svrha naći prostorne promjene geomagnetskog polja (Newitt i sur. 1996, Mandea i Korte 2011). Uvijek prisutne vremenske promjene geomagnetskog polja tijekom trajanja izmjere, krive stvarnu sliku prostornih varijacija polja. Opservatorijski podaci se koriste za vremensku korekciju podataka izmjere kako bi se dobila čista predodžba o prostornim varijacijama geomagnetskih elemenata premjerenog područja. Nadalje, jedino kvalitetni, dugoročni (> 10 god.) opservatoriji podaci mogu dati uvid u geodinamičke procese u dubokoj unutrašnjosti Zemlje, koji generiraju i održavaju preko 95% Zemljinog magnetskog polja.

Kontinuirana mjerenja vektorskim magnetometrima (variometrima) ne daju apsolutne vrijednosti komponenata polja i pod utjecajem su temperaturnih varijacija, nestabilnosti stupova/postolja na kojima su postavljeni senzori magnetometara te instrumentalnog drifta (npr. starenje elektroničkih komponenti). „Drift" jest signal u magnetskim podacima koji je posljedica nedostatka idealnih laboratorijskih uvjeta, odnosno potječe od okoline u kojoj magnetometar mjeri te same nesavršenosti magnetometra. Kako ti signalu nisu „prirodne" magnetske promjene, nužno ih je eliminirati iz podataka. Iz tog razlog manualna apsolutna motrenja još uvijek su nužna u modernim geomagnetskim opservatorijima. Vrše se obično jednom tjedno, u svrhu kalibracije kontinuiranih mjerenja i eliminacije drifta. Iz ovih opažanja u kombinaciji s podacima vektorskog i skalarnog magnetometra dobivaju se opažene bazne vrijednosti. Ove bazne vrijednosti se kasnije koriste za računanje kontinuiranih, prilagođenih baznih linija koje služe za dobivanje apsolutnih variometarskih podataka iz kojih su eliminirani driftovi. Prilagođene bazne vrijednosti se dobivaju numeričkom ili ručnom (manualnom, eng. *hand scaling*) prilagodbom iz opaženih vrijednosti. U današnje vrijeme, konačna prilagodba baznih linija se radi na godišnjem nivou i podaci kalibrirani s godišnjim baznim linijama zovemo definitivni (D) podaci. Ti podaci ujedno moraju biti očišćeni od šuma, tj. magnetskih kontaminacija, naglih skokova i ostalih degradacija u kontinuiranim mjerenjima (Jankowski i

Sucksdorff 1996).

Od uspostave INTERMAGNET-a (eng. INTErnational Real-time MAGnetic observatory NETwork, http://www.intermagnet.org) krajem osamdesetih, do nedavno INTERMAGNET opservatoriji (IMO) publicirali su tri tipa podataka, definitivne, preliminarne i sirove podatke. Sirovi podaci geomagnetskih varijacija izmjereni variometrom trebali bi biti dostupni unutar 3 dana od samih mjerenja te su prikladni jedino za studije kratkoročnih varijacija polja. Ovi podaci mogu sadržavati degradacije poput magnetskih šumova i kontaminacija, diskontinuitete i rupe u podacima. Unutar 7 dana opservatoriji mogu raditi korekcije na sirovim podacima kako bi producirali preliminarne podatke. To obično uključuje: upotpunjavanje rupa u podacima, korekcije diskontinuiteta, djelomično i li potpuno uklanjanje šumova te preliminarna korekcija baznih linija. Bez obzira to, preliminarnih podaci nisu slobodni od driftova i nemaju ciljanu apsolutnu točnost. S druge strane definitivni podaci koji su nužni za studije sekularne varijacije i geodinamičkih procesa u Zemljinoj jezgri, publiciraju se s vremenskim kašnjenjem od nekoliko mjeseci pa i više od godinu dana. Za razliku od opservatorijskih podataka, u potpunosti kalibrirani satelitski podaci dostupni su unutar nekoliko dana od samih mjerenja.

Na temelju dosadašnjih satelitskih misija (CHAMP, Ørsted, SAC-C) u nekoliko studija (Lesur i sur. 2006, Macmillan i Olsen 2013, Olsen i sur. 2006) demonstrirana je važnost apsolutnih opservatorijskih podataka u gotovo realnom vremenu. Trenutna satelitska misija Swarm (Friss-Christensen i sur. 2006), konstelacija je tri satelita, čiji podaci omogućuju separaciju unutarnjih i vanjskih izvora polja bolje nego ikada do sada. Obrada, selekcija i verifikacija satelitskih podataka bazira se na podacima opservatorija i njihovim produktima, npr. geomagnetskim indeksima. Apsolutne satne srednje vrijednosti opservatorija širom svijet igraju važnu ulogu sat-po-sat (eng. hour-by-hour) sfernoj harmonijskoj analizi.

Kako bi se povećala iskoristivost opservatorijskih podataka i ispunile potrebe znanstvenih grupa koja se bave globalnim modeliranjem, INTERMAGNET je definirao novi tip „kvazi-definitivnih" podataka (Peltier i Chulliat 2010, Clarke i sur. 2013, Matzka 2013). Kvazi-definitivni podaci su popravljeni s privremenim baznim linijama, trebali bi imati vrijednosti bliske definitivnim i publicirani puno prije (unutar 1-3 mjeseca) nego konačni definitivni podaci. Kvaliteta zapisa varijacije polja kvazi-definitivnih podataka bi trebala biti ista (ili slična) kao kod definitivnih podataka, tj. bez magnetskih kontaminacija i šumova. Drugim riječima kvazi-definitivni podaci premošćuju prazninu između preliminarnih i definitivnih podataka. Time se omogućuje puno veća iskoristivost i efikasnije kombiniranje opservatorijskih podataka sa satelitskim, kao i s podacima terenskih izmjera.

Privremene kvazi-definitivne bazne linije se računaju iz svih apsolutnih mjerenja obavljenih u tekućoj godini. Neki opservatoriji publiciraju kvazi-definitivne podatke u gotovo realnom vremenu koristeći bazne linije dobivene ekstrapolacijom. U tim slučajevima godišnja amplituda varijacije bazne linije ne

bi smjela prelaziti 5 nT. Ovakvo promptno publiciranje također zahtjeva brzu i efikasnu obradu variometarskih podataka. U današnje vrijeme, pregled i uklanjanje degradacija iz magnetograma može se obaviti relativno brzo, u roku nekoliko dana od akvizicije. Naravno ovo uvelike ovisi o raspoloživom opservatorijskom osoblju, efikasnosti računalnih programa za obradu podataka te o količini i kompleksnosti problema u variometarskim podacima. Isto vrijedi za kontrolu apsolutne točnosti podataka samo na duljim vremenskim skalama, a uključuje: prebacivanje rezultata manualnih opažanja u digitalni format, obradu opažanja, kontrolu kvalitete i verifikaciju rezultata, donošenje odluka u toku prilagodbe baznih linija itd. Ovi koraci su nužni tijekom kalibracije definitivnih i kvazi-definitivnih podataka. Vremenski interval od 1 do 3 mjeseca potreban je za produkciju kvazi-definitivnih podataka, dok za konačnu pripremu definitivnih podataka potrebno sakupiti rezultate opažanja tijekom čitave godine.

Danas, većina opservatorija koristi parametarsku (npr. polinomi) ili polu-parametarsku (eng. *semi-parametric*, npr. izglađivanje splajn funkcijama) prilagodbu na godišnjem nivo kako bi dobili definitivne bazne linije (DBL). Računanje baznih linija na taj način ima dva glavna nedostatka: (1) Opažene vrijednosti kroz cijelu godinu moraju biti prikupljene kako bi se izračunale definitivne bazne linije. (2) U slučaju parametarske prilagodbe konvergencija kumulativnih kvazi-definitivni linija, prema definitivnoj, vrlo je spora. To znači da odstupanja apsolutnih vrijednosti kvazi-definitivnih podataka od vrijednosti konačnih definitivnih podataka mogu značajno odstupati (do 5 nT) ovisno o generalnoj stabilnosti baznih linija u opservatoriju. Slično vrijedi i za polu-parametarsku prilagodbu u slučaju da je vremenska razdioba opažanja neuniformna ili se mijenjaju parametri izglađivanja kako se podatkovni set opažanja ažurira (vidi poglavlje 3.2). Općenito, globalna prilagodba (na godišnjem nivou) dobra je za procjenu generalnog trenda varijacije baznih linija. S druge strane imamo li značajnije varijacije bazne linije unutar kraćeg vremenskog perioda (npr. zbog problema s mehaničkom stabilnosti senzora variometra), globalna prilagodba možda neće dati zadovoljavajuće rezultate tj. imati zadovoljavajuću dobrotu prilagodbe u periodima gdje bazna linija varira jače bez da se naruši kvaliteta prilagodbe u ostalim dijelovima domene. Povećanjem stupnja polinoma ili fleksibilnosti splajna postići će se bolja prilagodba u periodima gdje bazna linija varira jače, ali to može unijeti i „lažnu" varijaciju u periodima gdje opažanja ukazuju na stabilan trend, osobito u periodima gdje imamo rijetka opažanja (za detalje vidi poglavlje 8.2.1).

U ovom radu biti će demonstrirano da se definitivni podaci opservatorija mogu biti producirati unutar godine dana. Pokazati će se kako je dovoljno sakupiti razuman broj opažanja tijekom određenog perioda koja će omogućiti ispravnu lokalnu (definitivnu) prilagodbu za taj period. S tjednim apsolutnim motrenjima, unutar nekoliko mjeseci moguće je sakupiti dovoljan broj uzoraka za dio definitivne bazne linije unutar godine. Konstrukcijom po segmentima kontinuirane krivulje, s glatkim prijelazima na rubovima segmenata (prozora), zapravo se konstruira godišnja definitivna bazna linija po dijelovima. Prednost konstrukcije po segmentima je ta što opažanja u budućnosti neće utjecati na

oblik bazne linije u prošlosti. Ova činjenica je opravdana i s fizikalne točke gledišta. Naime, opažene bazne vrijednosti odražavaju odziv variometra na trenutne meteorološke uvjete u njegovoj okolini. Bazne vrijednosti u različitim trenutcima (danima) su neovisne, tj. opažena bazna vrijednost u sadašnjosti neovisna je od one u budućnosti. To znači kako trebamo sakupiti razuman broj opažanja (4-10) u određenom periodu kako bismo ispravno procijenili trend bazne linije za dane kada nemamo opažanja. Ispravna interpretacija opažanja u periodima gdje bazna linija varira jače i izbjegavanje unošenja „lažne" varijacije u periodima dobre stabilnosti bazne linije dodatne su prednosti prilagodbe po segmentima.

8.2. Metoda

Predložena metoda bazira se na izglađivanju kubičnim splajn funkcijama (De Boor 1978). Kako bi se dobile visoko-kvalitetne bazne linije na automatiziran način, koristilo se glađenje kubičnim splajn funkcijama (dalje u tekstu samo splajn) u sprezi s dodatnim restrikcijama. Prvi korak podrazumijeva računanje dijela bazne linije unutar segmenta (prozora). Empirijski se utvrdilo kako je duljina prozora od osam opažačkih dana ($L = 8$) u većini slučajeva dobar izbor (jedan motriteljski dan može imati više setova opažanja). Ovisno o učestalosti opažanja širina vremenskog prozora može varirati od tjedan dana pa do nekoliko mjeseci. Dodatno, uzorci iz dva opažačka dana ($d = 2$) prije i nakon prozora koriste se za računanje bazne linije unutar prozora. Na ovaj način umanjuju se diskontinuiteti na rubovima prozora između baznih linija unutar prozora. Sama bazna linija unutar prozora je izglađena kubična splajn funkcija $f(t)$ koja minimizira izraz (3.1). U izrazu (3.1), $f_i = f(t_i)$ predstavlja vrijednosti bazne linije $f(t)$ u vremenima opažanja t_i, a $f''(t)$ predstavlja drugu derivaciju. Granice integrala a i b predstavljaju granice proširenog prozora koji sadrži $L + 2d$ opažanja. Opažanja su označena s y_i, a w_i su pripadne težine. Parametar izglađivanja $p \in [0,1]$ definira glatkoću funkcije $f(t)$ i za veće vrijednosti p, bazna linija biti će bliža opažanjima. U slučaju $p = 0$ bazna linija biti će konstantna (srednjak opažanja), a za $p = 1$ bazna linija biti će interpolacijska splajn funkcija koja interpolira opažanja. Procjena težina se radi na način da izračuna preliminarna bazna linija $\tilde{f}(t)$, pri čemu sva opažanja imaju iste težine, jednake 1. Zatim, iz razlika $y_i - \tilde{f}_i$, odrede se težine prema metodi najčešće vrijednosti (Steiner 1988). Na ovaj način relativno fleksibilni dijelovi bazne linije (veće vrijednosti p) su robusni na veće pogreške u mjerenjima ili nepouzdana mjerenja.

Za automatsko određivanje optimalnog parametra izglađivanja koristi se relacija (3.2), prema De Boor, 2003. U relaciji (3.2) h predstavlja prosječno uzorkovanje, tj. prosječni period između opažačkih dana. Trenutna verzija programa pretpostavlja isti koeficijent glađenja c za tri vektorske komponente,

dok za skalarnu komponentu c može biti isti ili različiti. Koeficijent c varira se u rasponu od 10^{-3} do 10^2 i za svaki c (vektorske i skalarne) bazne linije se računaju. U svrhu automatskog odabira prikladnog koeficijenta c te provjeru kvalitete izračunatih familija baznih linija također se računa i tzv. „Delta F" (ΔF). Rezidual ΔF predstavlja razliku totalnog intenziteta dobivenu iz podataka vektorskog magnetometra i neovisnog skalarnog magnetometra (vidi poglavlje 2.1). Ovdje je skalarni totalni intenzitet popravljen za razliku intenziteta polja između referentne lokacije i lokacije senzora skalarnog magnetometra (vidi poglavlje 2.3). Optimalan koeficijent c odgovara minimalnoj vrijednosti ΔF. Iz ovog razloga, osim samih opažanja, program za kalkulaciju baznih linija koristi variometarske i skalarne zapise. U slučaju da podaci skalarnog magnetometra nisu dostupni, nije moguće izračunati ΔF i u tom slučaju vrijednost koeficijenta c iznosi 0.5.

U određenim slučajevima INTERMAGNET opservatorija, godišnji dugoročni drift baznih linija je malen odnosno usporediv ili reda veličine kao nasumični rasap opažanja. S druge strane, određeni opservatoriji imaju česta apsolutna opažanja (gotova svaki dan po nekoliko setova) u određenim vremenskim intervalima. U ovom slučaju opažanja mogu ukazivati na (nasumične) fluktuacije koje se ne očekuju u „prirodi" bazne linije. Primijetimo također da se p povećava kako h pada (učestala opažanja). Prema jednadžbi (3.1), to znači da će izračunate bazne linije biti bliske opažanjima te će nastojati pratiti, gore spomenute, nasumične fluktuacije u opažanjima. Iz tog razloga preferira se „glatkoća" u odnosu na „fleksibilnost". Odabirom unaprijed zadanog $c < 1$ ($c = 0.5$), desni član u relaciji (3.1) ima veću težinu, a fleksibilnost splajn funkcije je ograničena da slijedi trend u podacima, a ne nasumični rasap.

Kada se odrede bazne linije unutar prozora, prema izrazu (3.1) i gore opisanim restrikcijama, dijelovi baznih linija imati će slične (ali ne indentične) vrijednosti na rubovima susjednih prozora. Iz tog razloga bazne linije unutar prozora dodatno se glade (preko cijele domene) spline funkcijom s fiksnim koeficijentom c. Unaprijed zadana vrijednost $c = 0.005$ koristi se za vektorske bazne linije, a $c = 0.0005$ za skalarnu baznu liniju. U slučaju da nismo u potpunosti zadovolji rezultatima dobivenim automatskim putem, korisnik uvijek može ručno podešavati vrijednosti c koeficijenata. Na ovaj način dobivamo glatke prijelaze između rubova prozora, a da se pritom ne naruši oblik individualnih baznih linija unutar pojedinih prozora. Ovo će rezultirati glatkim, kontinuiranim baznim linijama kroz cijelu godinu. Osim u posljednjem, recentnom prozoru, oblik bazne linije dobiven na ovakav način je definitivan i neće biti narušen kako se podatkovni niz ažurira novim budućim opažanjima.

Umjeravanje, pomicanje ili premještanje pozicije senzora rezultirati će diskontinuitetima odnosno skokovima u variometarskoj ili skalarnoj baznoj liniji. Općenito, broj diskontinuiteta može biti različit za vektorski ili skalarni instrument. Razlozi ovih diskontinuiteta su obično poznati u opservatorijima i trenutci u kojima su se dogodili označeni su markerom „d", u INTERMAGNET podatkovnom formatu u kojima se doznačuju informacije o opažanjima i prilagođenim baznim linijama (.BLV). Marker „d" i

vrijednosti originalnih, publiciranih baznih linija koriste se za identifikaciju ovih skokova i njihovih iznosa. Stoga, za pravovaljanu prilagodbu u slučaju diskontinuiteta, predložena rutina za prilagodbu baznih linija koristi referentnu listu s vremenima i iznosima diskontinuiteta. Za potrebe testova u ovom radu, ova referentna lista se kreira automatski iz spomenutih informacija koji se publiciraju u INTERMAGNET-ovim .BLV podatkovnim datotekama. Koristeći ove informacije, opažanja se korigiraju na jedan referentni nivo u svrhu pravovaljane prilagodbe novih baznih linija. Na slikama u Prilogu B1 diskontinuiteti su označeni vertikalnim zelenim linijama u vektorskim komponentama i ružičastim linijama u skalarnoj komponenti.

8.2.1. Specijalni slučajevi: nedostajući podaci u vremenskim nizovima i nepodudaranje u intenzitetu skalarnih baznih linija

Primjer opservatorija BOX (Borok) iz rada Peltier and Chulliat (2010) izabran je da se demonstrira kako ne-uniformno uzorkovanje i pretpostavka o unaprijed *a priori* poznatom parametru izglađivanja p može unijeti „umjetnu" varijaciju bazne linije koja nije podržana uzorcima. Na Sl. 3.1, predstavljene su samo horizontalna (H) i vertikalna (Z) bazna linija, zajedno s veličinom ΔF. Originalne bazne linije i ΔF (publicirane na INTERMAGNET DVD-u) dobivene su uzimajući u obzir sva opažanja. Zamislimo sada da iz određenog razloga opažanja nisu bila moguća tijekom proljeća zbog operativnih problema (npr. lokacija opservatorija nije bila pristupačna ili su bili neki problemi s instrumentarijem). Rezultati dobiveni IPGP (Institut de Physique du Globe de Paris) metodom, pod pretpostavkom nedostajućih podataka u proljeću, predstavljeni su plavim linijama. Rezultati dobiveni novom predloženom metodom, pod istom pretpostavkom predstavljeni su crnim linijama. Vertikalne sive linije označavaju automatski definirane prozore u predloženoj metodi. Originalne bazne linije i dobivene IPGP metodom imaju savršeno preklapanje svugdje osim u trećem prozoru. Ukoliko se zanemare proljetna opažanja, očito je kako IPGP metoda daje procjenu baznih linija s većom greškom nego nova metoda. Unaprijed određen parametar izglađivanja u IPGP metodi neće biti dobar je su u slučaju BOX opservatorija bazne linije poprilično fleksibilne, a nemamo opažanja u proljeće koji bi onemogućili krivu procjenu bazne linije u periodu nedostajućih podataka. Nove bazne linije daju puno razumniju procjenu baznih linija zahvaljujući ograničenjima predstavljenim u prethodnom poglavlju. S druge strane na Sl. 3.1, bazne linije dobivene novom metodom, u studenom i prosincu malo su glatkije o originalnih. Ovo je posljedica nedostatka informacije o razlici intenziteta totalnog intenziteta referentne lokacije i lokacije skalarnog senzora, tj. skalarne bazne linije. Prije 2009. INTERMAGNET opservatoriji nisu publicirali informaciju o skalarnim baznim linijama. Dodatno, krajem studenog i prosinca nemamo informaciju o ΔF odnosno podaci skalarnog magnetometra nisu dostupni. U mnogim slučajevima, skalarna bazna linija ima najveći utjecaj na rezidual ΔF. U određenim

slučajevima skalarna opažanja ne mogu pravovaljano reducirati totalni intenzitet skalarnog magnetometra na referentnu lokaciju. Iako su skalarni magnetometri apsolutni instrumenti, potencijalna varijabilnost skalarnih baznih linija dolazi od činjenice da se apsolutna opažanja te vektorska i skalarna mjerenja odvijaju na tri različite lokacije. U konačnici, prilikom pripreme definitivnih podataka sva mjerenja se svode na referentnu (apsolutnu lokaciju). Razliku totalnog intenziteta između referentne i lokacije skalarnog magnetometra kao i vremenske promjene te razlike definiraju skalarnu baznu liniju. Kao što je prikazano na Sl. 3.2 („S" dijagram) , u slučaju originalnih podataka imamo očitu degradaciju u ΔF. Glavni razlog ovome je prisutnost konstantnog odstupanja uzoraka i skalarne bazne linije, tj. odstupanja ΔF od nule za otprilike -0.5 nT.

Generalno govoreći, pouzdanost (odstupanja, varijabilnost i raspršenje) skalarnih opažanja također ovise o magnetskoj homogenosti lokacije opservatorija. Kvalitetna mjerenja (bez magnetske kontaminacije) vektorskog i skalarnog magnetometra, kao i gradiometarske razlike između svih lokacija u opservatoriju koje trebaju biti što manje, a informacije o njima učestalo ažurirane, osnovni su preduvjet za dobivanje kvalitetnih opažanja i redukciju vremenskih nizova na referentnu lokaciju. U situacijama kada imamo nepodudaranje intenzitet u skalarnoj baznoj liniji (tj. odstupanje u ΔF), ili imamo preveliko raspršenje skalarnih opažanja, nova metoda procjenjuje skalarnu (S) baznu liniju kao konstantno odstupanje ΔF od nule. To znači da se u iterativnom postupku opisanom u gornjem poglavlju, unaprijed zada početna pretpostavka daje S bazna linija jednaka nuli, a konačna vrijednost ovisiti će o odstupanju ΔF od nule, ukoliko ono postoji. Bazna linija S dobivena na ovaj način prikazana je na Sl. 3.2 („S" dijagram, crna točkasta linija). Po dijelovima konstantni segmenti godišnje bazne linije S odgovaraju prozorima koji označeni na „H" dijagramu (Sl.3.2, vertikalne sive linije). U nekim opservatorijima broj skalarnih opažanja je značajnije manji od vektorskih, u određenim periodima ili tijekom cijele godine. Ukoliko nemamo informacija o baznoj liniji S ili imamo manje od tri uzorka nužnih za računanje splajna unutar prozora, nova metoda procjenjuje S baznu liniju kao konstantu. Pretpostavka o konstantom S također važi ukoliko je ΔF izračunat koristeći splajn baznu liniju S, dobivenu iz raspršenih opažanja, veći od ΔF-a koji je izračunat koristeći konstantnu baznu liniju S. Nadalje, ukoliko postoje diskontinuiteti veći od 0.5 nT između konstantnih segmenata bazne linije S, tada se ti skokovi eliminiraju izglađivanjem splajn funkcijom s koeficijentom izglađivanja c = 0.0005. Na Sl. 3.3 („S" dijagram), možemo vidjeti preliminarne, po dijelovima konstantne bazne linije (šarene točkaste linije). Konačna prilagođena bazna linija dobivena glađenjem konstantnih segmenata prikazana je crnom točkastom linijom.

Pogledamo li prilagodbu vektorskih baznih linija na Sl. 3.2 i 3.3, možemo vidjeti da nove bazne linije puno bolje prate trend uzoraka nego originalne bazne linije. Ova činjenica je posebno izražena u Z komponenti na Sl. 3.3. U prvoj polovici godine, originalne bazne linije ne mogu u potpunosti kompenzirati drift u Z komponenti. Kao posljedica, u tom periodu imamo veće iznose ΔF reziduala. Primijetimo da u tom periodu, originalne i nove skalarne bazne linije imaju praktički identične

vrijednosti. Na Sl. 3.2, osim konstantnog odstupanja ΔF reziduala od nule, također imamo prisutnost dugoročnog drifta kroz cijelu godinu. Originalne bazne linije i u ovom slučaju podcjenjuju varijabilnost trenda baznim linijama H i Z komponente.

8.2.2. Manualno podešavanje i kvazi-definitivne bazne linije

Općenito govoreći jedna računska metoda nije prikladan alat za obradu i manipulaciju različitih podatkovnih setova i u nekim slučajevima možda neće dati zadovoljavajuće rezultate. Ovo je posebno moguće u slučajevima gdje imamo relativno malen broj podataka, različit broj podataka u različitim komponentama, nejednoliko uzorkovanje, iznenadne promjene u vrijednostima te kada svatki podatkovni set ima različite karakteristike (poput trendova, amplituda, kvalitete uzoraka i sl.). Sve navedeno su zapravo karakteristike opažačkih podatkovnih nizova koji se dobivaju iz standardnih apsolutnih opažanja u geomagnetskim opservatorijima. Testiranje nove metode na INTERMAGNET opservatorijima pokazalo je da u određenim slučajevima, rezultate dobivene automatiziranim procesom moguće poboljšati manualnim ugađanjem na temelju vizualne inspekcije. Ovo se postiže ručnim odabirom L i d parametara, ili ručnim ugađanjem parametra glatkoće splajn funkcije koja se koristi za izglađivanje i povezivanje baznih linija unutar prozora. Ova procedura je demonstrirana na Sl. 3.4a i 3.4b. Rezultati dobiveni u potpunosti automatskim putem su predstavljeni na Sl. 3.4a. U ovom slučaju nove bazne linije nisu dovoljno fleksibilne da se prilagode naglim varijacijama baznih linija u početku godine. Uslijed nepravilne kompenzacije drifta imamo degradaciju u ΔF prikazanom na posljednjem dijagramu na Sl. 3.4a. Ručnim ugađanjem i povećanjem koeficijenta c (u jednadžbi 3.2) konačnog splajna, koji gladi i povezuje bazne linije unutar pojedinih prozora, rezultiralo je fleksibilnijim baznim linijama. Ovo je ilustrirano na Sl. 3.4b. S ovom manjom intervencijom (L i d su ostali isti), dobiveni su puno bolji rezultati od onih dobivenih automatski.

Ukoliko detaljnije pogledamo Sl. 3.2, 3.3, 3.4a i b, nove privremene kvazi-definitivne bazne (QDBL) linije istovremeno su prikazane ispod definitivne bazne linije (DBL). Zbog skoro savršenog preklapanja kumulativnih QDBL i konačne DBL, na Sl. 3.2 i 3.3, vidljivi su samo mali segmenti QDBL na desnoj strani pojedinih prozora. Na primjer, na Sl. 3.2 u blizini kraja jedanaestog prozora možemo primijetit dijelove vektorskih QDBL (narančasta linija). Slično možemo uočiti na Sl. 3.3, u komponenti deklinacije na rubu trećeg prozora. U svrhu boljeg grafičkog prikaza, razlike između QDBL i DBL prikazani su na zasebnim dijagramima, na Sl. 3.4a i b („QD_{RSD}" dijagrami). Ovdje jasno možemo uočiti da male razlike između kumulativnih setova QDBL i konačne DBL postoje samo uz blizini desnog ruba svakog prozora. Označimo li broj prozora s N, tada imamo savršeno preklapanje QDBL i DBL u svim prozorima od prvog do $N-1$, tj. QD_{RSD} su jednaki nuli. To znači da je DBL izračunata i definirana u svim prozorima od prvog do $N-1$. Manja odstupanja postoje samo uz desni

rub N-tog prozora. Sve dok ne prikupimo dodatna opažanja i definiramo $N + 1$ prozor, baznu liniju unutar N-tog prozora definiramo kao kvazi-definitivnu. Općenito, za sve opservatorije korištene u ovom radu, ove male razlike između QDBL i DBL su unutar 1 nT.

8.3. Odabir podataka i verifikacija predložene metode

U svrhu usporedbe rezultata prilagode baznih linija koristili su se podaci INERMAGNET opservatorija u periodu od 2009. do 2011. godine. Ovaj period je izabran jer su se informacije o kalibracijskim parametrima neovisnog skalarnog magnetometra počeli publicirati tek od 2009. godine. U trenutku pripreme rezultata prezentiranih u ovoj disertaciji, posljednji INTERMAGNET-ov DVD publiciran je za 2011. godinu. U tom periodu korišteni su samo podaci opservatorija koji su publicirali podatke o ΔF odnosno vektorske podatke zajedno s podacima neovisnog skalarnog magnetometra.

U trećem poglavlju predstavljeno je samo nekoliko odabranih primjera od ukupno 255 analiziranih slučajeva. Kako bismo prikazali sve rezultate u sažetom obliku, korištena statistička analiza predstavljena je u daljnjem tekstu.

Kako bismo dobili ideju o dobroti prilagodbe novim i originalnim DBL, izračunati su kvadrati koeficijenta korelacije (R^2). Tablica 4.1 prikazuje ove koeficijente za primjere na Sl. 3.2, 3.3, 3.4a i 3.4b. Iz numeričkih vrijednosti u Tablici 4.1 i grafičkih rezultata možemo zaključiti kako su koeficijenti R^2 popriličn dobri indikatori dobrote prilagodbe. Na godišnjoj razini određena su maksimalna apsolutna odstupanja($max|RSD|$) i srednja apsolutna odstupanja($avg|RSD|$) vrjednoti između novih i originalnih baznih linija. Ovo je učinjeno za svaki od 255 testnih slučaja, za vektorske i skalarne bazne linije te za rezidual ΔF. U svrhu ljepšeg grafičkog prikaza izbačeno je 5 slučajeva u kojima su $max|RSD|$ i $avg|RSD|$ za dvije standardne devijacije veći o prosječnog rezultata. U svim odbačenim slučajevima nove bazne linije daju bolje rezultate prema koeficijentu R^2 i rezidualu ΔF. Preostali reziduali su sortirani u razrede od 0.5 nT, a koeficijenti R^2 u razrede širine 0.1 i prikazani u obliku histograma.

Slična analiza napravljena je za nove, kumulativne setove privremenih baznih linija (tj. QDBL) unutar godine. Ovdje, QD_{RSD} razlike su određene samo u odnosu na novu DBL. Za ove kvazi-definitivne slučajeve, unutar svakog prozora određivali su se samo maksimalni apsolutni reziduali ($max|RSD_{QD}^i|$), gdje je $i = 1, \ldots, N$, a N predstavlja broj prozora. Naposljetku, da bi se odredila QD_{RSD} razlika na godišnjem nivou određene su maksimalne ($max(max|RSD_{QD}^i|)$) i srednje ($max(max|RSD_{QD}^i|)$)

vrijednosti svih apsolutnih maksimalnih reziduala $max\left|RSD^i_{QD}\right|$ unutar prozora. Uzimajući u obzir samo $max\left|RSD^i_{QD}\right|$, isključili smo periode u kojima imamo savršeno preklapanje QDBL i DBL (Sl. 3.4a i 3.4b, „QD_{RSD}" dijagrami). U suprotnom, dobili bismo premale razlike (manje od 0.01 nT), tj. puno manje od apsolutne pouzdanosti kalibracijske procedure baznim linijama. Razlike između novih QDBL i publiciranih DBL nisu računate posebno. Iz razloga što ta odstupanja približno odgovaraju razlikama između novih i publiciranih DBL. Drugim riječima, srednjaci razlika QD_{RSD} ($avg\left|RSD^i_{QD}\right|$), daleko su manji nego razlike $max\left|RSD\right|$ i $avg\left|RSD\right|$.

8.4. Rezultati i diskusija

Na Sl. 4.1 (gore), prikazani su maksimalni i srednji ΔF reziduali. Nove bazne linije, automatski izračunate, s unaprijed zadanim postavkama prikazani su crnim histogramima. Rezultati originalnih ΔF reziduala prezentirani su bijelim histogramima. Općenito uzevši, možemo primijetiti kako nove bazne linije daju bolje rezultate prema ΔF parametru. Ovdje se treba naglasiti da je u pojedinim slučajevima manualna intervencija od strane čovjeka ključna u poboljšanju rezultata prilagodbe baznim linijama. U tu svrhu, na temelju vizualne kontrole kvalitete, manje manualne intervencije su napravljene u 46 slučajeva (tj. 18%). Nakon re-kalkulacije baznih linija dodatna poboljšanja se mogu uočiti kroz ΔF parametar (Sl. 4.1, sivi histogrami). Značajnija poboljšanja u obliku i trendu nakon manualnih korekcija ilustrirani su dodatnim primjerima u Prilogu B (pod-Prilog B3). Histogrami razlika između novih i originalnih DBL pokazuju da su u otprilike 80 % slučajeva razlike $max\left|RSD\right|$ unutar 1 nT, a $avg\left|RSD\right|$ unutar 0.2 nT. Najveće razlike su u Y (ili D) komponenti, a najmanje u S komponenti. Ovi rezultati su očekivani iz razloga što je obično varijabilnost Y bazne linije najveća dok je s druge strane bazna linija S najstabilnija. Stabilnost bazne linije S je također evidentna iz Sl. 4.2, gdje je oko 30 % bazne linije S aproksimirano kao konstanta ili po dijelovima konstanta, tj. $R^2 \leq$ 0.1. U slučaju vektorskih komponenti s novom prilagodbom, također možemo uočiti veći broj slučajeva s koeficijentom R^2 unutar razreda između 0.5 i 0.9.

Nešto veći broj opservatorija s R^2 oko 1 imamo u slučaju originalne prilagodbe. U ovim slučajevima originalne bazne linije prilagođene su tehnikama linearne interpolacije ili po segmentima linearnom prilagodbom. Prilikom korištenja ovih tehnika detaljna ljudska intervencija i kontrola kvalitete je nužna. To uključuje kontrolu kvalitete opažanja tj. uklanjanje nepouzdanih i pogrešnih opažanja, zatim u toku prilagodbe donose se odluke, npr. koja opažanja uključiti u računanju jednog segmenta bazne linije, različite komponente mogu imati različit broj segmenata, različite tehnike prilagodbe se mogu

koristiti u različitim komponentama i sl. Ovakvi slučajevi pokazuju kako je ponekad nužna detaljna analiza i intervencija od strane iskusnog osoblja kako bi se dobili visoko-kvalitetni podaci.

Isti test je proveden s novim baznim linijama koje su izračunate s fiksnim, unaprijed zadanim koeficijentom izglađivanja c ($c = 0.5$). U ovom slučaju prilagodba se nije vršila iterativno kako bi se minimizirao ΔF i na taj način našao optimalan c. Prosječne razlike između novih baznih linija izračunatih iterativno i koristeći fiksni c su poprilično malene. Za sve komponente u više od 90 % slučajeva prosječne razlike su unutar 0.1 nT, a maksimalna odstupanja su unutar 1 nT. Detaljnija razdioba ovih razlika je prikazana na Sl. 4.3. Usprkos ovim rezultatima treba napomenuti da se u pojedinim slučajevima, na temelju vizualne kontrole, mogu uočiti značajnija poboljšanja u kvaliteti prilagodbe kada se bazne linije računaju iterativno minimiziranjem ΔF.

Prema tome, nova metoda ima nekoliko prednosti u usporedbi s tradicionalnim. Prvo, nove bazne linije su uistinu točnije jer su u većini slučajeva bolje prilagođena na opažanja te posljedično rezultiraju manjim ΔF (npr. Sl. 3.2 i 3.3). Drugo, razlike između novih QDBL i DBL su jako malene (Sl. 4.4) i prisutne su samo u neposrednoj blizini desnog ruba posljednjeg prozora. U prosjeku više od 90 % ovih reziduala manji su od 0.3 nT (Sl. 4.4, desno), dok su godišnji maksimumi u svih 250 slučajeva rijetko prelaze 1 nT (Sl. 4.4, ljevo). Primijetimo kako su ove razlike prisutne samo u malom vremenskom periodu, kao sto je demonstrirano na Sl. 3.4a i b. Neposredno nakon kalkulacije bazne linije koristeći uzorke iz slijedećeg prozora (tj. nakon ažuriranja podatkovnog niza), ova diskrepancija se popravlja. Posljednja, ali najvažnija činjenica jest da su nove definitivne bazne linije određene unutar godine. Vremensko kašnjenje u produkciji definitivne bazne linije može varirati od nekoliko tjedana pa do nekoliko mjeseci što ovisi o učestalosti apsolutnih opažanja.

Nove privremene bazne linije također ispunjavaju kriterije da ih definiramo kao QDBL čak i u odnosu na originalne, publicirane DBL. Prema INTERMAGNET standardima, razlike između QDBL i DBL trebale bi biti manje od 5 nT, a za mnoge opservatorije te razlike su unutar 1 nT. Na Sl. 4.1 možemo vidjeti da su srednje razlike $avg|RSD|$ unutar 1 nT u svim komponentama, u otprilike 80 % slučajeva te su razlike unutar 0.2 nT. U ovom razmatranju napravljena je pretpostavka da nove privremene QDBL imaju savršeno preklapanje s novim DBL. Ova pretpostavka je opravdana iz razloga što su razlike između novih DBL i njenih privremenih QDLB segmenata puno manji nego razlike između novih i originalnih DBL. To se jasno vidi sa Sl. 4.1 koja prikazuje srednja i maksimalna odstupanja, dok Sl. 4.4 prikazuje godišnje maksimume i srednjake svih maksimalnih odstupanja unutar prozora.

8.5. Zaključci

Tradicionalno definitivni geomagnetski podaci se publiciraju na godišnjem nivou s zakašnjenjem od nekoliko mjeseci pa do više od godinu dana. Dva su osnovna razloga za to. Nemogućnost promptne obrade variometarskih podataka (vizualna kontrola kvalitete, uklanjanje pikova i šumova, korekcije skokova u podacima, itd.) nedugo nakon prikupljanja zbog nedostataka opservatorijskog osoblja i numeričkih rutina za brzu i kvalitetnu obradu podataka. S druge strane prilagodba baznih linija i kalibracija podataka na godišnjem nivou današnji je standard.

U ovoj studiji istražena je mogućnost kontinuiranog publiciranja definitivnih opservatorijskih podataka s manjim vremenskim kašnjenjem. Predložena je nova metoda za prilagodbu baznih linija na gotovo u potpunosti automatski način. Definitivne bazne linije mogu biti procijenjene unutar prozora koji sadrže dovoljan broj opažanja i to na način da rezultati budućih opažanja i prilagodbe neće utjecati na oblik bazne linije u prošlosti. Na ovaj način je puno lakše raditi fleksibilnu prilagodbu baznih linija u periodima većih nestabilnosti variometra, a da pri tome prilagodba bude dovoljno glatka u intervalima kada je bazna linija variometra stabilna. Detaljnom re-analizom opažanja INTERMAGNET-ovih opservatorija u periodu od 2009. do 2011. god. pokazano je da definitivne bazne linije izračunate predloženom metodom u većini slučajeva daju iste ili bolje rezultate (prema ΔF i R^2 kriteriju) od originalnih definitivnih baznih linija.

Većina rezultata u ovoj disertacije se oslanja na verifikaciju veličine ΔF. Kontinuirane i točne skalarne opservacije su nužne kako bi dobili pravovaljani skalarni F na referentnoj lokaciji te kako bismo dobili pouzdanu vrijednost ΔF. Stoga, najbolja opservatorijska praksa bi bila držati skalarnu baznu liniju na nuli, tj. vršiti kontinuirana skalarna mjerenja na referentnoj lokaciji (osim kada se vrše manualna DI-flux motrenja). Alternativno, gradiometarska razlika između referentne lokacije i lokacije skalarnog magnetometra, koja je ujedno i potrebna za obradu DI-flux motrenja, trebala bi se učestalo ažurirati nakon svakog DI-flux motrenja. To bi značilo, neposredno nakon DI-flux motrenja, drugim skalarnim magnetometrom bi trebalo mjeriti F (10-ak minuta) na referentnoj lokaciji. Koristeći ovaj 10-minutni F i simultana mjerenja neovisnog skalarnog magnetometra (koji mjeri kontinuirano) nađe se reprezentativna gradiometarska razlika za određenu seriju DI-flux motrenja. Ova gradiometrijska razlika može se vidjeti u Prilogu A, Slika A.3 i iznosi -3.4 nT (označeno zelenom bojom).

U ovoj disertaciji demonstrirano je da većina INTERMANET opservatorija može publicirati definitivne podatke relativno brzo nakon što prikupi recentna apsolutna mjerenja. Dostupnost podataka najbolje kvalite, tj. definitivnih podataka unutar tekuće godine biti će cijenjena od strane korisnika opservatorijskih podataka. S tjednim opažanjima, većina opservatorija bi trebala moći publicirati definitivne podatke kontinuirano u periodima od 2 do 3 mjeseca nakon samih mjerenja. Povećanje

broja opažanja ili skraćenje duljine prozora moglo bi značajnije skratiti ovo kašnjenje. Dodatno, s predloženom metodom maksimalna odstupanja između definitivnih i kvazi-definitivnih podataka (koji mogu biti dostupni unutar nekoliko dana/tjedana) rijetko prelaze 0.3 nT (odnosno < 0.1 lučnu minute za *D* i *I*).

Činjenica da u većini slučajeva nova metoda daje dobre rezultate bez ljudske intervencije utire put prema automatizaciji cijelog procesnog lanca u geomagnetskim opsevatorijima kada automatski apsolutni instrumenti (Gonsette i sur. 2013, Korte i sur. 2013, Poncelet i sur. 2017) postanu dio instrumentarija standardnog opservatorija. S povećanjem broja digitalnih, automatski prikupljenih opservacija (npr. svakih sat vremena) javit će se potreba za rutinom za prilagodbu baznih linija i kalibraciju podataka u gotovo realnom vremenu. Nasuprot tome automatski instrumenti pokazuju veći rasap u podacima i možemo očekivati velik broj pogrešnih opservacija. Stoga, protokol za automatsku obradu podataka mora biti robustan na raspršenja i greške u mjerenjima. Podaci iz opservatorija Lonjsko polje (LON) korišteni su kako bi se simulirali podatkovni setovi automatskog apsolutnog instrumenta koji vrši 24 opažanja na dan. Rezultati ovih testova su također potvrdili robusnost i pouzdanost predložene metode. Ovime se također pokazalo da ukoliko posjedujemo automatski apsolutni instrument, koji radi mnoštvo opažanja u toku dana, moguće je raditi kalibraciju podataka na dnevnoj bazi što znači da bi krajnji definitivni podaci mogli biti dostupni unutar nekoliko dana nakon prikupljanja.

Appendix A

Most observatories use three-component fluxgate magnetometers as the main observatory variometer. Therefore, in this appendix, the absolute measurement protocol (the null method) and derivation of base values will be demonstrated through data processing template for the LON supplement variometer LEMI-035.

Every DI-flux measurement begins with levelling of the theodolite. At the start and end of each set, the circle readings of the azimuth mark when the fluxgate sensor is above or under the telescope are taken (Fig. A1, table "Myra readings"). In LON, the azimuth mark is located north-east from the reference pillar at the distance of 512 m. True bearing of the azimuth mark with respect to the reference pillar is $A_Z = 64°58'08''$.

Measurement of declination: Before each reading we need to set the telescope exactly horizontal (the vertical scale reads exactly 90° or 270°). By turning the theodolite until the sensor measures almost no magnetic field, the sensor is then brought almost perpendicular to the horizontal component of the field. At this moment, we need to check if the sensor is exactly horizontal. A small deviation from horizontal can occur due to imperfect levelling of the theodolite. If this is the case, the telescope must be adjusted so that vertical scale shows exactly 90° or 270°. Next, the theodolite is finely adjusted until the sensor measures no magnetic field, i.e. the electronic unit displays 0 nT. The exact time and angle at which this occurred are noted. In LON, we initiate the sequence of measurement with position E_{UP}, indicating that the theodolite telescope has been turned toward the east with the fluxgate sensor on the upper side of the telescope. In the given example (Fig. A1), zero-field reading was taken at 09 hours, 13 minutes and 20 seconds according to UTC time and associated angle is 311°30'50''. The next position W_{UP} (telescope toward the west and the sensor is on the top) is obtained after turning the theodolite by approximately 180° around its vertical axis. Again, we need to check and adjust the telescope if necessary so that vertical scale shows 90° or 270°. After fine tuning, we read the exact time and angle of zero-field position. The third horizontal reading E_{DN} is taken after turning the telescope around its horizontal axis by 180° and finding (after fine tuning) the position giving a zero reading on the magnetometer. The last declination reading, W_{DN}, is found by turning the theodolite approximately 180° around its vertical axis to the opposite null position. This way, we obtain four observations (Fig. A1, green cells in table "D") that compensate misalignment between the magnetic

axis of the sensor and the optical axis of the telescope, and for zero-field offset of the fluxgate magnetometer. The observations can be taken in any order, but it is advisable to always use the same order.

Measurement of inclination: Immediately after the measurement of declination four circle readings (Fig. A1, green cells in table "D") are used to calculate the position of magnetic meridian. The magnetic meridian is the mean of the four declination readings and is used to orientate the theodolite telescope in the vertical plane of the magnetic meridian. In our example, this means that the sensor and telescope lie in the vertical plane that corresponds to the horizontal circle reading of 221°32'11''. The null readings in in the inclination observation are found by rotating the telescope around its horizontal axis and vertical circle readings are noted. The first reading, N_{DN}, indicates that the theodolite telescope has been turned toward the north with the fluxgate sensor under the telescope. In this and all other positions in the inclination observation, the null reading is achieved when the sensor axis is perpendicular to the total field vector. The second position, S_{UP}, is obtained by turning the telescope around the horizontal axis by approximately 180°. This brings the telescope toward the south with the fluxgate sensor on the upper side of the telescope. After this reading, we need to rotate the theodolite around its vertical axis by exactly 180°. In this position, the sensor and telescope lie in the same plane of the magnetic meridian, but now the horizontal circle reading corresponds to 41°32'11''. The remaining two readings N_{UP} and S_{DN} are done in analogue way as N_{UP} and S_{DN}.

Measurement of the total field: Ideally, we would like to measure *F* simultaneously at the same place as *D* and *I* measurements. This is not possible because *F* is measured with a different instrument, which is far enough from the absolute pillar so it does not disturb the DI-flux measurements. The *F* difference between the absolute pillar and the remote site of the scalar sensor is easy to determine by measuring *F* at both places many times so the difference is known to 0.1 nT. This difference has to be checked at least once a year, but more frequently is recommended. This, of course, depends on the magnetic homogeneity of the observatory location. In general, this difference changes very slowly or can be considered as constant for a long time (except during intensive magnetic storms). In the ideal case, simultaneous measurements of *F* should be done after each DI-flux measurement. At LON, this difference in 2016 was -3.4 ± 0.1 nT, which means that the difference is practically constant, and *F* at the main pillar was 3.4 nT lower than at the scalar magnetometer site. Complementary *F* for LEMI magnetometer is provided by dIdD magnetometer. The dIdD *F* recording is most complete, with the smallest number of data gaps and is closest to the LEMI sensor. The table on Fig. A4 contains the variation and *F* recordings during the observational times.

Processing of the D absolute measurements: Since the theodolite circle has a scale from 0° to 360° (or 0-400 in grad-scale), two *D* readings are rewritten as follows:

$$E_{UP} \rightarrow E_{UP} - 180°$$

$$W_{DN} \rightarrow W_{DN} - 180°$$

To obtain correct absolute and base values, the next step is to reduce every reading to the reference time, i.e. reading. The reference time can be arbitrary, and in the LON case, this is the time of the first D reading. Because geomagnetic field is continuously changing between individual readings, the purpose of temporal reduction is to obtain readings as if they are all taken at the same moment. For this, we also need simultaneous vector and scalar recordings. To explain this let us look at "D" table (Fig. A1). The column denoted with (2) presents the previous column in decimal degrees. Raw variation values of D (Var_D) in nT are in column (3). Conversion of Var_D in nT to Var_D in decimal degrees (colum (4)) is done according to formula

$$Var_D° = Var_D^{nT}/(H^{nT} \sin(1°)) = Var_D^{nT}/(F^{nT} \cos(I°)0.0175). \tag{1.A}$$

Relative variations, i.e. variations with the respect to the first variation value are given in column (5). By subtracting the values in column (2) with corresponding values in column (5), we obtain readings reduced to the reference time (denoted with [1] in some tables) in column (6). The average D reading reduced to the reference time is A_D and the magnetic declination is

$$D = A_D - 90° + A_Z - A_M . \tag{2.A}$$

In the formula above the subtraction by 90° comes because, in fact, we measure the position perpendicular to D. To convert ($A_D - 90°$), i.e. the D value in the theodolite system into D in the geographical system, we need to know the average direction of azimuth mark reading (A_M) and true bearing of the mark (A_Z).

Processing of the I absolute measurements: Again, since the theodolite circle has scale from 0° to 360°, some of I readings are rewritten as follows:

$$N_{DN} \rightarrow 360° - N_{DN}$$

$$S_{UP} \rightarrow 180° - S_{UP}$$

$$S_{DN} \rightarrow S_{DN} - 180°$$

Temporal reduction of I readings is performed using Var_H^{nT} and Var_Z^{nT} variometer outputs. Firstly, we compute I variations in nT according to formula

$$Var_I^{nT} = \cos(I_p°) Var_Z^{nT} - \sin(I_p°) Var_H^{nT}, \tag{3.A}$$

where I_p stands for preliminary uncorrected inclination, the average of column (8) (Fig. A2, table "I").

To convert Var_I to degrees using expression

$$Var_I^\circ = Var_I^{nT}/(F^{nT} \sin(1^\circ)),$$ (4.A)

the raw dIdD F recordings during the I observations are used (Fig. A3, table "F", column (15)). Var_I° obtained in this manner is presented in column (11) (Fig. A3). Relative variations with respect to the reference time (the first D reading) are in column (12), while in column (13), we have reduced inclination readings. The magnetic inclination is the average of column (13).

Processing of the F measurements: In Fig. A3, table "F", column (15), contain the raw dIdD F recordings at the time of the first D reading and during the I readings. Firstly, we reduce F to the main pillar by -3.4 nT. Using Var_H^{nT} and Var_Z^{nT} variometer outputs and I_p, we can calculate Var_F^{nT}, i.e. the variometer F output using formula

$$Var_F^{nT} = \cos(I_p^\circ)\, Var_H^{nT} + \sin(I_p^\circ)\, Var_Z^{nT}.$$ (5.A)

Values obtained according to the above expression are presented in column (18), Fig A3. These values are equivalent to the F variometer output if the sensor orientation was in the spherical *DIF* frame. Relative variations with respect to the reference time are in column (19), and column (20) is obtained by subtracting column (15) and (19). This means we have used F variations at the variometer site to reduce F measurements at the main pillar. Finally, the total field at the main pillar is the average of column (20).

Base values: When we know the direction (D, I) and intensity of the field (F), it is trivial to find other intensive elements. Observed geomagnetic elements referred to the main pillar at the reference time 09:34:30 UTC [1] are shown in Fig. A3, table "Absolute values". D and I are expressed in degrees and decimal minutes, while intensive elements are in nT. Now, variometer base values are simply

$$
\begin{aligned}
H_B &= H - Var_H^{nT} \\
D_B &= D - Var_D^{nT} \\
Z_B &= Z - Var_Z^{nT}
\end{aligned}
$$ (6.A)

Recordings of F from an independent scalar magnetometer should also be reduced to the main pillar for the absolute verification of the final vector data. Scalar base values (S) are defined as a difference between F at the main pillar minus raw scalar F_{GSM} at the reference time. Variometer and scalar baselines are shown in Fig. A3, table "Base values". Later, during the preparation of the definitive data, a full year of the observed base values is used to calculate continuous baselines and calibrate scalar and vector data.

Calculation of the offset of the fluxgate electronics and misalignment of the fluxgate sensor

Parallel with computing the absolute *D* and *I* values from the observations described above it is recommended that one should also calculate two angles (δ, ε) between the direction of the fluxgate sensor and the optical axis of the theodolite, and the offset of the fluxgate electronics (S_0). δ is the angle between the direction of the fluxgate sensor and optical axis of the theodolite in the horizontal plane when the telescope is horizontal and ε is the corresponding vertical angle. Both ε and S_0 can be found from the *D* and *I* observations according to formulas:

$$\delta = \frac{\left(A_1 + A_2 - A_3 - A_4\right)}{4}$$

$$\varepsilon_D = \frac{\left(A_1 - A_2 - A_3 + A_4\right)}{4\,tan\,I}$$

$$S_{0D} = \frac{\left(A_2 - A_1 + A_4 - A_3\right)}{4\,sin\left(1°\right)} H$$

$$\varepsilon_I = \frac{\left(V_1 + V_2 - V_3 - V_4\right)}{4}$$

$$S_{0I} = \frac{\left(A_1 - A_2 + A_3 - A_4\right)}{4\,sin\left(1°\right)} F$$

where ε_D and S_{0D} correspond to the *D* observations while ε_I and S_{0I} correspond to the *I* observations. A_i ($i = 1,\dots4$) are values in column (6) in table "D" (Fig. A1). Similarly, V_i are values in column (13) in table "I" (Fig. A2). As demonstrated in Fig. 3A, quantities δ, ε and S_0 should be calculated in connection with every absolute measurement, because they provide a good check of the fluxgate theodolite and are good indicators of the observation quality.

Geomagnetic Observatory Lonjsko Polje (LON)
Department of Geophyisics, Faculty of Science, Zagreb,Croatia
Analysis of DI-Flux-Measrements - H - D - Z
Green fields should be filled

Location:	LON
Date:	15.9.2015
Pillar:	Absolute
First reading:	9:34:30
Absolutes:	THEO-010A
Variations:	LEMI-035
Observer: Igor Mandić	

Myra readings:

	Degrees						
	°	'	"				
Myra Sensor up:	282	33	31	102	33	31	102,55861
Myra Sensor down:	102	33	28	102	33	28	102,55778

Mean
Myra reading:

		°	'	"	
A_M =		102	33	30	102,55819

	°	'	"	
Azimuth A_z =	64	58	8	64	58	8	64,96889

	Sens.	A Nr. [ ]	UTC (1)	Theodolite Readings ° ' "					D/° (2)	Var. D/nT (3)	Var D/° (4)	Red.Var/° (5)-(5)[1]) (5)	Red.Abl./° (2)-(6) (6)
D	E_{up}	1	9:34:30	311	30	50	131	30	50	131,51389	18,462	0,0472	0,00000	131,51389
	W_{up}	2	9:36:25	131	35	19	131	35	19	131,58861	18,165	0,0465	-0,00076	131,58937
	E_{dn}	3	9:39:10	131	31	39	131	31	39	131,52750	17,461	0,0447	-0,00256	131,53006
	W_{dn}	4	9:41:25	311	30	57	131	30	57	131,51583	16,976	0,0434	-0,00380	131,51963
	Means:							A_P=	131,53646	$sinD_P$= 0,06884		A_D=	131,53824
										$cosD_P$= 0,99763			

$$D = A_D + A_z - A_M - 90 = \quad 3,94893 \quad °$$

$$D_p = A_p + A_z - A_M - 90° = \quad 3,94715 \quad °$$

(4) Var. D/° = (3) / (0.01745 * F_P * $cosI_P$)

δI '= 0,80
εI ' = -0,68

Figure A1. Template for processing the *D* measurements.

Geomagnetic Observatory Lonjsko Polje (LON)
Department of Geophyisics, Faculty of Science, Zagreb, Croatia
Analysis of DI-Flux-Measrements - H - D - Z
Green fields should be filled

Location:	LON
Date:	15.9.2015
Pillar:	Absolute
First reading:	9:34:30
Absolutes:	THEO-010A
Variations:	LEMI-035
Observer: Igor Mandić	

	Sens.	A Nr. [ ]	UTC (7)	Theodolite Readings ° ' "				I/° (8)	Var. H/nT (9)	Var Z/nT (10)	Var. I° (11)	Red.Var/° (11)-(11[1]) (12)	Red.Abl./° (9)-(14) (13)
		1	9:34:30						30,129	128,433	0,04016	0,00000	
	N$_{dn}$	5	9:46:05	297	55	44	62 4 16	62,07111	31,529	127,808	0,03833	-0,00183	62,07294
	S$_{up}$	6	9:48:20	117	56	43	62 3 17	62,05472	32,214	127,673	0,03753	-0,00263	62,05736
I	N$_{up}$	7	9:54:00	62	5	45	62 5 45	62,09583	30,224	127,638	0,03961	-0,00055	62,09638
	S$_{dn}$	8	9:55:10	242	4	48	62 4 48	62,08000	30,149	127,597	0,03967	-0,00049	62,08049
Means:							I$_p$ =	62,07542	sinI$_p$ = 0,88356			I =	62,07679
									cosI$_p$ = 0,46831				

(11) Var. I/° = (cosI$_p$ * (10) - sinI$_p$ * (9)) / U$_I$ εI ' = -0,70

Figure A1. Template for processing the *I* measurements.

Geomagnetic Observatory Lonjsko Polje (LON)
Department of Geophyisics, Faculty of Science, Zagreb, Croatia
Analysis of DI-Flux-Measrements - H - D - Z
Green fields should be filled

Location:	LON
Date:	15.9.2015
Pillar:	Absolute
First reading:	9:34:30
Absolutes:	THEO 010A
Variations:	LEMI-035
Observer:	Igor Mandić

	A Nr [ ]	UTC (14)	GSM F/nT (15)	Reduced to A pillar (15) -3,4	Var. H/nT (16)	Var. Z/nT (17)	Var. F/nT (18)	Red.Var F/nT (19-(19[1])) (19)	A pillar F/nT (red. Var.) (20)
	1	9:34:30	47840,28	47836,88	30,129	128,433	127,589	0,000	
	5	9:46:05	47840,20	47836,80	31,529	127,808	127,692	0,103	47836,70
F	6	9:48:20	47840,36	47836,96	32,214	127,673	127,893	0,305	47836,66
	7	9:54:00	47839,37	47835,97	30,224	127,638	126,931	-0,658	47836,63
	8	9:55:10	47839,25	47835,85	30,149	127,597	126,859	-0,729	47836,58

Means: F_p = 47839,80 U_I = 0,01745 F_p = 834,80   F = 47836,64
H_P = 22403,80 U_D = 390,95

(18) Var.F/nT = $\cos I_p$ * (16) + $\sin I_p$ * (17) $H_P = F_P * \cos I_P$

Absolute values:

UTC [1]	D ° '	I ° '	F/nT	H/nT F·cosI	X/nT H·cosD	Y/nT H·sinD	Z/nT F·sinI
9:34:30	3 56,94	62 4,61	47836,64	22401,31	22348,13	1542,72	42267,31

Base values:

UTC [1]	H_B nT	D_B ° '	Z_B Z - (10[1]) nT	I_B ° '	S = F - F_{GSM} F/nT -(15)[1]
		3,901713 °		62,036633 °	
		3 °		62 °	
9:34:30	22371,18	54,10 '	42138,87	2,20 '	-3,64

H_B = H - 9[1]	δI ' = 0,80		
D_B = D - 4[1]	DEC: εI ' = -0,68	DEC: S_0 /nT= 6,36	
Z_B = Z - 10[1]	INC: εI ' = -0,70	INC: S_0 /nT= 6,57	

Figure A3. Final absolute and base values obtained from absolute observations in conjunction with scalar and variometer recordings (Fig A4).

Date	Time	Var H/nT	Var D/nT	Var Z/nT	F/nT		
15.9.2015	9:34:30	30,129	18,462	128,433	47840,28	[1]	
15.9.2015	9:36:25	30,649	18,165	128,290	47840,40		
						D	
15.9.2015	9:39:10	31,144	17,461	128,057	47840,37		
15.9.2015	9:41:25	31,223	16,976	127,846	47840,26		
							LEMI-035
15.9.2015	9:46:05	31,529	16,055	127,808	47840,20		
15.9.2015	9:48:20	32,214	15,215	127,673	47840,36		
						I	
15.9.2015	9:54:00	30,224	14,815	127,638	47839,37		
15.9.2015	9:55:10	30,149	14,652	127,597	47839,25		

Green fields should be filled

Figure A4. Variometer and scalar recordings during the DI-flux zero-field positions. The first reading presents the reference time.

Appendix B

All supplemental figures have the same labelling, i.e. "Vector baselines obtained with the new method (black line) and original baselines (blue dotted line). Vertical grey lines (top diagram) designate the automatically defined windows in the proposed method. Scalar baseline obtained with the new method is displayed by black dotted lines and original by blue dotted line. Observations are denoted with red circles. Original ΔF (blue line) corresponds to original baselines (blue dotted lines). Fractions of the new temporary (quasi-definitive) baselines, barely noticeable, near the right edge of some windows are presented by coloured lines." Only special characteristics related to each figure are commented in the figure captions.

SUB-APPENDIX B1: Examples of discontinuities in baselines.
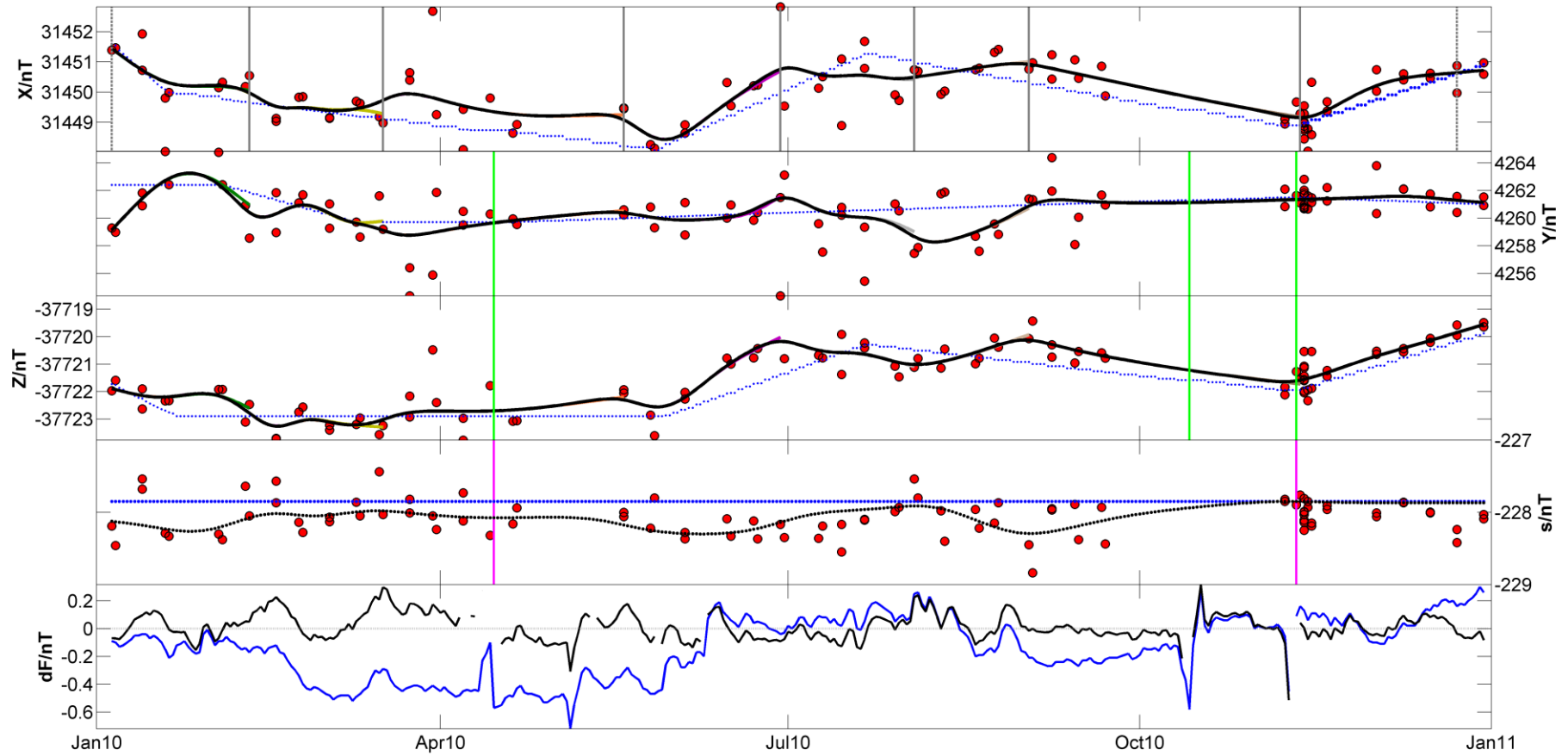
Figure B1.1. Green vertical lines show three discontinuities in vector baselines (only second and third diagram). Two discontinuities in scalar baseline are presented by magenta vertical lines. Generally, the number of discontinuities in vector and scalar baselines is different.
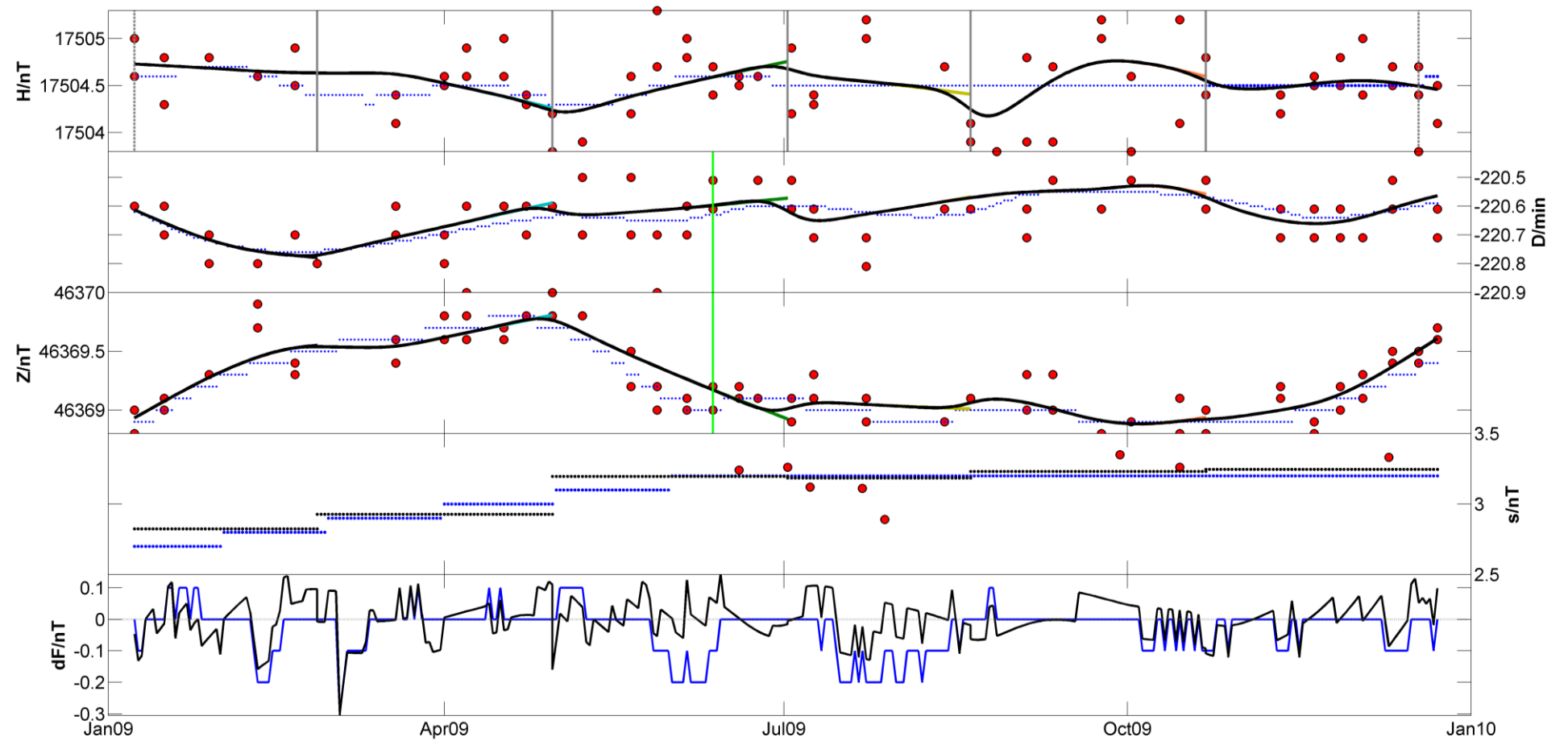
Figure B1.2. Green vertical lines show only one discontinuity in vector baselines.

SUB-APPENDIX B2: Disagreeing intensities in scalar baselines.
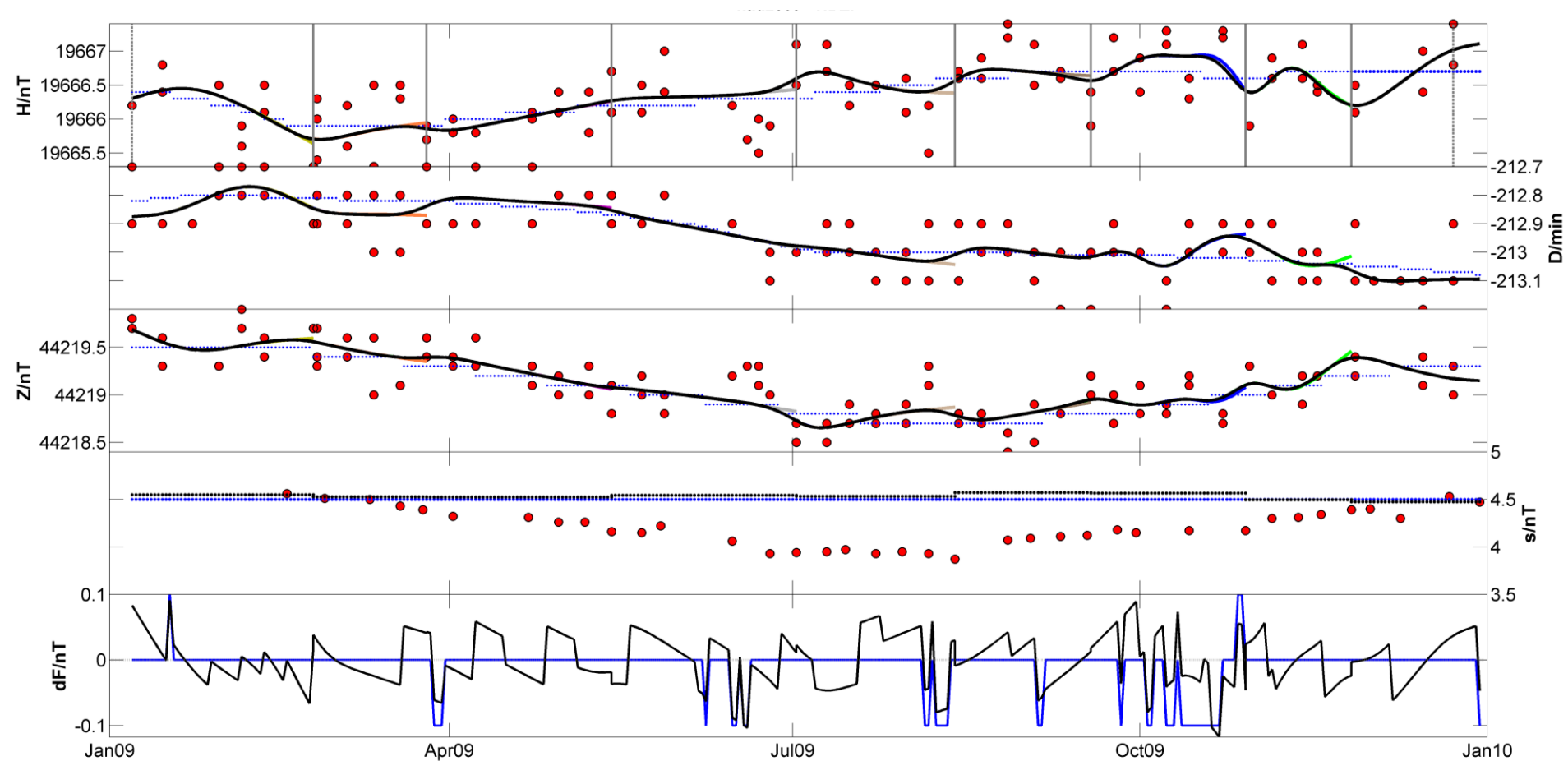
Figure B2.1. Both scalar baselines are estimated in order to minimize and centre *ΔF* to zero.
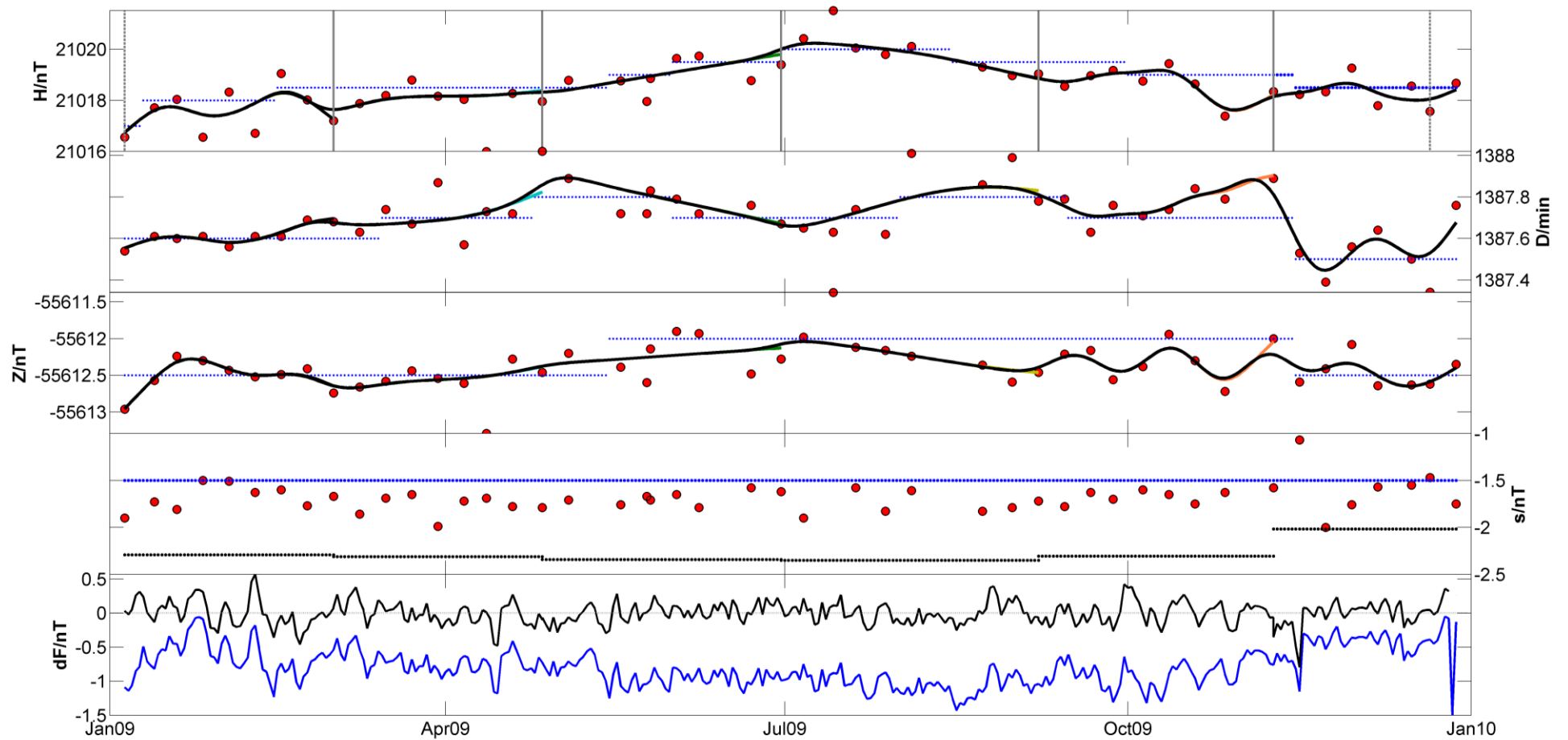
Figure B2.2. The reported scalar baseline overestimates the samples. On the other hand the new baseline underestimates the samples. The *ΔF* diagram shows improvements in reduction of the scalar data to the reference site, after applying the new scalar baseline.

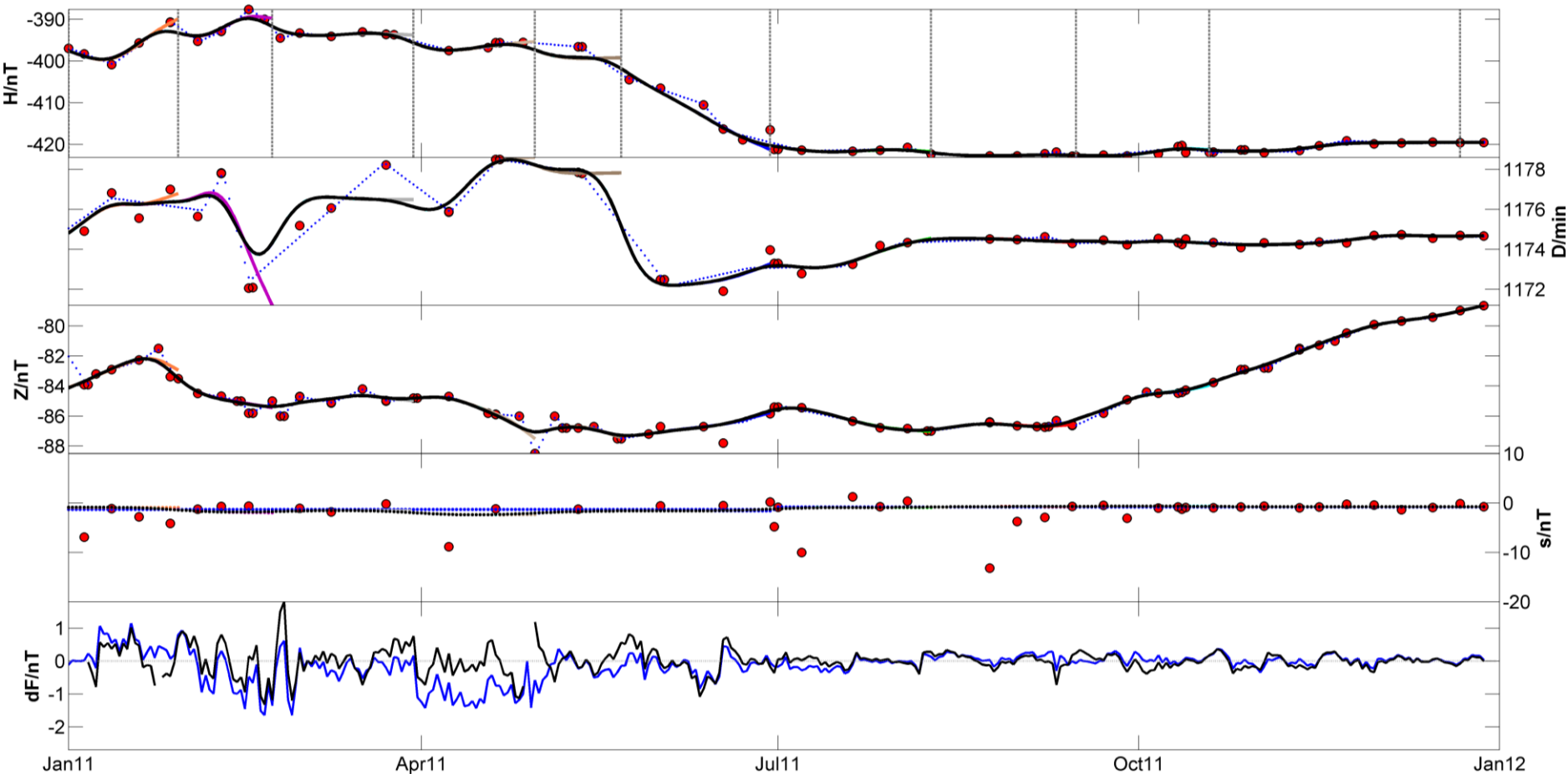SUB-APPENDIX B3: The new baselines obtained by manual adjustment.

Figure B3.1a. The new automatically created baselines (with default settings).
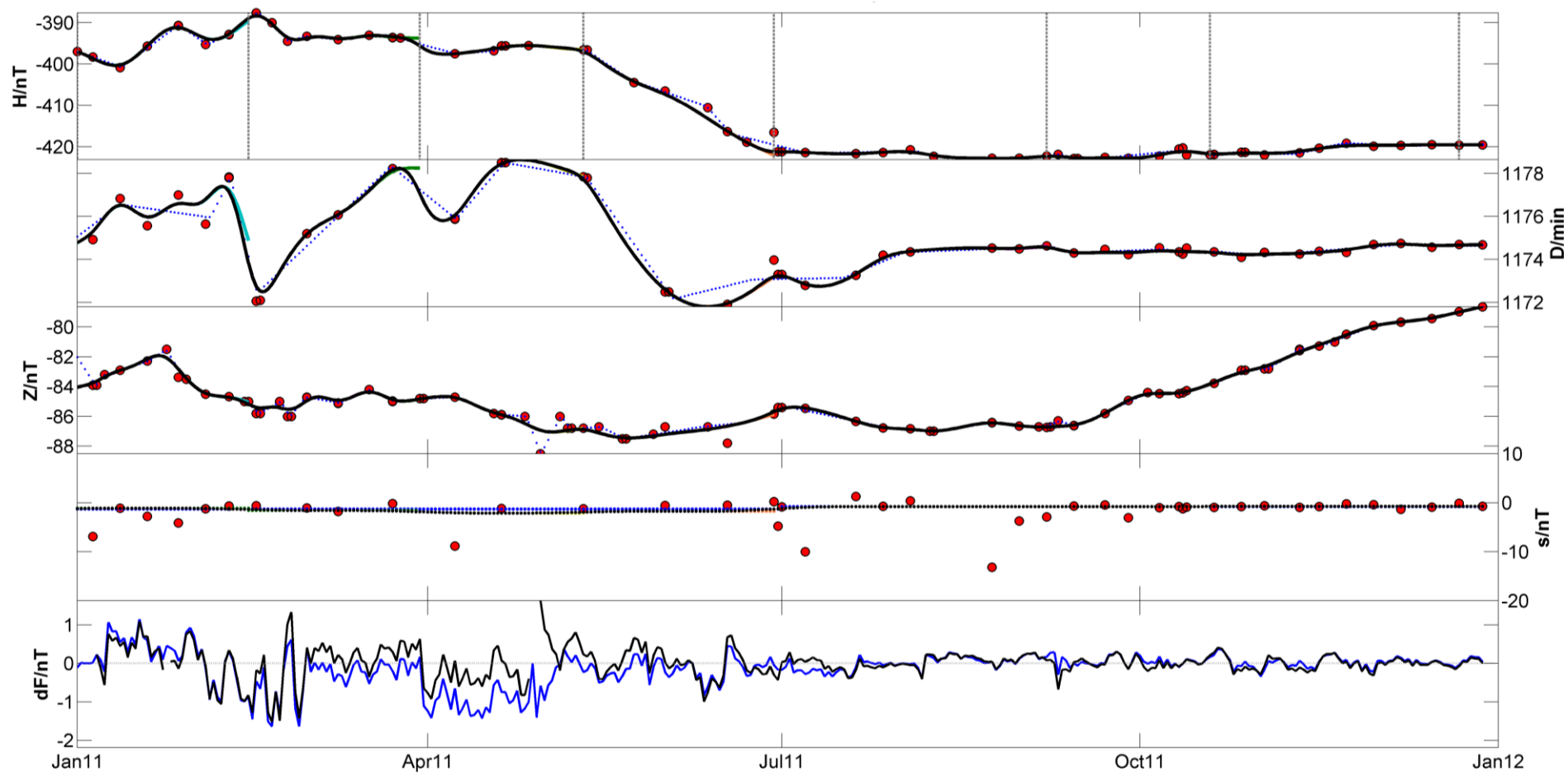
Figure B3.1b. The new baselines obtained after increasing the window size.
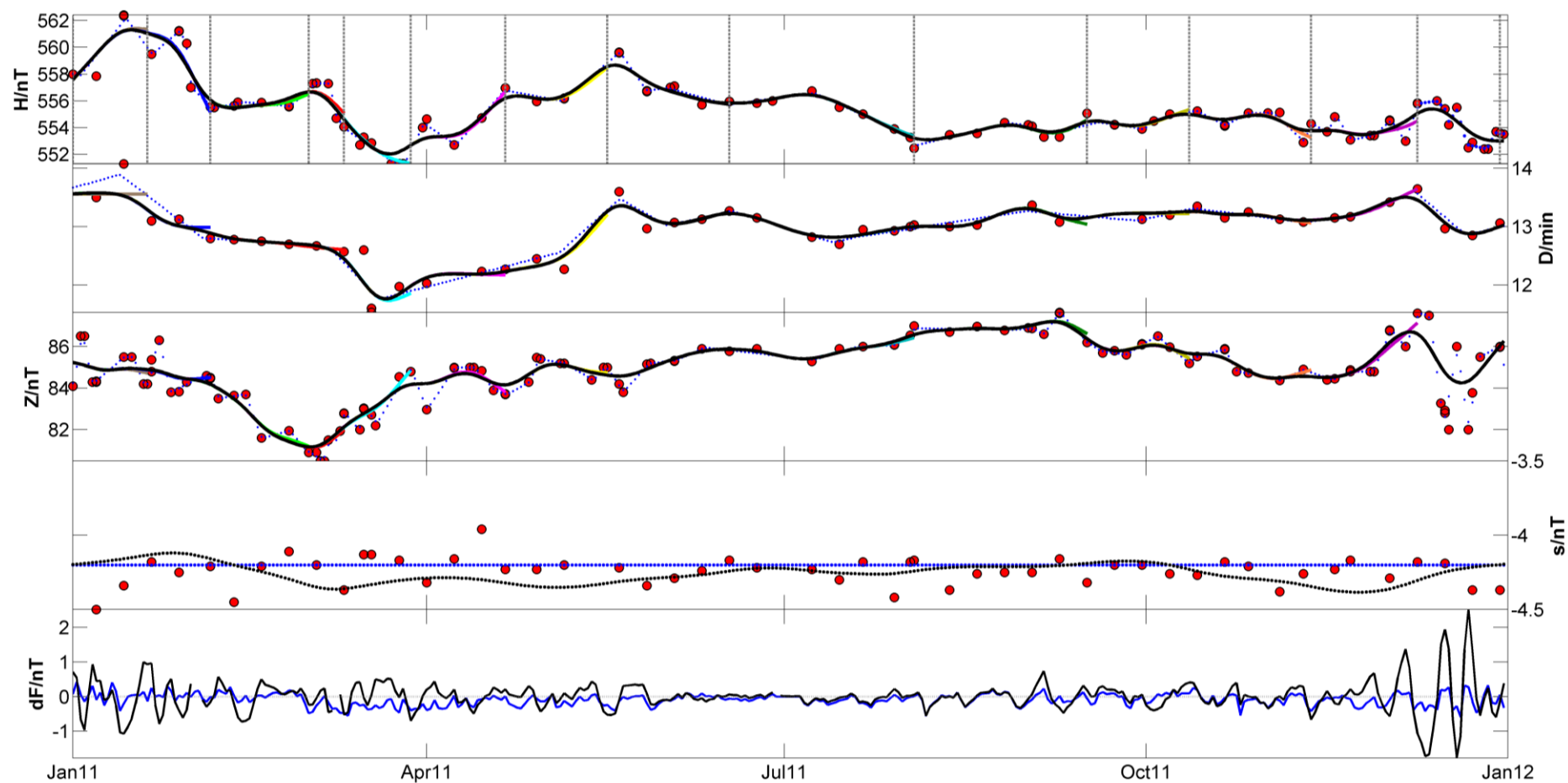
Figure B3.2a. The new automatically created baselines (with default settings).
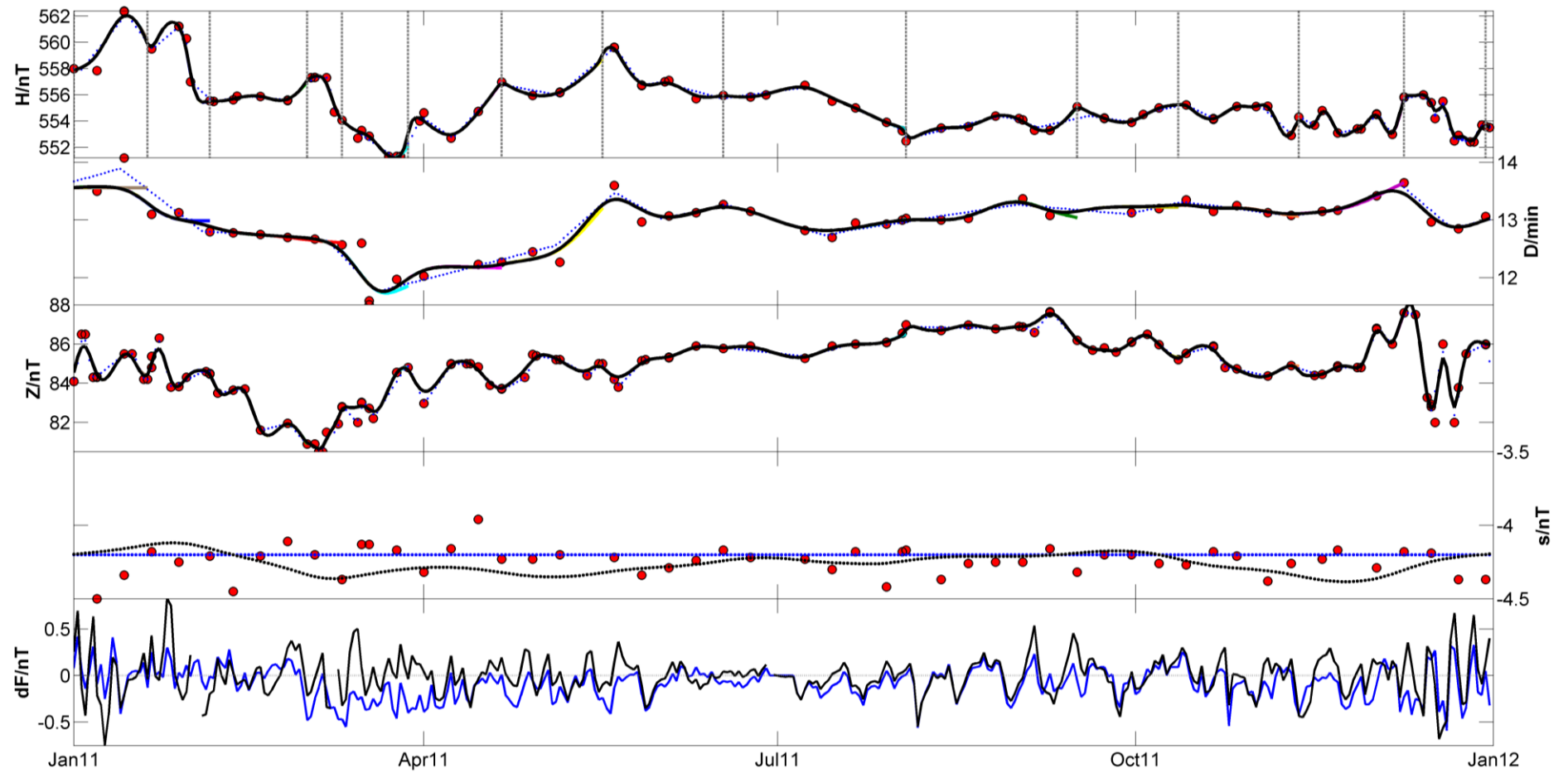
Figure B3.2b. The new baselines obtained after increasing the smoothing parameter of a final spline that joins and smooths sub-splines within the windows.

SUB-APPENDIX B4: Examples of the original baselines determined by linear interpolation or piecewise linear fits.
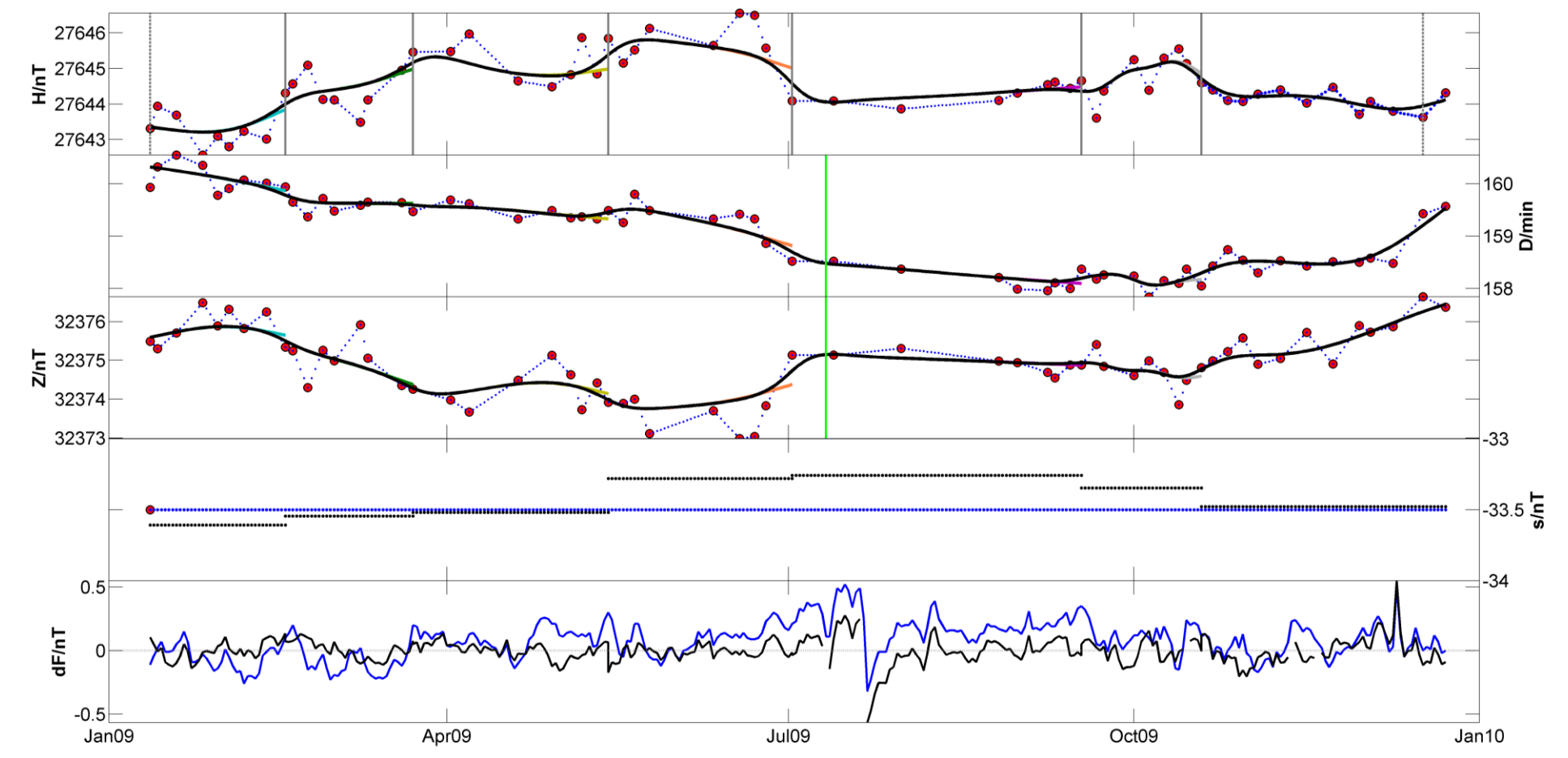

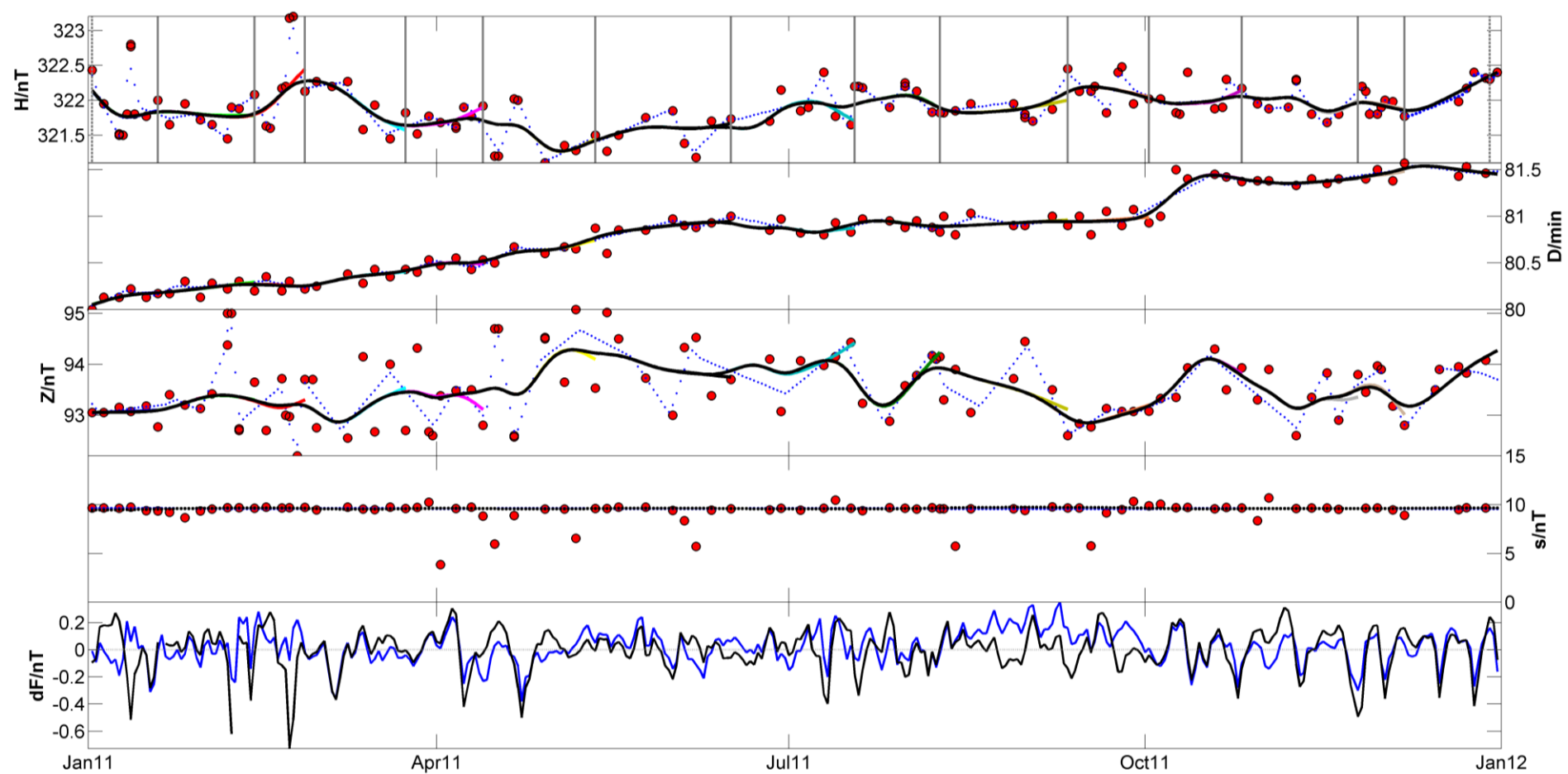**Figure B4.1.** Reported baselines are obtained by linear interpolation.

Figure B4.2. Reported baselines are obtained by piecewise linear fits.

Curriculum vitae

Name   Igor Mandić

Personal data

Birth date: 01 July 1983

Place of birth: Zagreb, Croatia

Address: Vladimira Ruždjaka 2c, 10000 Zagreb, Croatia

E-Mail: mandici@gfz.hr

Education

2010 – Graduated at the University of Zagreb, Faculty of Science, Department of Geophysics, Study of Physics, Geophysics with seismology, qualification: Dipl. Ing. Physics

2003 – Graduated at the First Technical School "Tesla", Zagreb, qualification: Electro-technician

Training

2012 – XVth IAGA Workshop on Geomagnetic Observatory Instruments, Data Acquisition and Processing, San Fernando, Spain

2014 – Visiting scholar at the GFZ German Research Centre for Geosciences, Potsdam, Germany (eight months)

2015 – 7th European MagNetE Workshop, Budapest, Hungary

2016 – XVIIth IAGA Workshop on Geomagnetic Observatory Instruments, Data Acquisition and Processing, Dourbes, Belgium

Work experience

2016-today – Expert Associate at the Department of Geophysics, Faculty of Science, University of Zagreb

2011-2016 – Teaching and Research Assistant at the Department of Geophysics, Faculty of Science, University of Zagreb

Research Projects

2017-2021 – Participant in the project "Renewal of the geomagnetic information on the territory of Republic Croatia – second cycle", the Croatian Ministry of Defence and State Geodetic Administration

2011-2014 – Participant in the project "Study of the geomagnetic field and heterogeneities of the lithosphere in Croatia", the Croatian Ministry of Science, Education and Sports, project No. 119-1193086-1314

2012-2014 – Participant in the project FP7 "Plasmon", European Community's Seventh Framework Programme, project No. 263218.

Awards and Recognitions

2014 – DAAD research grant (No. 91529536-50015537)

2014 – ERASMUS exchange programme grant (No. ERA-2013-166).

2015 – Award from International Union of Geodesy and Geophysics for the attendance at the 26th IUGG General Assembly, Prague, Czech Republic

2016 – INTERMAGNET certification of the Lonjsko Polje Observatory

2016 – Award from International Association of Geomagnetism and Aeronomy for the attendance at the XVIIth IAGA Workshop on Geomagnetic Observatory Instruments, Data Acquisition and Processing, Dourbes, Belgium

Other Activities

2011-today – Maintenance of the Lonjsko Polje Observatory, software development, data analyst

2016-today – Data analyst at the Croatian Seismological Survey

2011-today – Teaching assistant of graduate courses *Geomagnetism* and *Geophysical practicum*

2011-2016 – Teaching assistant of graduate courses *Aeronomy* and *Planetology*

2017-today – Member of the coordination committee in the project "Renewal of geomagnetic information on the territory of Republic Croatia – second cycle"

2017 – Reviewer for the journal "*Geoscientific Instrumentation, Methods and Data Systems*"

List of publications

CC/SCI journals:

1. **Mandić, Igor**; Korte, Monika.

   On the possibility of producing definitive magnetic observatory data within lessthan one year // *Acta Geophysica*, 2017, **65**, 2, 275-286.

2. Jorgensen, Anders M.; Heilig, Balazs; Vellante, Massimo; Lichtenberger, Janos; Reda, Jan; Valach, Fridrich; **Mandić, Igor**.

   Comparing the Dynamic Global Core Plasma Model with ground-based plasma mass density observations // *Journal of Geophysical Research, Space Physics*, 122, 8, 7997-8013.

3. **Mandić, Igor**; Vujić, Eugen; Heilig, Balazs; Pelajić, Izidor; Herak, Davorka

   Recent efforts toward the establishment of the Lonjsko Polje Geomagnetic Observatory // *Acta Geophysica*, 2016, **64**, 5, 1311-1339.

Other journals:

1. Markušić, Snježana; Herak, Davorka; **Mandić, Igor**.

   First Croatian Geomagnetic Observatory in Croatia// *Cartograph and geoinformation*, 2012, **11**, 18; 194-199.

Conference papers:

1. **Mandić, Igor**; Csontos, Andras; Heilig, Balazs.

   A new geomagnetic observatory in Croatia // BOLETÍN ROA N.º 3/2013, *Proceedings of the XVth IAGA Workshop on Geomagnetic Observatory Instruments, Data Acquisition, and Processing* / Hejda, Pavel ; Chulliat, Arnaud ; Catalán, Manuel (ur.). Madrid : MINISTERIO DE DEFENSA, 2013. 111-114.

2. Heilig B.; Lichtenberger, J.; Vellante, M.; Reda, J.; Raita, T.; Sutcliffe, P.; Váczyová, M.; Herak, Davorka; Neska, M.; Merényi, L.; Csontos, A.; Kovács, P., Srbecky, M.; **Mandić, Igor**.

    EMMA for near real time Monitoring of the Plasmasphere // BOLETÍN ROA N.º 3/2013, *Proceedings of the XVth IAGA Workshop on Geomagnetic Observatory Instruments, Data Acquisition, and Processing* / Pavel Hejda ; Arnaud Chulliat ; Manuel Catalán (ur.). San Fernando, Cádiz, Spain : MINISTERIO DE DEFENSA, 2013. 127-130

Conference reports:

1. **Mandić, Igor**.

    Data management at the Lonjsko Polje geomagnetic observatory // *XVIIth IAGA Workshop on Geomagnetic Observatory Instruments, Data acquisition and Processing Dourbes, Belgium, Book of Abstracts*, 2016, 39-39.

2. **Mandić, Igor**; Korte, Monika.

    A routine for the automatic determination of quasi-definitive observatory data // *XVIIth IAGA Workshop on Geomagnetic Observatory Instruments, Data acquisition and Processing Dourbes, Belgium, Book of Abstracts*, 2016, 34-34.

3. **Mandić, Igor**.

    Current status of the Lonjsko Polje geomagnetic observatory // *The abstract book MagNetE 2015*, Geological and Geophysical Institute of Hungary, 2015.

4. **Mandić, Igor**; Korte, Monika.

    Baseline adaptation based on weighted cubic smoothing splines // *Abstracts – 26th IUGG General Assembly*, 2015.

5. Telisman Prtenjak, Maja; **Mandić, Igor**; Horvat, Igor; Tomažić, Igor; Kvakić, Marko; Viher, Mladen; Grisogono, Branko.

    Impact of mesoscale meteorological processes on anomalous radar propagation conditions // *Abstracts – 26th IUGG General Assembly*, 2015.

6. Reda, Jan; Vellante, Massimo; Heilig, Balazs; Raita, Tero; Collier, Andrew; **Mandić, Igor**; Neska, Mariusz.

EMMA/SANSA ground magnetometer network for studies of the plasmasphere // *Geophysical Research Abstracts*, Vol. 16 / Vienna, 2014, EGU2014-5863.

7. **Mandić, Igor**; Pelajić, Izidor; Herak, Davorka; Heilig, B.

    First results from the first Croatian geomagnetic observatory // *Geophysical Research Abstracts*, Vol. 15. Vienna, 2013. EGU2013-4080.

8. **Mandić, Igor**; Markušić, Snježana.

    Geomagnetism in Croatia // *Geophysical Challenges of the 21st Century: Book of abstracts*. Zagreb: Geofizički odjek Prirodoslovno-matematičkog fakulteta, 2011.